# MODERN TOPICS IN RELATIVISTIC SPIN DYNAMICS AND MAGNETISM

by

Andrew James Steinmetz



A Dissertation Submitted to the Faculty of the

DEPARTMENT OF PHYSICS

In Partial Fulfillment of the Requirements
For the Degree of

DOCTOR OF PHILOSOPHY
WITH A MAJOR IN PHYSICS

In the Graduate College

THE UNIVERSITY OF ARIZONA
2023

THE UNIVERSITY OF ARIZONA
GRADUATE COLLEGE

As members of the Dissertation Committee, we certify that we have read the dissertation prepared by Andrew James Steinmetz, titled *Modern topics in relativistic spin dynamics and magnetism* and recommend that it be accepted as fulfilling the dissertation requirement for the Degree of Doctor of Philosophy.

_____ Date:

_____ Date:

_____ Date:

_____ Date:

_____ Date:

_____ Date:

Final approval and acceptance of this dissertation is contingent upon the candidate's submission of the final copies of the dissertation to the Graduate College.

I hereby certify that I have read this dissertation prepared under my direction and recommend that it be accepted as fulfilling the dissertation requirement.

Date:

Dissertation Director: Johann Rafelski

## STATEMENT BY AUTHOR

This dissertation has been submitted in partial fulfillment of requirements for an advanced degree at the University of Arizona and is deposited in the University Library to be made available to borrowers under rules of the Library.

Brief quotations from this dissertation are allowable without special permission, provided that accurate acknowledgment of source is made. Requests for permission for extended quotation from or reproduction of this manuscript in whole or in part may be granted by the head of the major department or the Dean of the Graduate College when in his or her judgment the proposed use of the material is in the interests of scholarship. In all other instances, however, permission must be obtained from the author.

SIGNED: Andrew James Steinmetz

TABLE OF CONTENTS

TABLE OF CONTENTS – *Continued*

TABLE OF CONTENTS – *Continued*

# LIST OF FIGURES

LIST OF FIGURES – *Continued*

LIST OF FIGURES – *Continued*

# LIST OF TABLES

# ABSTRACT

Magnetism is a rich subject touching all aspects of physics. My goal with this dissertation is to explore spin and magnetic dipole moments in *relativistic* mechanics from both a quantum and classical perspective. We emphasize the special case of gyromagnetic ratio $g = 2$ and its relationship to the algebraic spin structure of the wave equations of motion.

In relativistic quantum mechanics, we investigate generalizations of the Dirac equation for arbitrary magnetic dipole moments for fermions. We analyze the homogeneous magnetic field case and the Coulomb problem for hydrogen-like atoms with emphasis on the role of the anomalous magnetic moment (AMM). We explore alternative approaches which combine mass and the magnetic moment. Extensions to include both electromagnetic and color dipole moments are considered. Classically, we propose a relativistic covariant model of the Stern-Gerlach force via the introduction of a magnetic four-potential. This model unites the Ampèrian and Gilbertian models for magnetic dipole moments.

We further study (transition) magnetic dipoles in Majorana neutrinos specifically analyzing the relationship between flavor mixing and electromagnetic fields. We demonstrate this explicitly in the 2-flavor model and develop electromagnetic flavor mixing into a dynamical mass basis.

An interesting application of these theoretical developments is to study primordial magnetization in the early universe during the hot dense electron-positron plasma epoch. We propose a model of magnetic thermal matter-antimatter plasmas. We analyze the paramagnetic characteristics of electron-positron plasma when exposed to an external primordial field. We determine the magnitude of a small polarization asymmetry is sufficient to generate field strengths in agreement with those measured today in deep intergalactic space.

# Publications and author contributions

In the course of satisfying the University of Arizona Department of Physics's requirements for a Ph.D. doctoral dissertation, I prepared the following publications which are reprinted in full in the appendices. These articles are not ordered chronologically, but in the contextual order of presentation in this document. My contribution to each work is described under each item.

- Appendix A - "Magnetic dipole moment in relativistic quantum mechanics" by Steinmetz, Formanek, and Rafelski (2019) is a study and comparison of DP and KGP wave equations for homogeneous magnetic fields and hydrogen-like atoms. I performed all computation, writing, and figure making in preparation of the first draft and approved the final draft before submission. I acknowledge the help and consultation of Martin Formanek (MF) and Johann Rafelski (JR) in research, writing and editing.

- Appendix B - "Strong fields and neutral particle magnetic moment dynamics" by Formanek, Evans, Rafelski, Steinmetz, and Yang (2018) is an overview of our research group's efforts in studying neutral particle dynamics in electromagnetic fields. I wrote Section 2.1 in collaboration with MF. I consulted and helped lead author MF and co-authors Stefan Evans (SE) and Cheng Tao Yang (CTY) in editing and revising the overall manuscript.

- Appendix C - "Relativistic dynamics of point magnetic moment" by Rafelski, Formanek, and Steinmetz (2018) introduces a new covariant formulation of classical spin dynamics and unifies Gilbertian and Ampèrian dipoles. I wrote Section 3 in collaboration with JR and MF and aided in the computation in Section 5.1. I otherwise consulted in the research, writing, and editing process of this publication.

- Appendix D - "Dynamic fermion flavor mixing through transition dipole moments" by Rafelski, Steinmetz, and Yang (2023c) is a study of Majorana neu-

trino flavor mixing in electromagnetic fields and proposes a novel dynamical EM-mass basis for propagating neutrinos. The article was written originally via invitation of JR by Gerhard Buchalla, Dieter Lüst and Zhi-Zhong Xing as a memorial chapter in a book dedicated to Harald Fritzsch. I performed all computation and writing in preparation of the first draft and approved the final draft before submission. I acknowledge the help and consultation of JR and CTY in research, writing and editing.

- Appendix E - "A Short Survey of Matter-Antimatter Evolution in the Primordial Universe" by Rafelski, Birrell, Steinmetz, and Yang (2023a) is a 50 page long review with many novel results describing the role of antimatter in the early universe. I supervised (in collaboration with CTY) the document creation, combining the writing contributions of all authors (including myself, Jeremiah Birrell (JB), CTY, and JR) into one coherent presentation. I also coordinated with all authors in formatting and editing the technical figures in this review by JB, CTY, and JR.

- Appendix F - "Matter-antimatter origin of cosmic magnetism" by Steinmetz, Yang, and Rafelski (2023) proposes a model of para-magnetization driven by the large matter-antimatter (electron-positron) content of the early universe. I carried out all writing in preparation of the first draft and approved the final draft before submission. Computation and figure making was done in collaboration with CTY who contributed key results and five technical figures. I acknowledge the help and consultation of CTY and JR in research, writing and editing.

This is not a total catalogue of my research efforts, but lists the works that form the foundation of Chapter 2, Chapter 3 and Chapter 4 of this dissertation. Where noted, these chapters also contain sections of complete yet unpublished work. Chapter **??** contains brief discussions of still-in-progress research efforts to be completed after submission of this dissertation.

I was also co-author on the following publications which are not used extensively in this dissertation and are not reprinted as appendices. They are listed in chronological

order below. In these three works I consulted with MF, CTY and JR in research and editing making content clarifying contributions to these manuscripts:

- "Classical neutral point particle in linearly polarized EM plane wave field" by Formanek, Steinmetz, and Rafelski (2019) explores the dynamical equations presented in Appendix C for neutral particles with magnetic moment.

- "Radiation reaction friction: Resistive material medium" by Formanek, Steinmetz, and Rafelski (2020) introduces a novel model of relativistic covariant friction within a medium.

- "Motion of classical charged particles with magnetic moment in external plane-wave electromagnetic fields" by Formanek, Steinmetz, and Rafelski (2021) is a followup to the above 2019 work and Appendix C for charged particles with magnetic moment.

- "Decomposition of Fermi gas into zero and finite temperature distributions with examples" by Yang, Formanek, Steinmetz, and Rafelski (2023) is a mathematical methods paper detailing a novel analytic form of the finite temperature behavior of the Fermi-Dirac distribution function. The cold magnetized gas is analyzed as an example.

# CHAPTER 1

## The importance of spin

All fundamental particles known in physics have a non-zero quantized spin angular momentum with the exception of the Higgs boson which is a scalar with spin-0. All other confirmed elementary particles (such as electrons, quarks, photons, etc...) have values of either spin-1/2 or spin-1. Particles with even values of spin are known as bosons while half-integer particles with spin are called fermions. Composite particles (such as atomic nuclei) can exhibit more exotic spin values and fundamental particles with higher spins such as spin-3/2 or spin-2 graviton are commonly predicted in beyond-standard-model (BSM) physics.

In the realm of the Poincaré group of spacetime symmetry (rotations, boosts and translations) transformations, each particle can be uniquely labeled by two distinct Casimir invariants: mass and spin. These two operators commute with all generators of the Poincaré group and act as labels which represent a particle. Therefore in a relativistic context, particle mass and spin are of fundamental importance on equal footing.

If a particle is electrically charged, then by virtue of its spin it will have a magnetic dipole moment. Most neutral particles with spin, though not all, will also have magnetic dipoles though for more complex reasons. Therefore the magnetic behavior of particle is an important window into probing one of the most fundamental properties in physics. As quantum mechanics is not well described in terms of forces or accelerations (except in the context of Ehrenfest-style equations), there is no simple operator description of torque and spin-forces despite having played a key role in the development of quantum mechanics. For a short historical overview of spin see Ohanian (1986).

This introduction serves to motivate the fundamental concepts of spin, magnetic moment and electromagnetism which have played a crucial role in the history physics

and will be explored in the subsequent research chapters. Magnetic (and electric) dipoles, anomalous magnetic moments (AMM), and the wave equations which describe spin-1/2 fermions are covered in Section 1.1. Lastly, Section 1.3 covers topics in ΛCDM cosmology which are particular relevance to Chapter 4. This chapter will also serve to establish notation and mathematical conventions. SI units will be used unless otherwise stated.

## 1.1 Quantum magnetic dipoles and wave equations

In classical theory, when charges rotate or circulate in some manner, a magnetic field is produced characterized by the magnetic dipole moment of the system. An Ampèrian loop of wire with a current is the quintessential example. This concept can be transplanted into quantum theory for spinning particles where the natural size of the magnetic moment of a particle (in this context a charged lepton) is given by the magneton value

$$\mu_\ell \equiv \frac{e\hbar}{2m_\ell} \tag{1.1}$$

where the lepton (denoted by $\ell$) has charge $e$ and mass $m_\ell$.

A quick word on notation: Euclidean three-vectors and matrices will be denoted by boldface font. If indices are specifically printed, they will be done so using Latin indices such as $s_i$. Inner products of three-vectors will be noted via $\boldsymbol{a} \cdot \boldsymbol{b} = a_i b_i$ using Einstein summation notation where repeated indices are summed over. For electrons, Eq. (1.1) is referred to as the Bohr magneton $\mu_B$. The non-relativistic spin operator $\boldsymbol{S}$ for a spin-1/2 particle is defined as

$$\boldsymbol{S} = \frac{\hbar}{2}\boldsymbol{\sigma} = \frac{\hbar}{2}\left(\sigma_1,\, \sigma_2,\, \sigma_3\right)^{\mathrm{T}} , \tag{1.2}$$

where $\boldsymbol{\sigma}$ is the three-vector comprised of the familiar $2 \times 2$ Pauli matrices which act upon two-component spinors $\chi = (\chi_1, \chi_2)^{\mathrm{T}}$. Spinor indices will be suppressed or noted with Latin indices. The algebra defined by the commutators of the Pauli

matrices serves as a representation of $SU(2)$ group structure

$$\{\sigma_i, \sigma_j\} = 2\delta_{ij}\,, \qquad [\sigma_i, \sigma_j] = 2i\varepsilon_{ijk}\sigma_k\,, \tag{1.3}$$

where $\varepsilon_{ijk}$ is the totally antisymmetric Levi-Civita symbol and $\delta_{ij}$ is the Kronecker delta.

The relativistic theory of spin-1/2 fermions however necessitates a four-component spinor $\psi = (\psi_1, \psi_2, \psi_3, \psi_4)^{\mathrm{T}}$ which as Dirac famously noted accommodates the required degrees of freedom for particles and antiparticles as well as both spin up ($\uparrow$) and spin down ($\downarrow$) eigenstates. The Hamiltonian density (in the Dirac representation) for the magnetic dipole moment interaction is given by

$$\mathcal{H}_{\mathrm{int}} = \frac{e\hbar}{2m_\ell}\psi^\dagger \begin{pmatrix} -\boldsymbol{\sigma}\cdot\boldsymbol{B} & i\boldsymbol{\sigma}\cdot\boldsymbol{E}/c \\ -i\boldsymbol{\sigma}\cdot\boldsymbol{E}/c & \boldsymbol{\sigma}\cdot\boldsymbol{B} \end{pmatrix} \psi\,, \tag{1.4}$$

where $\psi^\dagger$ is the complex conjugate transpose of the $\psi$ spinor. The electric $\boldsymbol{E}$ and magnetic $\boldsymbol{B}$ fields are defined in terms of the scalar potential $V$ and vector potential $\boldsymbol{A}$ in the usual way.

$$\boldsymbol{E} = -\boldsymbol{\nabla}V - \frac{\partial \boldsymbol{A}}{\partial t}\,, \qquad \boldsymbol{B} = \boldsymbol{\nabla}\times\boldsymbol{A}\,. \tag{1.5}$$

In the non-relativistic limit for particle states, the lower (antiparticle) components of $\psi$ are suppressed by $|\boldsymbol{p}|/mc$. We can approximate the particle states in terms of two-component spinors $\chi$ to first order as

$$\psi \approx \left(\chi,\ \frac{\boldsymbol{\sigma}\cdot\boldsymbol{\pi}}{2m_\ell c}\chi\right)^{\mathrm{T}}\,, \qquad \boldsymbol{\pi} = \boldsymbol{p} - e\boldsymbol{A}\,. \tag{1.6}$$

A more rigorous method of obtaining non-relativistic Hamiltonian can be found in Foldy and Wouthuysen (1950). The operator $\boldsymbol{\pi}$ is the kinetic momentum operator written in terms of canonical momentum $\boldsymbol{p}$ and vector potential $\boldsymbol{A}$. Making use

of the identity

$$\sigma_i \sigma_j = \delta_{ij} + i\varepsilon_{ijk}\sigma_k \,, \tag{1.7}$$

we insert Eq. (1.6) into Eq. (1.4) yielding to order $\mathcal{O}(1/m^3)$

$$\mathcal{H}_{\text{int}} \approx -\chi^\dagger \left( \frac{e\hbar}{2m_\ell} \boldsymbol{\sigma} \cdot \boldsymbol{B} + \frac{ie\hbar}{4m_\ell^2 c^2} \Big[ (\boldsymbol{\sigma} \cdot \boldsymbol{E}), (\boldsymbol{\sigma} \cdot \boldsymbol{\pi}) \Big] \right) \chi \tag{1.8}$$

$$\mathcal{H}_{\text{int}} \approx -\chi^\dagger \left( \frac{e\hbar}{2m_\ell} \boldsymbol{\sigma} \cdot \boldsymbol{B} + \frac{e\hbar^2}{4m_\ell^2 c^2} \boldsymbol{\nabla} \cdot \boldsymbol{E} + \frac{e\hbar}{4m_\ell^2 c^2} \boldsymbol{\sigma} \cdot (\boldsymbol{E} \times \boldsymbol{\pi} - \boldsymbol{\pi} \times \boldsymbol{E}) \right) \chi \,. \tag{1.9}$$

Keeping only up to first order, the dipole interaction Eq. (1.4) reduces to

$$\mathcal{H}_{\text{int}} \approx -\frac{e\hbar}{2m_\ell} \chi^\dagger \boldsymbol{\sigma} \cdot \boldsymbol{B} \chi \,, \tag{1.10}$$

which is the expected non-relativistic quantum dipole term. The second and third terms in Eq. (1.9) can be interpreted as a Darwin term $\sim \boldsymbol{\nabla} \cdot \boldsymbol{E}$ sensitive to charge density and spin orbit coupling $\sim \boldsymbol{\sigma} \cdot (\boldsymbol{E} \times \boldsymbol{p})$. We will return to relativistic notation and concepts in Section 1.1.2.

The magnetic moment operator $\boldsymbol{\mu}$, as suggested by Eq. (1.10) is defined in terms of the Pauli matrices as

$$\boldsymbol{\mu} = g \left( \frac{e\hbar}{2m_\ell} \right) \frac{\boldsymbol{\sigma}}{2} = g\mu_\ell \frac{\boldsymbol{\sigma}}{2} \,, \qquad \mu \equiv \frac{g}{2} \mu_\ell \,, \tag{1.11}$$

where $\mu$ is the 'total magneton' value representing the full magnetic moment. The parameter $g$ in Eq. (1.11) is the gyromagnetic ratio (or $g$-factor) of the particle. The 'natural' value is $g = 2$. While this prediction is normally attributed to the Dirac equation, it justified from the construction of the kinetic energy operator in the Schrödinger-Pauli equation; see Section 1.2.2 and Sakurai (1967).

In non-relativistic quantum mechanics, the time-dependant Schrödinger-Pauli

(SP) equation (with Hamiltonian $H_{\rm SP}$) for a charged particle is given by

$$H_{\rm SP}\chi = \left(\frac{1}{2m_\ell}\boldsymbol{\pi}^2 - \boldsymbol{\mu}\cdot\boldsymbol{B} + eV\right)\chi = i\hbar\frac{\partial}{\partial t}\chi\,, \qquad \boldsymbol{\pi} = \boldsymbol{p} - e\boldsymbol{A}\,, \tag{1.12}$$

where $\chi$ is again a two-component spinor. It is well known that Eq. (1.12) is obtainable from the Dirac equation (see Section 1.1.2) in the non-relativistic limit.

Before moving on, we will verify that the SP Eq. (1.12) contains within it an expression of the Stern-Gerlach force which was used to first provide evidence of the quantization of angular momentum (Gerlach and Stern, 1922). To accomplish this, we will work in the Heisenberg representation where operators obey the following equation of motion

$$i\hbar\frac{d\boldsymbol{O}}{dt} = [\boldsymbol{O}, H] + i\hbar\frac{\partial\boldsymbol{O}}{\partial t}\,, \tag{1.13}$$

To obtain a 'force' in quantum mechanics we need to find the time derivative of the kinematic momentum operator $\boldsymbol{\pi}$ which is given by

$$\frac{d\boldsymbol{\pi}}{dt} = -\frac{i}{\hbar}[\boldsymbol{\pi}, H_{\rm SP}] + \frac{\partial\boldsymbol{\pi}}{\partial t} = -\frac{i}{\hbar}\left[\boldsymbol{\pi}, \frac{(\boldsymbol{\sigma}\cdot\boldsymbol{\pi})^2}{2m} + eV\right] + \frac{\partial\boldsymbol{\pi}}{\partial t}\,, \tag{1.14}$$

$$\frac{\partial\boldsymbol{\pi}}{\partial t} = -\frac{\partial e\boldsymbol{A}}{\partial t}\,, \qquad [\pi_i, \pi_j] = ie\hbar\varepsilon_{ijk}B_k\,, \qquad [\pi_i, B_j] = -i\hbar\nabla_i B_j\,. \tag{1.15}$$

After some derivation and making use of the identities in Eq. (1.15), we arrive at the quantum analog of the Lorentz force for particles with spin

$$\boxed{\frac{d\boldsymbol{\pi}}{dt} = e\boldsymbol{E} + \frac{e}{2m}(\boldsymbol{\pi}\times\boldsymbol{B} - \boldsymbol{B}\times\boldsymbol{\pi}) + \frac{e\hbar}{2m}\sigma_i\boldsymbol{\nabla}B_i}\,. \tag{1.16}$$

The last term in the expression is the Stern-Gerlach force which is sensitive to inhomogeneous magnetic fields. We also note this equation is suggestive of the 'Ampérian' dipole force which is in the direction of the gradient $\boldsymbol{\nabla}$ rather than the 'Gilbertian' type of dipole force which is in the direction of the field $\boldsymbol{B}$; see Section 2.5. Eq. (1.16) can be connected to our classical understanding by taking the expectation value and casting it as an Ehrenfest-style theorem (Ehrenfest, 1927).

| particle | category | $g$-factor |
|---|---|---|
| electron | elementary | -2.002 319 304 362 56(35) |
| muon | elementary | -2.002 331 8418(13) |
| tau | elementary | -2.036(34) |
| neutron | composite | -3.826 085 45(90) |
| proton | composite | 5.585 694 6893(16) |
| deuterium | composite | 0.857 438 2338(22) |
| tritium | composite | 5.957 924 931(12) |

Table 1.1: The $g$-factor of various particles found in Workman et al. (2022).

### 1.1.1 Anomalous magnetic moment

In nature there is no particle with exactly $g = 2$. As seen in Table 1.1, composite particles often deviate from $g = 2$ greatly as the $g$-factor of a composite particle is related to its internal composition. In the case of the neutron and proton, the internal quarks themselves are responsible. The comparison between three listed isotopes of hydrogen also displays how magnetic moments can 'cancel out' or add together. While deuterium's value of $g$ is suppressed by the extra neutron, the two neutrons in tritium balance one another returning the ratio into one manifestly similar to the proton.

When $g \neq 2$ (which is true for all physical particles with magnetic moment; composite of otherwise) the anomalous magnetic moment (AMM) can be defined via

$$a \equiv \frac{g}{2} - 1\,, \qquad a\frac{e\hbar}{2m_\ell} \to \delta\mu \equiv \mu - \mu_\ell\,, \tag{1.17}$$

where $a$ is the anomaly parameter. We also introduce $\delta\mu$ as the anomalous magneton which will be helpful in our proposal to connect mass and magnetic moment in Section 2.4.1 and Section 3.1.

The anomalous magnetic moment of a particle can arise from a variety of physical sources with the most famous being the one-loop vacuum polarization contribution to the electron first computed by Schwinger (1951). In that work, the first correction to $g$ is given by

$$a_e = \frac{\alpha}{2\pi}\,, \qquad \alpha \equiv \frac{1}{4\pi\varepsilon_0}\frac{e^2}{\hbar c}\,, \tag{1.18}$$

where $\alpha$ is the fine structure constant with an approximate value of $1/137$. The measurement of the electron's $g$-factor is among the most precise measurements in all of physics (Tiesinga et al., 2021) and rapid advancements in the measurement of the muon's anomalous magnetic moment are occurring to this day (Aguillard et al., 2023). This makes the study of magnetic moment, and spin, an exciting area of physical research as new developments continue today.

### 1.1.2 Dirac and Dirac-Pauli equations

While it is always beneficial to be well-appraised of non-relativistic mechanics, nature is intrinsically relativistic and therefore this dissertation must be as well. The relativistic generalization of Eq. (1.12) is the Dirac equation given by

$$\left(\gamma_\alpha \left(i\hbar\partial^\alpha - eA^\alpha\right) - m_\ell c\right)\psi = 0\,, \tag{1.19}$$

$$\pi^\alpha = i\hbar\widetilde{\nabla}^\alpha = i\hbar\partial^\alpha - eA^\alpha\,. \tag{1.20}$$

The wave function $\psi$ in Eq. (1.19) is understood to be a four-component spinor and $\widetilde{\nabla}^\alpha$ in Eq. (1.20) is the covariant derivative. $\pi^\alpha$ is the four-vector version of the kinetic momentum versus the four-momentum $p^\alpha = i\hbar\partial^\alpha$. Four-vectors and tensors in this work will be denoted by Greek indices. Inner products of four-vectors will be noted by $a \cdot b = a^\alpha \eta_{\alpha\beta} b^\beta = a^\alpha b_\alpha$ again following Einstein notation. The four-derivative $\partial^\alpha$ and four-potential $A^\alpha$ are defined as

$$\partial^\alpha = \left(\frac{1}{c}\frac{\partial}{\partial t}, -\boldsymbol{\nabla}\right)\,, \qquad A^\alpha = \left(\frac{V}{c}, \boldsymbol{A}\right)\,. \tag{1.21}$$

We have written the Dirac equation here in the covariant form where $\gamma^\alpha$ are the gamma matrices which obey the anticommuting Clifford algebra

$$\{\gamma_\alpha, \gamma_\beta\} = \gamma_\alpha\gamma_\beta + \gamma_\beta\gamma_\alpha = 2\eta_{\alpha\beta}\,, \tag{1.22}$$

$$\eta_{\alpha\beta} = \mathrm{diag}(+1, -1, -1, -1)\,, \tag{1.23}$$

where $\eta_{\alpha\beta}$ is the flat spacetime Minkowski metric tensor defined with a positive time metric signature. The metric tensor is also responsible for raising and lowering covariant and contravariant indices e.g. $a_\alpha = \eta_{\alpha\beta}a^\beta$. As $\gamma^\alpha$ are also spinor matrices, the commutator in Eq. (1.22) carries implicit spinor indices which here computes to the $4 \times 4$ identity matrix $\mathbb{1}_4$ (which is suppressed). We also introduce the 'fifth' gamma matrix $\gamma^5$ which anticommutes with $\gamma^\alpha$ and the following standard conventions following Itzykson and Zuber (1980)

$$\boldsymbol{\alpha} = \gamma^0\boldsymbol{\gamma}\,, \qquad \boldsymbol{\Sigma} = \gamma^5\boldsymbol{\alpha}\,, \qquad \gamma^5 = i\gamma^0\gamma^1\gamma^2\gamma^3\,, \qquad \gamma_5^2 = 1\,. \tag{1.24}$$

As mentioned before, Eq. (1.19) predicts $g=2$ which is a standard calculation in many textbooks. The most straight-forward manner to generalize the Dirac equation allowing for an anomalous magnetic moment is to add a Pauli term proportional to the anomalous parameter $a$. While in most texts, the anomaly is given in terms of $g-2$ or $a$, we wish to keep our equations generalized to fermions of any given charge $e$ and magnetic moment $\mu$.

Therefore we make use of the substitution in Eq. (1.17) and write the Dirac-Pauli (DP) equation as

$$\left(\gamma_\alpha\left(i\hbar\partial^\alpha - eA^\alpha\right) - m_\ell c - \delta\mu\frac{1}{2c}\sigma_{\alpha\beta}F^{\alpha\beta}\right)\psi = 0\,, \tag{1.25}$$

where the antisymmetric spin tensor $\sigma_{\alpha\beta}$ is defined in terms of the commutator of the gamma matrices

$$\sigma_{\alpha\beta} = \frac{i}{2}\left[\gamma_\alpha, \gamma_\beta\right] = \frac{i}{2}\left(\gamma_\alpha\gamma_\beta - \gamma_\beta\gamma_\alpha\right)\,. \tag{1.26}$$

Exact solutions to the DP equation are relatively scarce due to the complicating nature of the anomalous term. The most extensively studied solutions are those with high symmetries or constant external fields (Thaller, 2013). When the anomalous part $\delta\mu$ is zero, the Dirac equation is recovered. $F^{\alpha\beta}$ is the standard antisymmetric

electromagnetic field tensor defined by

$$F^{\alpha\beta} = \partial^\alpha A^\beta - \partial^\beta A^\alpha = \begin{pmatrix} 0 & -E_1/c & -E_2/c & -E_3/c \\ E_1/c & 0 & -B_3 & B_2 \\ E_2/c & B_3 & 0 & -B_1 \\ E_3/c & -B_2 & B_1 & 0 \end{pmatrix} . \tag{1.27}$$

The electromagnetic field tensor can also be defined in terms of the commutators of the covariant derivative Eq. (1.20) as

$$\left[\widetilde{\nabla}^\alpha, \widetilde{\nabla}^\beta\right] = \frac{ie}{\hbar} F^{\alpha\beta} . \tag{1.28}$$

It is also useful to define the Hodge dual of the electromagnetic field tensor

$$F^*_{\alpha\beta} = \frac{1}{2}\varepsilon_{\alpha\beta\mu\nu}F^{\mu\nu} = \begin{pmatrix} 0 & -B_1 & -B_2 & -B_3 \\ B_1 & 0 & -E_3/c & E_2/c \\ B_2 & E_3/c & 0 & -E_1/c \\ B_3 & -E_2/c & E_1/c & 0 \end{pmatrix} , \tag{1.29}$$

where we use the four-dimensional fully antisymmetric Levi-Civita pseudo-tensor $\varepsilon_{\alpha\beta\mu\nu}$ with the $\varepsilon_{0123} = +1$ convention. The contracted portion $\sigma_{\alpha\beta}F^{\alpha\beta}$ in the Pauli term in Eq. (1.25) can be further expressed as

$$\frac{1}{2}\sigma_{\alpha\beta}F^{\alpha\beta} = i\boldsymbol{\alpha}\cdot\boldsymbol{E}/c - \boldsymbol{\Sigma}\cdot\boldsymbol{B} = i\gamma^0\boldsymbol{\gamma}\cdot\boldsymbol{E}/c - \gamma^5\gamma^0\boldsymbol{\gamma}\cdot\boldsymbol{B} , \tag{1.30}$$

which captures that relativistic magnetic moments should be sensitive to electric as well as magnetic fields as required by Lorentz transformations of the $\boldsymbol{E}$ and $\boldsymbol{B}$ fields. We note that Eq. (1.30) is the matrix which appears in Eq. (1.4) specifically in the Dirac representation of $\boldsymbol{\alpha}$ and $\boldsymbol{\Sigma}$. This should be unsurprising if one considers how the non-relativistic dipole form must generalize under Lorentz boosts which mix electric and magnetic fields.

The DP equation can be obtained from perturbative QED as an effective field

theory for leptons due to vacuum polarization; see standard texts Itzykson and Zuber (1980); Schwartz (2014). However, if a particle's anomalous magnetic moment is not sourced by perturbative QFT, then the Pauli term introduced in Eq. (1.25) must be added by hand *ad hoc* or obtained via non-perturbative means such as Lattice calculations (Aoyama et al., 2020). This is the case for the hadronic contribution to anomalous magnetic moment of leptons as well as any composite particle such as the proton or neutron whose moment is determined by internal structure (Hewett et al., 2012).

Therefore we can describe the AMM as an added Lagrangian interaction term

$$\mathcal{L}_{\mathrm{DP,AMM}} = -\bar{\psi}\left(\delta\mu\frac{1}{2}\sigma_{\alpha\beta}F^{\alpha\beta}\right)\psi\,, \tag{1.31}$$

where $\bar{\psi} = \psi^\dagger\gamma^0$ is the Dirac adjoint. While the focus of this dissertation is not on quantum field theory (QFT), it is valuable to note that the Pauli Lagrangian term in Eq. (1.31) is considered 5-dimensional as the $\psi$ fields have natural units of $[\text{length}]^{-3/2}$ as determined from the Dirac Lagrangian

$$\mathcal{L}_{\mathrm{D}}/c = \bar{\psi}\left(i\hbar\gamma_\alpha\widetilde{\nabla}^\alpha - m_\ell c\right)\psi\,, \qquad \mathcal{L}_{\mathrm{DP}} = \mathcal{L}_{\mathrm{D}} + \mathcal{L}_{\mathrm{DP,AMM}}\,. \tag{1.32}$$

To demonstrate, we note that the electromagnetic field tensor has natural units of $F^{\alpha\beta} \sim [\text{length}]^{-2}$. Therefore the product $\psi\sigma_{\alpha\beta}F^{\alpha\beta}\psi$ has natural units of $[\text{length}]^{-5}$ and the coefficient of Eq. (1.31) (given by $\delta\mu$) has to compensate with $\delta\mu \sim [\text{length}]^{1}$. This makes the DP Lagrangian unsuitable for renormalization which is an essential feature required for well-behaved QFTs. While this does not stop us using DP as an effective QFT with some natural cutoff scale responsible for the anomalous moment, it does reduce the usefulness of the equation as a general description of quantum dipole moments.

As such, there is no reason to expect non-perturbative sources of magnetic moment to strictly adhere to the DP form. Additionally, the DP equation has the physically inelegant consequence of splitting the spin dynamics of fermions into (a) natural $g=2$ behavior (see Section 1.2.2) encompassed by the spinor structure of the Dirac equation

and (b) the anomalous behavior contained in the Pauli term.

### 1.1.3 Electric dipole moments and CP symmetry

While this dissertation is primarily concerned with the dynamics of magnetic dipoles, we note that the techniques and methods discussed here may also find application in other important topics such as electric dipoles. I stress that the following section should be treated as an interesting avenue for future, not present, work.

The structure of the Pauli term in Eq. (1.31) informs us how to construct the relativistic electric dipole moment (EDM); see Knecht (2004); Jegerlehner (2017). The generalization to include the electric dipole is

$$\delta\mu \to \delta\tilde{\mu} \equiv \delta\mu + i\epsilon\gamma^5\,, \tag{1.33}$$

where $\epsilon$ is the EDM of the particle. As the natural electric dipole within the Dirac equation is zero, the presence of $\epsilon$ is always considered anomalous. The EDM Pauli Lagrangian term is

$$\mathcal{L}_{\text{EDM}} = -\bar{\psi}\left(i\epsilon\gamma^5\frac{1}{2}\sigma_{\alpha\beta}F^{\alpha\beta}\right)\psi\,, \tag{1.34}$$

which is of interest because of the inclusion of $\gamma^5$. Taking advantage of the properties of $\gamma^5$, we can write the EDM in Eq. (1.34) as

$$\gamma^5\sigma_{\mu\nu} = \frac{i}{2}\varepsilon_{\mu\nu\alpha\beta}\sigma^{\alpha\beta} \;\to \mathcal{L}_{\text{EDM}} = +\bar{\psi}\left(\epsilon\frac{1}{2}\sigma^{\alpha\beta}F^{*}_{\alpha\beta}\right)\psi\,. \tag{1.35}$$

which is more closely analogous to the structure of the AMM in Eq. (1.31) making use of the dual form of the electromagnetic field tensor shown in Eq. (1.29).

Following a procedure similar to the one found in Section 1.1, Eq. (1.35) reduces in the non-relativistic limit to the Hamiltonian density EDM interaction

$$\mathcal{H}_{\text{EDM}} \approx \epsilon\chi^{\dagger}\boldsymbol{\sigma}\cdot\boldsymbol{E}\chi\,. \tag{1.36}$$

The electric dipole is important because the presence of one would signify charge-parity (CP) violation in the theory which provides a method to distinguish between matter and antimatter. We discuss briefly using the parity (P) and time (T) symmetries of the relevant spin $\boldsymbol{s}$ and field vectors $(\boldsymbol{E}, \boldsymbol{B})$ and their inner products. The even and odd symmetries of each are printed in Table 1.2.

| | $\boldsymbol{E}$ | $\boldsymbol{B}$ | $\boldsymbol{s}$ | $\boldsymbol{s}\cdot\boldsymbol{E}$ | $\boldsymbol{s}\cdot\boldsymbol{B}$ |
|---|---|---|---|---|---|
| T symmetry $(t \to -t)$ | **even** | odd | odd | odd | **even** |
| P symmetry $(\boldsymbol{x} \to -\boldsymbol{x})$ | odd | **even** | **even** | odd | **even** |
| PT symmetry $(x^\alpha \to -x^\alpha)$ | odd | odd | odd | **even** | **even** |

Table 1.2: Time (T), parity (P) and PT symmetries of electric $\boldsymbol{E}$, magnetic $\boldsymbol{B}$, spin $\boldsymbol{s}$ three-vectors and the inner products which describe the dipole Hamiltonian terms.

The EDM term Eq. (1.36) is overall T-odd and P-odd while the magnetic dipole is T-even and P-even. While EDM dipoles are common in molecular systems, no electric dipole has ever been measured for an elementary particle nor composite particles like the proton or neutron despite extensive searching. As a point of comparison, the EDM of the electron is excluded (Andreev et al., 2018; Roussy et al., 2023) by a bound of $|\epsilon_e/c| < 4.1 \times 10^{-30}\, e\,\mathrm{cm}$.

For CPT symmetry to hold, Table 1.2 implies that both the electric and magnetic dipoles must be C-even. C-symmetry is a more complicated concept to discuss as it is only well-defined relativistically where particle and antiparticle states are simultaneously described by the theory. The Dirac spinor charge conjugates as

$$C : \psi \to \psi_c = \eta_c C(\bar{\psi})^{\mathrm{T}} = \eta_c C\gamma_0^{\mathrm{T}}\psi^* \,, \tag{1.37}$$

where $C$ is the charge conjugation matrix satisfying the conjugation relation

$$-C\gamma_\alpha^{\mathrm{T}}C^{-1} = \gamma_\alpha \,, \tag{1.38}$$

and $\eta_c$ is an arbitrary complex phase. The exact matrix expression of $C$ depends

on the representational basis used (Dirac, Weyl, Majorana, etc...). We're specifically interesting in the following conjugations

$$C : \bar{\psi}\gamma_\alpha\psi \to -\bar{\psi}\gamma_\alpha\psi\,, \qquad C : \bar{\psi}\sigma_{\alpha\beta}\psi \to -\bar{\psi}\sigma_{\alpha\beta}\psi\,, \qquad C : A^\alpha \to -A^\alpha\,. \tag{1.39}$$

As the spin density $\bar{\psi}\sigma_{\alpha\beta}\psi$ and vector potential $A^\alpha$ (and thus $F^{\alpha\beta}$) are both odd under charge conjugation, the combination present in the AMM Lagrangian Eq. (1.31) is C-even under charge conjugation. The same is true of the EDM Lagrangian Eq. (1.35) which is more easily seen when cast in terms of the dual tensor.

We note that the fields $\psi$, $\bar{\psi}$ and $A^\alpha$ are considered dynamical *operators* within an interacting quantum field theory. C-symmetry is therefore broken when considering an externally fixed background field such as $A^\alpha_{\text{ext}}(x)$ as $C : A^\alpha_{\text{ext}}(x) \to A^\alpha_{\text{ext}}(x)$.

## 1.2 Klein-Gordon-Pauli equation

While the DP equation is more commonly used, there exists an alternative wave equation which describes the magnetic behavior of fermions called the Klein-Gordon-Pauli (KGP) equation. This equation was first introduced by Fock (1937) and found usefulness in the quantum electrodynamics (Feynman, 1951) and in studying weak interactions (Feynman and Gell-Mann, 1958) due to the ease of describing chiral states.

The KGP equation is generally considered to be the 'square' of the Dirac equation as unlike the Dirac or DP equations, it is a second order equation wave equation for the four-component spinor $\Psi$

$$\left((i\hbar\partial^\alpha - eA^\alpha)^2 - m_\ell^2 c^2 - \left(g\mu_\ell + i\epsilon\gamma^5\right) m_\ell \frac{1}{2}\sigma_{\alpha\beta}F^{\alpha\beta}\right)\Psi = 0\,. \tag{1.40}$$

In the above we printed both the AMM and EDM for theoretical interest, but will drop the EDM term for the remainder of this dissertation. The initial benefit of the KGP formulation is that the wave equation fully commutes with $\gamma^5$ making eigenfunctions explicitly good chiral states. This equation is physically distinct from the

DP and Dirac equations and only share solutions when $g=2$ which is seen if one tries to naïvely square the DP Eq. (1.25).

Eq. (1.40) is mathematically similar to the Klein-Gordon equation which describes charged scalar particles. In the same manner as scalar-QED, the squared covariant derivative contains a $e^2A^2$ term which in QFT results in the presence of a 4-vertex seagull interaction (Schwartz, 2014) at tree-level.

It is important to emphasize that the KGP Eq. (1.40) and DP Eq. (1.25) are distinct wave equations which do not share solutions except when $g=2$ whereas both reduce to the Dirac Eq. (1.19); a detail that has occasionally gone missed in the literature. We will clarify on the relationship between the KGP and Dirac equations here by rewriting the Dirac equation in Eq. (1.19) as

$$\mathcal{D}_\pm = i\hbar\gamma_\alpha\widetilde{\nabla}^\alpha \pm m_\ell c\,, \qquad \mathcal{D}_-\psi = 0\,, \tag{1.41}$$

with a 'Dirac operator' $\mathcal{D}_\pm$ defined in terms of positive and negative mass. This operator has the following properties

$$\mathcal{D}_- = -\gamma^5\mathcal{D}_+\gamma^5\,, \qquad [\mathcal{D}_+, \mathcal{D}_-] = 0\,. \tag{1.42}$$

Ignoring the proportionality factor of $\sqrt{\hbar/m_\ell c}$ which accommodate the units of $\psi$ versus $\Psi$, we can complete the square of the Dirac equation via the substitution $\psi \to \mathcal{D}_+\Psi$

$$\mathcal{D}_-\psi \to \mathcal{D}_-\mathcal{D}_+\Psi\,, \qquad \mathcal{D}_+\mathcal{D}_-\Psi = \left(-\hbar^2\widetilde{\nabla}^2 - m_\ell^2c^2 - e\hbar\frac{1}{2}\sigma_{\alpha\beta}F^{\alpha\beta}\right)\Psi = 0\,. \tag{1.43}$$

This procedure yields the KGP equation for $g=2$. This algebraic 'square root' will be elaborated on further in Section 1.2.2.

For $g \neq 2$ the relationship between the DP and KGP equation becomes more complicated. Instead of a clean algebraic separation, the substitution between $\psi$ and

$\Psi$ requires an infinite series expansion resulting from the non-local inverse substitution

$$\Psi \to \frac{1}{\mathcal{D}_+}\psi = \frac{1}{m_\ell c}\left(1 - \frac{\hbar}{m_\ell c} i\gamma_\alpha \widetilde{\nabla}^\alpha - \frac{\hbar^2}{m_\ell^2 c^2}\left(\gamma_\alpha \widetilde{\nabla}^\alpha\right)^2 + \dots\right)\psi\,. \tag{1.44}$$

The expansion in Eq. (1.44) is considered non-local because it requires an infinite number of initial conditions to determine.

While this procedure 'square roots' the KGP equation ($\sqrt{\text{KGP}}$), the resulting AMM Pauli Lagrangian Eq. (1.31) picks up an infinite number of derivative and field terms which makes the theory rather unpalatable.

$$\mathcal{L}_{\sqrt{\text{KGP}}} = \mathcal{L}_{\text{D}} + \mathcal{L}_{\sqrt{\text{KGP}},\text{AMM}}\,, \tag{1.45}$$

$$\mathcal{L}_{\sqrt{\text{KGP}},\text{AMM}} = -\bar{\psi}\left(\delta\mu \frac{1}{2}\sigma_{\alpha\beta}F^{\alpha\beta}\left(1 - \frac{\hbar}{m_\ell c} i\gamma_\alpha \widetilde{\nabla}^\alpha - \frac{\hbar^2}{m_\ell^2 c^2}\left(\gamma_\alpha \widetilde{\nabla}^\alpha\right)^2 + \dots\right)\right)\psi\,. \tag{1.46}$$

We note each term in Eq. (1.46) is preceded by powers of the reduced Compton wavelength $\lambda_{\text{C}} \equiv \hbar/m_\ell c$ therefore the $\sqrt{\text{KGP}}$ model still might be of interest to study assuming the physical system that admits a reasonable cutoff.

While the first term present in Eq. (1.46) is indeed the correct $\mathcal{L}_{\text{DP,AMM}}$ term, the resulting non-local behavior ultimately breaks the unitarity of the theory making it unsuitable as a fundamental particle theory (Veltman, 1998). While the above is suggestive that there exists no unitary transform between the KGP and DP wave equations, we do not claim it as an absolute proof. If a generalized description of $g=2$ magnetic moment theories exists and makes a good fundamental quantum field theory, then likely non-minimal electromagnetic terms are required to maintain both renormalization and unitarity.

### 1.2.1 Features of the KGP Lagrangian

Before continuing to specific physical problems, we consider how current conversation functions in the KGP formulation of fermions and how it might differ from the Dirac current $\mathcal{J}^\mu_{\text{D}} \propto -i\bar{\psi}\gamma^\mu\psi$. The KGP equation can be obtained from a Lagrangian not

dissimilar to the Klein-Gordon Lagrangian (Delgado-Acosta et al., 2011) and has the expression

$$\mathcal{L}_{\mathrm{KGP}}/c^2 = \left(i\hbar\widetilde{\nabla}^{\mu}\right)^{\dagger}\bar{\Psi}h_{\mu\nu}\left(i\hbar\widetilde{\nabla}^{\mu}\right)\Psi - m^2c^2\bar{\Psi}\Psi\,, \qquad h_{\mu\nu} = \eta_{\mu\nu} - i\frac{g}{2}\sigma_{\mu\nu}\,. \tag{1.47}$$

The matrix $h_{\mu\nu}$ acts an 'effective' metric which has been modified to account for the presence of an AMM. We note that the field $\Psi$ must have units $[\text{length}]^{-1}$ such that the Lagrangian density itself has natural units of $[\text{length}]^{-4}$.

In comparison to the DP AMM Lagrangian Eq. (1.31), the KGP magnetic moment Lagrangian obtained from Eq. (1.47) is

$$\mathcal{L}_{\mathrm{KGP,MM}}/c^2 = -\bar{\Psi}\left(\frac{g}{2}\mu_{\ell}m_{\ell}\sigma_{\alpha\beta}F^{\alpha\beta}\right)\Psi\,. \tag{1.48}$$

While they are mathematically similar both being 'Pauli terms', there are some important differences. Here the combination of fields $\Psi$ and $F^{\alpha\beta}$ have natural units $[\text{length}]^{-4}$ and the coupling coefficient $\mu m_{\ell} \propto g$ is manifestly dimensionless. This means the KGP Lagrangian is at first inspection renormalizable which is an improvement over the DP Lagrangian (Rafelski et al., 2023b). Literature however suggests that the KGP Lagrangian requires additional fermion self-interactions $\mathcal{L}_{\mathrm{int}} \sim \mathcal{O}(\bar{\Psi}\Psi)^2$ to be fully renormalizable (unless $g = 0, \pm 2$) which are not forbidden at tree-level (Angeles-Martinez and Napsuciale, 2012; Vaquera-Araujo et al., 2013).

The conserved current obtained from Eq. (1.47) can be expressed as

$$\mathcal{J}^{\mu} = -\frac{1}{c^2}\frac{\partial\mathcal{L}}{\partial eA_{\mu}} \equiv \mathcal{J}^{\mu}_{\mathrm{Conv}} + \mathcal{J}^{\mu}_{\mathrm{Mag}}\,, \tag{1.49}$$

$$\mathcal{J}^{\mu} = \bar{\Psi}\left(i\hbar\widetilde{\nabla}^{\mu}\right)\Psi + \left(i\hbar\widetilde{\nabla}^{\mu}\right)^{\dagger}\bar{\Psi}\Psi + i\frac{g}{2}\bar{\Psi}\sigma^{\mu\nu}\left(i\hbar\widetilde{\nabla}_{\nu}\right)\Psi + i\frac{g}{2}\left(i\hbar\widetilde{\nabla}_{\nu}\right)^{\dagger}\bar{\Psi}\sigma^{\nu\mu}\Psi\,. \tag{1.50}$$

The conserved current Eq. (1.49) can be interpreted as the sum of a convection current

$\mathcal{J}_{\text{Conv}}$ and magnetization current $\mathcal{J}_{\text{Mag}}$.

$$\mathcal{J}^{\mu}_{\text{Conv}} = \bar{\Psi}\left(i\hbar\widetilde{\nabla}^{\mu}\right)\Psi + \left(i\hbar\widetilde{\nabla}^{\mu}\right)^{\dagger}\bar{\Psi}\Psi\,, \tag{1.51}$$

$$\mathcal{J}^{\mu}_{\text{Mag}} = \frac{g}{2}\hbar\partial_{\nu}\left(\bar{\Psi}\sigma^{\nu\mu}\Psi\right)\ . \tag{1.52}$$

This is nearly identical to the Gordon Decomposition of the Dirac current $\mathcal{J}^{\mu}_{\text{D}}$, with the exception that the magnetization current is proportional to the $g$-factor of the particle.

The covariant derivative happens to simplify as $\widetilde{\nabla} \to \partial$ in Eq. (1.52) such that the current is a divergence of the spin density $\bar{\Psi}\sigma_{\mu\nu}\Psi$. Because of the antisymmetry of $\sigma_{\mu\nu}$ the spin tensor, the magnetization current is conserved independently of the the charge current. That both are independently conserved indicates conservation in both charge ($e$) and magnetic moment ($\mu$).

### 1.2.2 The special case of g = 2

There is a strong predilection in nature towards $g = 2$ which can be explained by the requirements of kinetic operator in quantum mechanics. Rather than taking the non-relativistic limit of the Dirac equation, $g=2$ can also be derived as a consequence of replacing the definition of the inner product for vectors which accounts for spinor structure via an argument attributed to R. P. Feynman; see footnote in Chap. 3.2 of Sakurai (1967).

The Schrödinger equation can be extended into the Schrödinger-Pauli Eq. (1.12) via the replacement

$$\boldsymbol{\pi}^2 \to (\boldsymbol{\sigma}\cdot\boldsymbol{\pi})^2 = \pi_i\sigma_i\sigma_j\pi_j\,. \tag{1.53}$$

We note that because the $2\times 2$ Pauli matrices $\sigma_i$ all anticommute, we can write down the relation

$$(\boldsymbol{\sigma}\cdot\boldsymbol{a})(\boldsymbol{\sigma}\cdot\boldsymbol{b}) = \boldsymbol{a}\cdot\boldsymbol{b} + i\boldsymbol{\sigma}\cdot(\boldsymbol{a}\times\boldsymbol{b})\,. \tag{1.54}$$

The non-relativistic kinetic energy (KE) Hamiltonian from Eq. (1.12) then reads as

$$H_{\mathrm{SP,KE}} = \frac{1}{2m}\left(\boldsymbol{\sigma}\cdot\boldsymbol{\pi}\right)^2 = \frac{1}{2m}\boldsymbol{\pi}^2 + i\boldsymbol{\sigma}\cdot\left(\boldsymbol{\pi}\times\boldsymbol{\pi}\right) = \frac{1}{2m}\boldsymbol{\pi}^2 - \frac{e\hbar}{2m}\boldsymbol{\sigma}\cdot\boldsymbol{B}\,. \tag{1.55}$$

As the kinetic momentum operator $\boldsymbol{\pi}$ does not self-commute, its cross product is non-zero resulting in a magnetic moment term with magneton size $\mu_\ell = e\hbar/2m_\ell$ and $g=2$. Therefore, we see there is conceptual value in replacing the inner dot product with a more intricate algebraic structure; in this case: $\delta_{ij} \to \sigma_i\sigma_j$.

The natural gyromagnetic ratio then appears to arise from the $SU(2)$ Lie algebra representation that the Pauli matrices describe and electromagnetic minimal coupling. The natural scale of the magnetic moment can be interpreted as originating from group symmetry requirements on charged particles.

An almost identical argument that $g$-factor arises from spin-structure and electromagnetic coupling can be made for the relativistic case as well. First we consider the quantum analog to the energy-momentum relation

$$\eta_{\alpha\beta}p^\alpha p^\beta\Phi = m^2c^2\Phi\,. \tag{1.56}$$

Eq. (1.56) as written evaluates to the Klein-Gordon equation on scalar field $\Phi$ where the four-momentum is written in the position basis $p^\alpha \to i\hbar\partial^\alpha$. Much like the non-relativistic example, we can introduce spin by replacing the momentum inner product with one sensitive to a Clifford algebra (Weinberg, 2005). Rather than the Pauli matrices, the relativistic replacement utilizes the gamma matrices yielding

$$\eta_{\alpha\beta} \to \gamma_\alpha\gamma_\beta\,, \qquad \gamma_\alpha\gamma_\beta p^\alpha p^\beta\Psi = m^2c^2\Psi\,. \tag{1.57}$$

Here $\Psi$ is understood to be a four-component spinor unlike in Eq. (1.56). The corresponding $4\times4$ matrix contraction identity analog to Eq. (1.54) is then

$$\gamma_\alpha\gamma_\beta a^\alpha b^\beta = \eta_{\alpha\beta}a^\alpha b^\beta - i\sigma_{\alpha\beta}a^\alpha b^\beta\,. \tag{1.58}$$

In both the relativistic and non-relativistic cases, the distinction between spin-

1/2 and spinless particles is only made apparent in the kinematics in the presence of electromagnetic fields. For minimal coupling $\pi^\alpha = p^\alpha - eA^\alpha$ we take advantage of the fact that any tensor product of vectors can be decomposed as a sum of commuting (symmetric) and anticommuting (antisymmetric) parts

$$\pi^\alpha\pi^\beta = \frac{1}{2}\left\{\pi^\alpha, \pi^\beta\right\} + \frac{1}{2}\left[\pi^\alpha, \pi^\beta\right] , \qquad \gamma^\alpha\gamma^\beta = \frac{1}{2}\left\{\gamma^\alpha, \gamma^\beta\right\} + \frac{1}{2}\left[\gamma^\alpha, \gamma^\beta\right] . \tag{1.59}$$

From the above and Eq. (1.57) and Eq. (1.28) we obtain

$$\gamma_\alpha\gamma_\beta\pi^\alpha\pi^\beta\Psi = \left(\eta_{\alpha\beta}\pi^\alpha\pi^\beta - \frac{e\hbar}{2}\sigma_{\alpha\beta}F^{\alpha\beta}\right)\Psi = m^2c^2\Psi\,. \tag{1.60}$$

Eq. (1.60) is the square of the Dirac equation with precisely $g = 2$ but in a different sense than the argument established in Eq. (1.43). Rather than squaring the Dirac equation, from this perspective, we are enlarging the structure of the energy-momentum relation. The spin-1 Proca equations and spin-3/2 Rarita-Schwinger equations can also be justified via this line of reasoning with different replacements for the field and inner-product definition.

How $g \neq 2$ AMM 'breaks' the inner product substitution is seen more explicitly when we write the effective metric tensor $h_{\mu\nu}$ from Eq. (1.47) as

$$h_{\mu\nu} = \frac{1}{2}\{\gamma_\mu, \gamma_\nu\} + \frac{1}{2}(1+a)[\gamma_\mu, \gamma_\nu] = \gamma_\mu\gamma_\nu + \frac{a}{2}[\gamma_\mu, \gamma_\nu]\,. \tag{1.61}$$

The anomalous part in Eq. (1.61) is inconveniently unable to be packaged as the elementary tensor product of two four-vectors like in Eq. (1.57). The same issue occurs with any anomalous EDM introduction as well. We suggest that more elaborate algebraic structures might accommodate such terms more naturally though we leave that to future work.

Furthermore, compelling arguments can be made that all elementary particles of any spin must have a natural gyromagnetic factor of $g=2$, though a competing idea is Belinfante's conjecture of $g=1/s$. To paraphrase the arguments by Ferrara, Porrati, and Telegdi (1992), $g=2$ is likely the natural scale for particles of any spin because:

1. The W boson, as the only known higher spin charged elementary particle, has at tree level $g=2$ via a Proca-like equation.
2. The relativistic TBMT torque equation is the same for any classical spin value and is most simple when the anomalous moment is zero.
3. For arbitrary spin, $g=2$ facilitates finite Compton scattering cross sections without additional physical requirements.
4. For charged interacting particles with arbitrary spin, open bosonic and supersymmetric string theory predicts $g=2$.

We would like to add the additional argument that rotating charged black holes described by the Kerr-Newman metric also have a magnetic dipole moment with fixed $g=2$ character (Carter, 1968). This illustrates that in some sense the spin of a black hole is 'particle-like' and dissimilar to the orbital Ampèrian motion of matter which has an orbital $g$-factor of $g_{\mathrm{L}}=1$; see Section 2.1.

While the above provide a nice justification for why particles should tend to this specific $g$-factor, the reality is no particle has exactly $g=2$ with all of them displaying some form of anomaly. The charged leptons come the closest to the natural value, but famously have vacuum polarization contributions (Schwinger, 1951) from QED, non-perturbative hadronic contributions (Jegerlehner, 2017), and potentially BSM interactions (Knecht, 2004) contributing to their anomalous magnetic dipole moment.

While the perturbative approach has proven to be exceedingly successful for the charged leptons, it is not appropriate for particles whose moments are dramatically different from $g=2$ or if the origin of the anomaly comes from internal structure such as the hadrons whose moments are determined by non-perturbative QCD (Pacetti et al., 2015) and not weakly coupled $\alpha \sim 1/137 \ll 1$ electromagnetic vacuum structure.

## 1.3 A few words on cosmology

This section introduces some necessary concepts which will be useful in describing the magnetization of the electron-positron primordial plasma in Chapter 4. We operate under the $\Lambda$ Cold Dark Matter ($\Lambda$CDM) model of cosmology where the contemporary

universe is approximately 69% dark energy, 26% dark matter, 5% baryons, and $< 1\%$ photons and neutrinos in energy density (Davis and Lineweaver, 2004; Aghanim et al., 2020). The standard picture of the universe's evolution is outlined in Figure 1.1.

The Friedmann-Lemaître-Robertson-Walker (FLRW) line element and metric (Weinberg, 1972) in spherical coordinates is

$$ds^2 = dt^2 - a^2(t)\left[\frac{dr^2}{1-kr^2} + r^2 d\theta^2 + r^2 \sin\theta^2 d\phi^2\right], \tag{1.62}$$

$$g_{\alpha\beta} = \begin{pmatrix} 1 & 0 & 0 & 0 \\ 0 & -\frac{a^2(t)}{1-kr^2} & 0 & 0 \\ 0 & 0 & -a^2(t)r^2 & 0 \\ 0 & 0 & 0 & -a^2(t)r^2\sin\theta^2 \end{pmatrix}. \tag{1.63}$$

The Gaussian curvature $k$ informs the spatial shape of the universe with the following possibilities: infinite flat Euclidean ($k = 0$), finite spherical but unbounded ($k = +1$), or infinite hyperbolic saddle-shaped ($k = -1$). Observation indicates our universe is flat or nearly so.

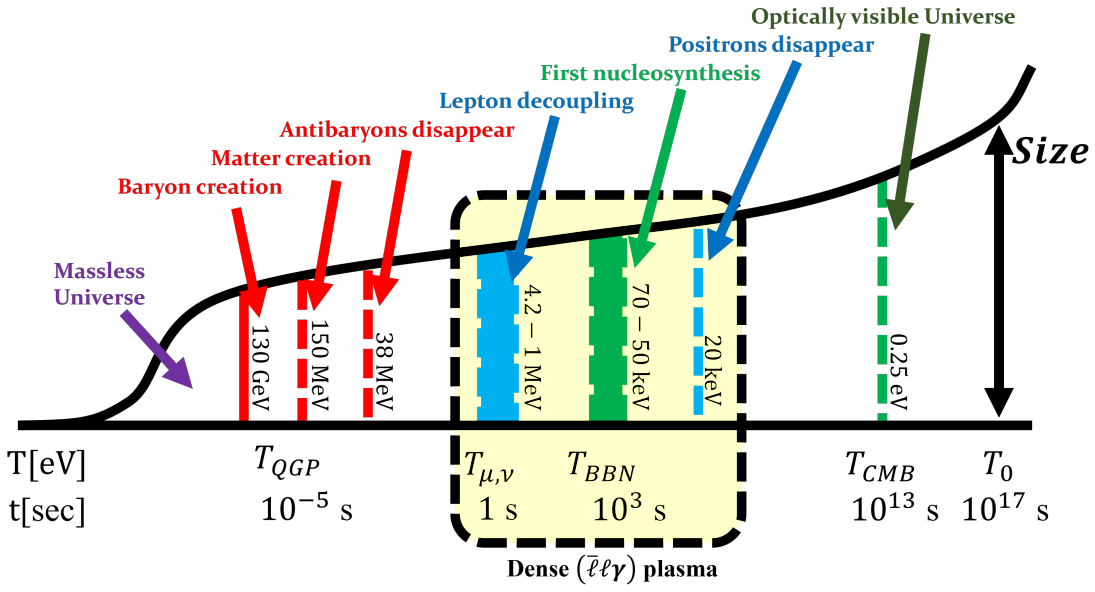


Figure 1.1: A schematic of the universe's evolution since the Big Bang. The region of interest studied in this dissertation is emphasized (in the highlighted box) to contain a dense nearly charge neutral matter-antimatter plasma.

The scale factor $a(t)$ denotes the change of proper distances $L(t)$ over time as

$$L(t) = L_0 \frac{a_0}{a(t)} \rightarrow L(z) = L_0(1+z)\,, \tag{1.64}$$

where $z$ is the redshift and $L_0$ the comoving length. In an expanding (or contracting) universe which is both homogeneous and isotropic, this implies volumes change with $V(t) = V_0/a^3(t)$ where $V_0 = L_0^3$ is the comoving Cartesian volume. The evolutionary expansion of the universe is then traditionally defined in terms of the Hubble parameter $H(t)$ as follows

$$H(t)^2 \equiv \left(\frac{\dot{a}}{a}\right)^2 = \frac{8\pi G_N}{3}\rho_{\text{total}}, \qquad \rho_{\text{total}}(t) = \rho_\Lambda + \rho_{\text{DM}}(t) + \rho_{\text{Baryons}}(t) + \dots \tag{1.65}$$

$$\frac{\ddot{a}}{a} = -qH^2, \qquad q \equiv -\frac{a\ddot{a}}{\dot{a}^2}, \qquad \dot{H} = -H^2(1+q). \tag{1.66}$$

where $G_N$ is the Newtonian constant of gravitation. Eq. (1.65) and Eq. (1.66) are also known as the Friedmann equations. The total density $\rho_{\text{total}}$ is the sum of all contributions from any form of matter, radiation or field. This includes but is not limited to: dark energy ($\Lambda$), dark matter (DM), baryons (B), leptons ($\ell, \nu$) and photons ($\gamma$). Depending on the age of the universe, the relative importance of each group changes as each dilutes different under expansion with dark energy infamously remaining constant in density and accelerating the universe today.

The parameter $q$ is the cosmic deceleration parameter where for historical reasons expansion is slowing down for $q > 0$. before the discovery of dark energy. The early universe was radiation dominated with $q = 1$, subsequently matter dominated with $q = 1/2$, and the contemporary universe is undergoing a transition from matter to dark energy dominated whereas the deceleration settles on the asymptotic value of $q = -1$; see Rafelski and Birrell (2014).

We can consider the expansion to be an adiabatic process (Abdalla et al., 2022) which results in a smooth shifting of the relevant dynamical quantities. As the uni-

verse undergoes isotropic expansion, the temperature decreases as

$$T(t) = T_0 \frac{a_0}{a(t)} \rightarrow T(z) = T_0(1+z)\,, \tag{1.67}$$

where $z$ is the redshift. The entropy within a comoving volume is kept constant until gravitational collapse effects become relevant. The comoving temperature $T_0$ is given by the the present CMB temperature $T_0 = 2.7$ K $\simeq 2.3 \times 10^{-4}$ eV (Aghanim et al., 2020), with contemporary scale factor $a_0 = 1$.

As the universe expands, redshift reduces the momenta of particles lowering their contribution to the energy content of the universe. This cosmological redshift is written as

$$p_i(t) = p_{i,0} \frac{a_0}{a(t)}\,. \tag{1.68}$$

Momentum (and the energy of massless particles $E = pc$) scales with the same factor as temperature. The energy of massive free particles in the universe however scales differently based on their momentum (and thus temperature).

When hot and relativistic, particle energy scales inversely like radiation. As the particles transition to non-relativistic (NR) momenta, their energies scale with the inverse square of the scale factor

$$E(t) = E_0 \frac{a_0}{a(t)} \xrightarrow{\text{NR}} E_0 \frac{a_0^2}{a(t)^2}\,. \tag{1.69}$$

This occurs because of the functional dependence of energy on momentum in the relativistic $E \sim p$ versus non-relativistic $E \sim p^2$ cases.

# CHAPTER 2

## Dynamics of charged particles with arbitrary magnetic moment

In Section 1.1, we addressed two different models of introducing anomalous magnetic moment in QM:

(a) the Dirac-Pauli (DP) first order equation which is the Dirac equation where $g$-factor is precisely fixed to the $g=2$, with the addition of an incremental Pauli term; and

(b) the Klein-Gordon-Pauli (KGP) second order equation which "squares" the Dirac equation and thereafter allows the magnetic moment $\boldsymbol{\mu}$ to vary independently of charge and mass, unlike Dirac theory.

These two approaches coincide when the anomaly $a$ vanishes. However, all particles that have magnetic moments differ from the Dirac value $g=2$, either due to their composite nature, or, for point particles, due to the quantum vacuum fluctuation effect.

We find that even a small magnetic anomaly has a large effect in the limit of strong fields generated by massive magnetar stars (Kaspi and Beloborodov, 2017). Therefore it is not clear that the tacit assumption of $g=2$ in the case of strong fields (Rafelski et al., 1978; Greiner et al., 2012a; Rafelski et al., 2017) is prudent (Evans and Rafelski, 2018). This argument is especially applicable to tightly bound composite particles such as protons and neutrons where the large anomalous magnetic moment can be taken as an external prescribed parameter unrelated to the elementary quantum vacuum fluctuations. It is then of particular interest to study the dynamical behavior of these particles in fields of magnetar strength. This interest carries over to the environment of strong fields created in focus of ultra-intense laser pulses and the associated particle production processes (Dunne, 2014; Hegelich et al., 2014). We

consider also precision spectroscopic experiments and recognize consequences even in the weak coupling limit.

This chapter reviews our work done in exploring relativistic dynamics with arbitrary magnetic dipoles in both a quantum mechanical and classical context. Section 2.1 and Section 2.2 is primarily based on Steinmetz et al. (2019) and covers analytic solutions for the Klein-Gordon-Pauli (KGP) equation in the presence of homogeneous magnetic fields and the Coulomb problem for hydrogen-like atoms. Comparisons with the Dirac-Pauli (DP) and Dirac solutions are made and novel consequences for strong fields are discussed in Section 2.3.

Section 2.4 covers special topics related to KGP including a proposal which couples mass and magnetic moment (Section 2.4.1) and an extension to particles (such as quarks) which are charged under both Albelian and non-Albelian fields (Section 2.4.2). The second special topic is yet unpublished outside this dissertation.

Relativistic classical spin dynamics is discussed in Section 2.5 and is based on our work in Rafelski et al. (2018). We propose in Section 2.5.1 a covariant form of magnetic dipole potential which modifies the Lorentz force, extends the Thomas-Bargmann-Michel-Telegdi (TMBT) equation, and reproduces the Stern-Gerlach force in the non-relativistic limit.

## 2.1 Homogeneous magnetic fields

The case of the homogeneous magnetic field, sometimes referred to as the Landau problem, provides a stepping stone in which to examine the consequences of quantum spin dynamics in a concrete analytical fashion. We present here an abbreviated analysis and the full treatment of this solution in terms of Ladder operators can be found in Steinmetz et al. (2019) while alternative approaches are shown in texts such as Itzykson and Zuber (1980). We take a constant magnetic field in the $z$-direction to be

$$\boldsymbol{B} = (0, 0, B)\,. \tag{2.1}$$

For our choice of gauge, there are two common options: (a) the Landau $\boldsymbol{A}_{\mathrm{L}}$ gauge and (b) the symmetric $\boldsymbol{A}_{\mathrm{S}}$ gauge

$$\boldsymbol{A}_{\mathrm{L}} = B(0, x, 0)\,, \qquad \boldsymbol{A}_{\mathrm{S}} = \frac{B}{2}(-y, x, 0)\,. \tag{2.2}$$

As the system has a manifest rotational symmetry perpendicular to the direction of the homogeneous field, we will choose the symmetric gauge $\boldsymbol{A}_{\mathrm{S}}$ which preserves this symmetry explicitly.

Before we examine relativistic wave equations, it will be helpful to first consider the non-relativistic Schrödinger-Pauli case as the KGP-Landau problem can be written as equivalent to the Schroödinger-Pauli Hamiltonian. We consider energy eigenstates of and electron with $m_e$ described by Eq. (1.12) under Eq. (2.1) as

$$\chi \to \chi_{\mathrm{E}} \exp\left(-\frac{iEt}{\hbar}\right)\,, \qquad \left(\frac{1}{2m_e}\boldsymbol{\pi}^2 - \boldsymbol{\mu}\cdot\boldsymbol{B}\right)\chi_{\mathrm{E}} = E\chi_{\mathrm{E}}\,, \tag{2.3}$$

where $\mu$ is the magnitude of the magnetic moment as defined in Eq. (1.11). Eq. (2.3) can be further rewritten using angular momentum $\boldsymbol{L}$ and the symmetric gauge Eq. (2.2) as

$$\left(\frac{1}{2m_e}\boldsymbol{p}^2 + \frac{e^2B^2}{8m_e}(x^2+y^2) - \frac{eB}{2m_e}L_3 - \mu B\sigma_3\right)\chi_{\mathrm{E}} = E\chi_{\mathrm{E}}\,, \tag{2.4}$$

$$\boldsymbol{L} = \boldsymbol{r}\times\boldsymbol{p}\,, \qquad L_i = \varepsilon_{ijk}x_j p_k\,. \tag{2.5}$$

The above can be broken into a set of three mutually commuting Hamiltonian operators:

a. Free particle Hamiltonian (Free)
b. Quantum harmonic oscillator (HO)
c. Zeeman interaction (ZI)

given by

$$H_{\text{total}} = H_{\text{Free}} + H_{\text{HO}} + H_{\text{Mag.}}\,, \tag{2.6}$$

$$H_{\text{Free}} = \frac{p_3^2}{2m}\,, \tag{2.7}$$

$$H_{\text{HO}} = \frac{1}{2m_e}\left(p_1^2 + p_2^2\right) + \frac{1}{2}m_e\omega^2(x^2+y^2)\,, \tag{2.8}$$

$$H_{\text{ZI}} = -\mu_B B\frac{L_3}{\hbar} - \mu B\sigma_3\,. \tag{2.9}$$

The cyclotron frequency appears in Eq. (2.8) as $2\omega = \omega_{\text{C}} = eB/m_e$. We note that the Zeeman Eq. (2.9) is usually expressed as

$$H_{\text{ZI}} = -\frac{e}{2m}\left(g_{\text{L}}\boldsymbol{L} + g\boldsymbol{S}\right)\cdot\boldsymbol{B}\,, \qquad g_{\text{L}} = 1\,, \tag{2.10}$$

with $\boldsymbol{S}$ defined in Eq. (1.2). We see explicitly that the orbital gyromagnetic ratio $g_{\text{L}}$ which is a coefficient to the angular momentum operator $\boldsymbol{L}$ is unity unlike for spin. We refer back to our comment about black hole rotation in Section 1.2.2 as spin-like rather than orbital-like in terms of its magnetic behavior. As all the above Hamiltonian operators are mutually commuting, the energy eigenvalue of the total Hamiltonian is the sum of the individual energy eigenvalues. Our remaining goal will be to convert the KGP eigenvalue equation into the above three non-relativistic Hamiltonian operators.

We now return to the KGP equation and write expand Eq. (1.40) for the Landau problem with energy eigenstates $\Psi_{\text{E}}$ yielding

$$\left(\frac{E^2}{c^2} - m_e^2c^2 - \boldsymbol{p}^2 - \frac{1}{4}e^2B^2\left(x^2+y^2\right) + eBL_3 + 2\mu m_eB\sigma_3\right)\Psi_{\text{E}} = 0\,. \tag{2.11}$$

We introduce the substitutions

$$E \to m'c^2\,, \quad \frac{E^2 - m_e^2c^4}{2E} \to E'\,, \tag{2.12}$$

and recast KGP Eq. (2.11) into a Schrödinger-style Hamiltonian equation

$$\left(\frac{1}{2m'}\boldsymbol{p}^2+\frac{e^2B^2}{8m'}(x^2+y^2)-\frac{eB}{2m'}L_3-\mu\left(\frac{m_e}{m'}\right)B\sigma_3\right)\Psi_{\rm E}=E'\Psi_{\rm E}\,, \tag{2.13}$$

which matches the non-relativistic Hamiltonian presented in Eq. (2.6).

The energy eigenvalues of Eq. (2.6) are given by

$$E'_{n,s}(p_3,B)=\frac{p_3^2}{2m'}+\frac{e\hbar B}{m'}\left(n+\frac{1}{2}\right)-\mu B\left(\frac{m_e}{m'}\right)s\,, \tag{2.14}$$

where $n\in 1,2,3\ldots$ is the Landau orbital quantum number and $s\in\pm1$ is the spin quantum number. The physical relativistic energies can be obtained by undoing the substitutions in Eq. (2.12) yielding from Eq. (2.14)

$$E^2_{n,s}(p_3,B)=m_e^2c^4+p_3^2c^2+2e\hbar c^2B\left(n+\frac{1}{2}\right)-2\mu Bm_ec^2s\,, \tag{2.15}$$

$$E_{n,s}=\pm\sqrt{m_e^2c^4+p_3^2c^2+2e\hbar c^2B\left(n+\frac{1}{2}\right)-2\mu Bm_ec^2s}\,. \tag{2.16}$$

This expression for the relativistic Landau levels is the same as found by Weisskopf (1936) for the Dirac equation setting $g=2$ in Eq. (2.16). The Landau orbital part and spin portions can be combined when the magnetic moment is expressed in terms of $e/m$, but the form in Eq. (2.16) keeps it generalized for the case of neutral particles.

The 'Landau' problem for neutral particles (for example the neutron with mass $m_{\rm N}$) simplifies to

$$E_{n,s}|_{e=0}\rightarrow E_s(\boldsymbol{p},B)=\sqrt{m_{\rm N}^2c^4+\boldsymbol{p}^2c^2-2\mu Bm_{\rm N}c^2s}\,, \tag{2.17}$$

which is just the free particle motion with a magnetic dipole energy. We note the correspondence between the quantized Landau orbitals and continuous transverse momentum $\boldsymbol{p}^2=p_3^2+p_{\rm T}^2$. We can define an 'effective' polarization mass given by

$$\boxed{\tilde{m}_s^2(B)=m^2c^4-2\mu Bmc^2s}\,. \tag{2.18}$$

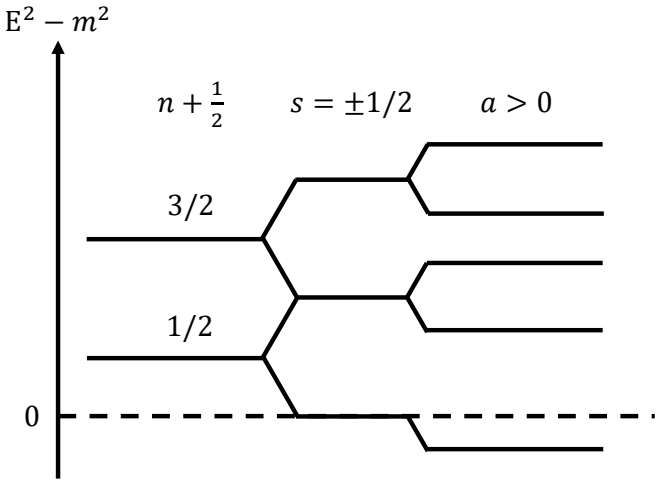


Figure 2.1: Diagram organizing the KGP-Landau levels for particles with zero z-component momentum. The Landau levels $n$ and spin $s$ serve to split levels while the anomaly $a$ controls the degeneracy among levels.

This effective polarization mass (which also is easily defined for charged particles) will find use when we consider cosmic thermodynamics and plasmas in Chapter 4.

Restricting ourselves to the positive energy spectrum, the non-relativistic reduction of Eq. (2.16) can be carried out in powers of $1/m$ in the large mass limit yielding

$$E_{n,s}|_{\rm NR} = m_e c^2 + \frac{p_3^2}{2m_e} + \mu_B B\left(2n+1-\frac{g}{2}s\right) - \frac{p_3^4}{8m_e^3c^2} \tag{2.19}$$
$$-\frac{p_3^2}{2m_e}\frac{\mu_B B}{m_e c^2}\left(2n+1-\frac{g}{2}s\right) - \frac{\mu_B^2 B^2}{2m_e c^2}\left(2n+1-\frac{g}{2}s\right)^2 + \mathcal{O}(1/m_e^5)\ ,$$

which contains the expected terms such as the non-relativistic kinetic energy in the z-direction, the first relativistic correction to kinetic energy, the Landau energies, and cross terms that behave like modifications to the mass of the particle.

The KGP-Landau levels above the ground state lose their (accidental) degeneracy for $g \neq 2$. This is shown schematically in Figure 2.1. The anomaly also causes the ground state to be pushed downward, such that $E^2 < m^2$; if the anomaly and the magnetic field are large enough, states above the ground state are also pushed below the rest mass energy of the particle.

However, we recognize a periodicity considering the energy as a function of $g$.

We recall that in Eq. (2.16) $n = 0, 1, 2 \ldots$. As $g$ varies, each time $gs/2$ crosses an integer value, for a different value of $n$ the energy eigenvalue $E$ repeat as a function of changing $g$. All possible values of energy $E$ are reached (at fixed $m$ and $p_3^2$) for $-2 \leq g \leq 2$. Moreover, while for almost all $g \neq 2$ the degeneracy is completely broken, this periodicity implies that energy degeneracy is restored for values Evans (2022); Evans and Rafelski (2022)

$$g_k/2 = 1 + k\,, \qquad \lambda'_{\rm L} = \lambda_{\rm L} - ks\,, \qquad \lambda_{\rm L} = n + \frac{1}{2} - s\,, \tag{2.20}$$

where $k = 0, \pm 1, \pm 2, \ldots$ The Landau levels Eq. (2.15) contain an infinite number of degenerate levels bounded from below. Certain states change the sign of the magnetic energy and their total energies become unphysical in the limit that $g_k B$ becomes large; for even $k$ there are $k/2$ such states and for odd $k$ there are $(k+1)/2$.

It is useful to compare the KGP solution to the the Landau levels for the DP equation which we obtained by Tsai and Yildiz (1971). The DP-Landua energy eigenstates are given by

$$E^2_{n,s}(p_3, B)|_{\rm DP} = \left(\sqrt{m_e^2c^4 + 2e\hbar c^2 B\left(n + \frac{1}{2} - s\right)} - \frac{eB\hbar}{2m_e}(g-2)s\right)^2 + p_3^2c^2, \tag{2.21a}$$

$$E_{n,s}|_{\rm DP} = \pm\sqrt{\left(\sqrt{m_e^2c^4 + 2e\hbar c^2 B\left(n + \frac{1}{2} - s\right)} - \frac{eB\hbar}{2m_e}(g-2)s\right)^2 + p_3^2c^2}\,, \tag{2.21b}$$

which in our opinion fails Dirac's principle of mathematical beauty when compared to the KGP result Eq. (2.16). Both Eqs. (2.16) and (2.21b) have the correct non-relativistic reduction at the lowest order though, the latter obscures the physical interpretation.

The most egregious issue with the DP-Landau levels is that, in a perturbative expansion, it includes cross terms between the $g=2$ magnetic moment and anomalous terms in $a = (g-2)/2$; thus the result does not depend on the particle magnetic moment alone; there is a functional dependence on the magnetic anomaly $a$. The

presence of these cross terms implies that above first order the results cannot be given in terms of the full magnetic moment alone. In comparison, for the KGP-Landau levels Eq. (2.21b), the entire effect of magnetic moment is contained in a single term.

## 2.2 Hydrogen-like atoms

The Coulomb problem, or sometimes referred to as the Kepler problem, provides us an important application of any quantum theory to explore. As the hydrogen-like atoms are the the most well understood atomic system in physics, any non-minimal behavior especially for high-$Z$ systems can lead to consequences for the resulting spectral lines. We take the Coulomb potential to be

$$eV_{\mathrm{C}} \equiv eA^0 = \frac{Z\alpha\hbar c}{r} , \qquad \boldsymbol{A} = 0 . \tag{2.22}$$

The KGP-Coulomb problem with arbitrary magnetic moment can be solved analytically and we will briefly sketch out the solution and its consequences.

For energy states $\Psi = e^{-iEt/\hbar}\Psi_{\mathrm{E}}$ the KGP equation yields the following differential equation

$$\left(\frac{E^2 - m^2c^4}{\hbar^2c^2} + \frac{Z^2\alpha^2}{r^2} + \frac{2E}{\hbar c}\frac{Z\alpha}{r} + \frac{1}{r}\frac{\partial \boldsymbol{L}^2}{\partial r^2}r - \frac{\boldsymbol{L}^2/\hbar^2}{r^2} - \frac{g}{2}Z\alpha\frac{i\boldsymbol{\alpha}\cdot\hat{\boldsymbol{r}}}{r^2}\right)\Psi_{\mathrm{E}} = 0 . \tag{2.23}$$

We recast the squared angular momentum operator $\boldsymbol{L}^2$ with the Dirac spin-alignment operator

$$\mathcal{K} = \gamma^0\left(1 + \boldsymbol{\Sigma}\cdot\frac{\boldsymbol{L}}{\hbar}\right) , \qquad \boldsymbol{L}^2/\hbar^2 = \mathcal{K}\left(\mathcal{K} - \gamma^0\right) . \tag{2.24}$$

The operator $\mathcal{K}$ commutes with $\boldsymbol{\alpha}\cdot\hat{\boldsymbol{r}}$ and its eigenvalues are given as either positive or negative integers $\kappa = \pm(j + 1/2)$ where $j$ is the total angular momentum quantum number. By grouping all terms proportional to $1/r^2$, we see the effective angular momentum eigenvalues take on non-integer values which in the limit of classical mechanics corresponds to orbits which do not close. The non-integer eigenvalues

depends explicitly on $g$-factor.

The difficulty of this equation is that the effective angular momentum operator is non-diagonal in spinor space due to the presence of $\boldsymbol{\alpha}\cdot\hat{\boldsymbol{r}}$ which mixes upper and lower components. The effective radial potential within Eq. (2.23) is then

$$\boxed{V_{\text{eff}} = -\frac{2E}{\hbar c}\frac{Z\alpha}{r} - \frac{Z^2\alpha^2}{r^2} + \frac{g}{2}Z\alpha\frac{i\boldsymbol{\alpha}\cdot\hat{\boldsymbol{r}}}{r^2}}\,. \tag{2.25}$$

We emphasize that the distinguishing characteristic which separates the KGP solutions (and Dirac for $g=2$) from the Klein-Gordon solutions is the last term in the effective potential Eq. (2.25). This is the dipole-charge interaction term which exists only because of the relativistic expression for the magnetic dipole and is entirely absent non-relativistically.

Following the procedure of Martin and Glauber (1958), we introduce the operator

$$\mathfrak{L} = -\gamma^0\mathcal{K} - \frac{g}{2}Z\alpha(i\boldsymbol{\alpha}\cdot\hat{\boldsymbol{r}})\,, \tag{2.26}$$

but with the novel modification that $g$-factor directly appears in the second term. This operator is also sometimes referred to as the Temple operator, therefore we will refer to it as the $g$-Temple operator. This operator then commutes with the spin-alignment operator $\mathcal{K}$ and has eigenvalues

$$\Lambda = \pm\sqrt{\kappa^2 - \frac{g^2}{4}Z^2\alpha^2}\,, \tag{2.27}$$

where the absolute values are denoted as $\lambda = |\Lambda|$. The angular momentum contributions to Eq. (2.23) can then be replaced by

$$\mathcal{K}(\mathcal{K}-\gamma^0) - Z^2\alpha^2 - \frac{g}{2}Z\alpha(i\boldsymbol{\alpha}\cdot\hat{\boldsymbol{r}}) = \mathfrak{L}(\mathfrak{L}+1) + \left(\frac{g^2}{4}-1\right)Z^2\alpha^2. \tag{2.28}$$

If the $g$-factor is taken to be $g=2$, then the differential Eq. (2.23) reverts to the one discussed in Martin and Glauber (1958). The coefficient $g^2/4-1$ will be commonly seen to precede new more complicated terms, which conveniently vanish for $|g|=2$

demonstrating that as function of $g$ there is a "cusp" (Rafelski et al., 2023b) for $|g| = 2$. This will become especially evident when we discuss strongly bound systems which behave very differently for $|g| < 2$ versus $|g| > 2$.

We omit further derivation which can be found in Steinmetz et al. (2019). We find the resulting energy levels of the KGP-Coulomb equation to be

$$E_{\pm\lambda}^{n_r,j} = mc^2 \left[1 + \frac{Z^2\alpha^2}{(n_r + 1/2 + \nu)^2}\right]^{-1/2}, \tag{2.29}$$

$$\nu = \sqrt{(\lambda \pm 1/2)^2 + \left(\frac{g^2}{4} - 1\right) Z^2\alpha^2}\,, \qquad \lambda = \sqrt{(j+1/2)^2 - \frac{g^2}{4} Z^2\alpha^2}\,. \tag{2.30}$$

where $n_r$ is the node quantum number which takes on the values $n_r = 0, 1, 2, \ldots$. Eq. (2.29) is the same "Sommerfeld-style" expression for energy that we can obtain from the Dirac or KG equations. The difference between them arises from the expression of the relativistic angular momentum which depends on $g$-factor for the KGP equation. The KGP eigenvalues Eq. (2.29) for arbitrary spin were obtained by Niederle and Nikitin (2006) using a tensor approach.

In the limit that $g \to 2$ for the Dirac case the expressions for $\lambda$ and $\nu$ reduce to

$$\lim_{g\to 2} \lambda = \sqrt{(j+1/2)^2 - Z^2\alpha^2}, \tag{2.31a}$$

$$\lim_{g\to 2} \nu_{\pm\lambda} = \lambda \pm 1/2\,. \tag{2.31b}$$

This procedure requires taking the root of perfect squares; therefore, the sign information is lost in Eq. (2.31a). As long as $Z^2\alpha^2 < 3/4$ we can drop the absolute value notation as $\nu$ is always positive. The energy is then given by

$$E_{\pm\lambda}^{n_r,j} = mc^2 \left[1 + \frac{Z^2\alpha^2}{\left(n_r \,{}^{+1}_{+0} + \sqrt{(j+1/2)^2 - Z^2\alpha^2}\right)^2}\right]^{-1/2}. \tag{2.32}$$

The ${}^{+1}_{+0}$ notation is read as the upper value corresponding to the $+\lambda$ states and the lower value corresponding to the $-\lambda$ states.

The ground state energy (with: $n_r = 0,\ \Lambda < 0,\ j = 1/2$) is therefore

$$E^{0,1/2}_{-\lambda(j=1/2)} = mc^2\sqrt{1 - Z^2\alpha^2}\ , \tag{2.33}$$

as expected for the Dirac-Coulomb ground state. Eq. (2.32) reproduces the Dirac-Coulomb energies and also contains a degeneracy between states of opposite $\lambda$ sign, same $j$ quantum number and node quantum numbers offset by one

$$E^{n_r+1,j}_{-\lambda} = E^{n_r,j}_{+\lambda}\ , \tag{2.34}$$

which corresponds to the degeneracy between $2S_{1/2}$ and $2P_{1/2}$ states. There is no degeneracy for the $E^{0,j}_{-\lambda}$ states.

In the limit that $g \to 0$, which is the KG case, the expressions are given by

$$\lim_{g\to 0} \lambda = j + 1/2, \tag{2.35a}$$

$$\lim_{g\to 0} \nu_{\pm\lambda} = \sqrt{\left(j \,{}^{+1}_{+0}\right)^2 - Z^2\alpha^2}\ , \tag{2.35b}$$

which reproduces the correct expressions for the energy levels for the Klein-Gordon case

$$E^{n_r,j}_{\pm\lambda} = mc^2\left[1 + \frac{Z^2\alpha^2}{\left(n_r + 1/2 + \sqrt{\left(j \,{}^{+1}_{+0}\right)^2 - Z^2\alpha^2}\right)^2}\right]^{-1/2}\ , \tag{2.36}$$

except that in this limit we are still considering the total angular moment quantum number $j$ rather than orbital momentum quantum number $\ell$. It is interesting to note that the KG-Coulomb problem's energy formula contains $\ell + 1/2$, which matches identically to our half-integer $j$ values; therefore, this artifact of spin, untethered and invisible by the lack of magnetic moment, does not alter the energies of the states.

The degeneracy in energy levels are given by

$$E_{-\lambda}^{n_r,j+1} = E_{+\lambda}^{n_r,j} \ , \tag{2.37}$$

with levels of opposite $\lambda$ sign, same node quantum number and shifted $j$ values by one. In a similar fashion to the Dirac case, here we have no degeneracy for $E_{-\lambda}^{n_r,1/2}$ states.

### 2.2.1 Non-relativistic Coulomb problem energies

The first regime of interest to understand the effect of variable $g$ in the KGP-Coulomb problem is the non-relativistic limit characterized by the weak binding of low-Z atoms. We now will convert from $n_r$, $j$ and $\pm\lambda$ to the familiar quantum numbers of $n$, $j$ and $\ell$ allowing for easy comparison with the hydrogen spectrum in standard notation. We start by expanding Eq. (2.29) in powers of $Z\alpha$ to compare to the known hydrogen spectrum.

To order $\mathcal{O}(Z^4\alpha^4)$ the energy levels are given by

$$\begin{aligned}\frac{E_{\pm\lambda}^{n_r,j}}{mc^2} = 1 &- \frac{1}{2}\frac{Z^2\alpha^2}{(n_r+1/2+(\nu_{\pm\lambda})|_{Z=0})^2} + \frac{(\nu_{\pm\lambda})|'_{Z=0}Z^3\alpha^3}{(n_r+1/2+(\nu_{\pm\lambda})|_{Z=0})^3} \\ &+ \frac{1}{2}\frac{(3/4-3(\nu_{\pm\lambda})|'^2_{Z=0})Z^4\alpha^4}{(n_r+1/2+(\nu_{\pm\lambda})|_{Z=0})^4} + \frac{1}{2}\frac{(\nu_{\pm\lambda})|''_{Z=0}Z^4\alpha^4}{(n_r+1/2+(\nu_{\pm\lambda})|_{Z=0})^3} + \mathcal{O}(Z^6\alpha^6) \ ,\end{aligned} \tag{2.38}$$

where primed $\nu_{\pm\lambda}$ indicate derivatives with respect to $Z\alpha$. These derivatives evaluate to

$$\begin{aligned}(\nu_{\pm\lambda})|_{Z=0} &= j+1/2\pm 1/2, \\ (\nu_{\pm\lambda})|'_{Z=0} &= 0, \\ (\nu_{\pm\lambda})|''_{Z=0} &= \frac{(g^2/4-1)}{j+1/2\pm 1/2} - \frac{g^2/4}{j+1/2} \ .\end{aligned} \tag{2.39}$$

Eq. (2.38) then simplifies to

$$\frac{E^{n_r,j}_{\pm\lambda}}{mc^2} = 1 - \frac{1}{2}\frac{Z^2\alpha^2}{\left(n_r + j\,{}^{+3/2}_{+1/2}\right)^2} + \frac{3}{8}\frac{Z^4\alpha^4}{\left(n_r + j\,{}^{+3/2}_{+1/2}\right)^4} + \frac{1}{2}\left(\frac{(g^2/4-1)}{j\,{}^{+1}_{+0}} - \frac{g^2/4}{j+1/2}\right)\frac{Z^4\alpha^4}{\left(n_r + j\,{}^{+3/2}_{+1/2}\right)^3} + \mathcal{O}(Z^6\alpha^6)\,. \tag{2.40}$$

In the non relativistic limit, the node quantum number corresponds to the principle quantum number via $n_r = n' - j - 1/2$ with $n' = 1, 2, 3\ldots$ Using Eq. (2.40) and Eq. (2.26) we see that in the non relativistic limit $+\lambda$ corresponds to $\kappa > 0$ or anti-aligned spin-angular momentum with $j = \ell - 1/2$ and $\ell \geq 1$. Conversely $-\lambda$ corresponds to $\kappa < 0$ or aligned spin-angular momentum with $j = \ell + 1/2$.

With all this input we arrive at

$$\frac{E^{n,j}_{\substack{\kappa>0\\ \kappa<0}}}{mc^2} = 1 - \frac{1}{2}\frac{Z^2\alpha^2}{\left(n'\,{}^{+1}_{+0}\right)^2} + \frac{3}{8}\frac{Z^4\alpha^4}{\left(n'\,{}^{+1}_{+0}\right)^4} + \frac{1}{2}\frac{(g^2/4-1)}{j\,{}^{+1}_{+0}}\frac{Z^4\alpha^4}{\left(n'\,{}^{+1}_{+0}\right)^3} - \frac{1}{2}\frac{g^2/4}{j+1/2}\frac{Z^4\alpha^4}{\left(n'\,{}^{+1}_{+0}\right)^3} + \mathcal{O}(Z^6\alpha^6)\,. \tag{2.41}$$

Lastly we recast, for the $\kappa > 0$ states, the principle quantum number as $n' + 1 \to n$ with $n \geq 2$ and we simply relabel $n' \to n$ for $\kappa < 0$ states. This allows Eq. (2.41) to be completely written in terms of $n$, $j$, and $\ell$ as

$$\frac{E^{n,j}_{\ell}}{mc^2} = 1 - \frac{1}{2}\frac{Z^2\alpha^2}{n^2} + \frac{3}{8}\frac{Z^4\alpha^4}{n^4} + \frac{1}{2}\frac{(g^2/4-1)}{\ell+1/2}\frac{Z^4\alpha^4}{n^3} - \frac{1}{2}\frac{g^2/4}{j+1/2}\frac{Z^4\alpha^4}{n^3} + \mathcal{O}(Z^6\alpha^6)\,, \tag{2.42}$$

where it is understood that $n - \ell \geq 1$, this condition allows us to write what was previously described in Eq. (2.41) as two distinct spectra now as a single energy spectra. In the limit $g \to 2$ or $g \to 0$ the correct expansion to order $Z^4\alpha^4$ of the Dirac or KG energies are obtained. In the following we explore some consequences of our principal non-relativistic result, Eq. (2.42).

### 2.2.2 g-Lamb Shift between 2S and 2P orbitals

The breaking of degeneracy in Eq. (2.42) between states of differing $\ell$ orbital quantum number, but the same total angular momentum $j$ and principle quantum number $n$ is responsible for the Lamb shift due to anomalous magnetic moment. The only term in Eq. (2.42) (up to order $Z^4\alpha^4$) that breaks the degeneracy between the $E^{n,j}_{\ell=j+1/2}$ and $E^{n,j}_{\ell=j-1/2}$ states for $n \geq 2$ is the fourth term. This is unsurprising as it depends exclusively on quantum number $\ell$ and $n$. The lowest order Lamb shift due to anomalous magnetic moment is then

$$\frac{\Delta E^{n,j}_{\text{gLamb}}}{mc^2} = E^{n,j}_{\ell=j-1/2} - E^{n,j}_{\ell=j+1/2} = \left(g^2/8 - 1/2\right)\left(\frac{1}{j} - \frac{1}{j+1}\right)\frac{Z^4\alpha^4}{n^3} \,. \tag{2.43}$$

For the $2S_{1/2}$ and $2P_{1/2}$ states Eq. (2.43) reduces to

$$\frac{\Delta E^{2S_{1/2}-2P_{1/2}}_{\text{gLamb}}}{mc^2} = \left(g^2/8 - 1/2\right)\frac{Z^4\alpha^4}{6} = \left(a + a^2/2\right)\frac{Z^4\alpha^4}{6} \,. \tag{2.44}$$

Our result in Eq. (2.43) and Eq. (2.44) is sensitive to $g^2/8 - 1/2 = a + a^2/2$. Traditionally the Lamb shift due to an anomalous lepton magnetic moment is obtained perturbatively (Itzykson and Zuber, 1980) by considering the DP equation which is sensitive to $g/2 - 1 = a$ the shift takes on the expression at lowest order

$$\frac{\Delta E^{2S_{1/2}-2P_{1/2}}_{\text{gLamb,DP}}}{mc^2} = \left(\frac{g-2}{2}\right)\frac{Z^4\alpha^4}{6} = a\frac{Z^4\alpha^4}{6} \,. \tag{2.45}$$

It is of experimental interest to resolve this discrepancy between the first order DP equation and the second order fermion formulation KGP. We recall the present day values

$$a_e = 1159.65218091(26) \times 10^{-6} \simeq \frac{\alpha}{2\pi} \,, \tag{2.46a}$$

$$a_\mu - a_e = 6.2687(6) \times 10^{-6} \,. \tag{2.46b}$$

The largest contribution to the anomalous moment for charged leptons is, as indicated the lowest order QED Schwinger result $a = \alpha/2\pi$. For the KGP approach, the anomalous $g$-factor mixes contributions of different powers of fine structure $\alpha$. Precision values for the fundamental constants are taken from Tiesinga et al. (2021). For the $2S_{1/2} - 2P_{1/2}$ states, the shift is

$$\frac{\Delta E_{\rm gLamb}^{2S_{1/2}-2P_{1/2}}}{mc^2} = \frac{Z^4\alpha^5}{12\pi} + \frac{Z^4\alpha^6}{48\pi^2} \ . \tag{2.47}$$

The scale of the discrepancy between KGP and DP for the hydrogen atom is then

$$\begin{aligned} \Delta E_{\rm gLamb,KGP}^{2S_{1/2}-2P_{1/2}} - \Delta E_{\rm gLamb,DP}^{2S_{1/2}-2P_{1/2}} &= \frac{\alpha^6 mc^2}{48\pi^2} \\ &= 1.62881214 \times 10^{-10}\ \text{eV} = 39.3845030\ \text{kHz} \ , \end{aligned} \tag{2.48}$$

without taking into account the standard corrections such as reduced mass, recoil, radiative, or finite nuclear size; for more information on those corrections please refer to Jentschura and Pachucki (1996); Eides et al. (2001); Tiesinga et al. (2021). It is to be understood that the corrections presented here are illustrative of the effect magnetic moment has on the spectroscopic levels, but that further work is required to compare these to experiment: for example we look here on behavior of point particles only.

While the discrepancy is small for the hydrogen system, it is $\approx 40$ kHz and will be visible in this or next generation's spectroscopic experiments. The discrepancy is also non-negligible for hydrogen-like exotics such as proton-antiproton because the proton $g$-factor is much larger

$$g_p = 5.585694702(17) \ , \qquad a_p = 1.792847351(9) \ . \tag{2.49}$$

The discrepancy for the proton-antiproton system is

$$\Delta E_{\rm gLamb,KGP}^{2S_{1/2}-2P_{1/2}} - \Delta E_{\rm gLamb,DP}^{2S_{1/2}-2P_{1/2}} = 0.71268151\ \text{eV} \ . \tag{2.50}$$

### 2.2.3 g-Fine structure effects within P orbitals

The fifth term in Eq. (2.42), which depends on $j$ and $n$, will shift the levels due to an anomalous moment, but does not contribute to the Lamb shift. Rather this expression, which contains the spin-orbit $\vec{L}\cdot\vec{S}$ coupling, is responsible for the fine structure splittings. From Eq. (2.42) the fine structure splitting is given by

$$\frac{\Delta E^{n,\ell}_{\rm gFS}}{mc^2} = E^{n,j=\ell+1/2}_{\ell} - E^{n,j=\ell-1/2}_{\ell} = \left(g^2/8\right)\left(\frac{1}{\ell} - \frac{1}{\ell+1}\right)\frac{Z^4\alpha^4}{n^3}\,. \tag{2.51}$$

The splitting between the $2P_{3/2}$ and $2P_{1/2}$ states is therefore

$$\frac{\Delta E^{2P_{3/2}-2P_{1/2}}_{\rm gFS}}{mc^2} = \left(g^2/8\right)\frac{Z^4\alpha^4}{16} = \left(1/2 + a + a^2/2\right)\frac{Z^4\alpha^4}{16}\,. \tag{2.52}$$

In comparison the fine structure dependence on $g$-factor in the DP equation is given as

$$\frac{\Delta E^{2P_{3/2}-2P_{1/2}}_{\rm gFS,DP}}{mc^2} = \left(\frac{g-1}{2}\right)\frac{Z^4\alpha^4}{16} = (1/2+a)\,\frac{Z^4\alpha^4}{16}\,. \tag{2.53}$$

Just as in the case of the Lamb shift, we find that the KGP and DP equations disagree for fine structure splitting. For the hydrogen atom this discrepancy is

$$\begin{aligned}\Delta E^{2P_{3/2}-2P_{1/2}}_{\rm gFS,KGP} - \Delta E^{2P_{3/2}-2P_{1/2}}_{\rm gFS,DP} &= \frac{\alpha^6 mc^2}{128\pi^2} \\ &= 6.10804553\times10^{-11}\ \text{eV} = 14.7691885\ \text{kHz}\,,\end{aligned} \tag{2.54}$$

and for proton-antiproton, the fine structure splitting discrepancy is

$$\Delta E^{2P_{3/2}-2P_{1/2}}_{\rm gFS,KGP} - \Delta E^{2P_{3/2}-2P_{1/2}}_{\rm gFS,DP} = 0.26725557\ \text{eV}\,. \tag{2.55}$$

For fine structure of the muonic-hydrogen system, the KGP-DP discrepancy is

$$\Delta E^{2S_{1/2}-2P_{1/2}}_{\rm gFS,KGP} - \Delta E^{2S_{1/2}-2P_{1/2}}_{\rm gFS,DP} = 1.272774\times10^{-8}\ \text{eV} \tag{2.56}$$

We can make a general observation that non minimal magnetic coupling, such as we have studied in the DP and KGP cases, enlarge energy level splittings. The above shows that these discrepancies will remain when calculating within more realistic finite nuclear size context.

## 2.3 Particles in strong electromagnetic fields

Care must be taken when interpreting the results presented in sections. For physical electrons the AMM interaction is the result of vacuum fluctuations whose strength also depends on the strength of the field. For example in the large magnetic field limit a QED computation shows that the ground state is instead of Eq. (2.16) given by Jancovici (1969)

$$E_0 \approx mc^2 + \frac{\alpha}{4\pi} mc^2 \ln^2\left(\frac{2e\hbar B}{m^2c^3}\right), \tag{2.57}$$

which even for enormous magnetic fields does not deviate significantly from the rest mass-energy of the electron. Further the AMM radiative corrections approach zero for higher Landau levels (Ferrer et al., 2015; Hackebill, 2022). Therefore the AMM in the case of electrons does not have a significant effect in highly magnetized environments such as those found in astrophysics (magnetars).

The situation is different for composite particles such as the proton, neutron and light nuclei whose anomalous magnetic moments are dominated by their internal structure and not by vacuum fluctuations. In this situation we expect that the AMM interaction in high magnetic fields remains significant. Therefore, asking whether the DP or KGP equations better describes the dynamics of composite hadrons and atomic nuclei in presence of magnetar strength fields is a relevant question despite the standard choice in literature being the DP equation (Broderick et al., 2000). The same question can be asked for certain exotic hydrogen-like atoms where the constituent particles have anomalous moments which can be characterized as an external parameter.

### 2.3.1 Strong homogeneous magnetic fields

The magnetic moment anomaly can flip the sign of the magnetic energy for the least excited states causing the gap between particle and antiparticle states to decrease with magnetic field strength. Setting $p_z = 0$ in Eq. (2.15), we show in Figure 2.2 that the energy of the lowest KGP Landau eigenstate $n = 0, s = 1/2$ reaches zero where the gap between particle and antiparticle states vanishes for the field

$$B^e_{\text{crit}} = \frac{B^e_S}{a_e} \simeq 861 B^e_S = 3.8006 \times 10^{16}\ \text{G}\ , \tag{2.58a}$$

$$B^p_{\text{crit}} = \frac{B^p_S}{a_p} \simeq \frac{1}{1.79} B^p_S = 8.3138 \times 10^{19}\ \text{G}\ , \tag{2.58b}$$

where $B_S$ is the so-called Schwinger critical field (Schwinger, 1951).

$$B^e_S \equiv \frac{m_e^2 c^2}{e\hbar} = \frac{m_e c^2}{2\mu_B} = 4.4141 \times 10^{13}\ \text{G}\ , \tag{2.59a}$$

$$B^p_S \equiv \frac{m_p^2 c^2}{e\hbar} = \frac{m_p c^2}{2\mu_N} = 1.4882 \times 10^{20}\ \text{G}\ . \tag{2.59b}$$

The numerical results are evaluated for the anomalous moment of the electron and proton, given by Eq. (2.46a) and Eq. (2.49). At the critical field strength $B_{\text{crit}}$ the Hamiltonian loses self-adjointness and the KGP loses its predictive properties. The Schwinger critical field Eq. (2.59a) denotes the boundary when electrodynamics is expected to behave in an intrinsically nonlinear fashion, and the equivalent electric field configurations become unstable (Labun and Rafelski, 2009). However, it is also possible that the vacuum is stabilized by such strong magnetic fields (Evans and Rafelski, 2018).

The critical magnetic fields as shown in Eq. (2.58a) appear in discussion of magnetars (Kaspi and Beloborodov, 2017). The magnetar field is expected to be more than 100-fold that of the Schwinger critical magnetic field which is on the same order of magnitude as $B_{\text{crit}}$ for an electron. While the critical field for a proton exceeds that of a magnetar, the dynamics of protons (and neutrons) in such fields is nevertheless significantly modified. A correct description of magnetic moment therefore has

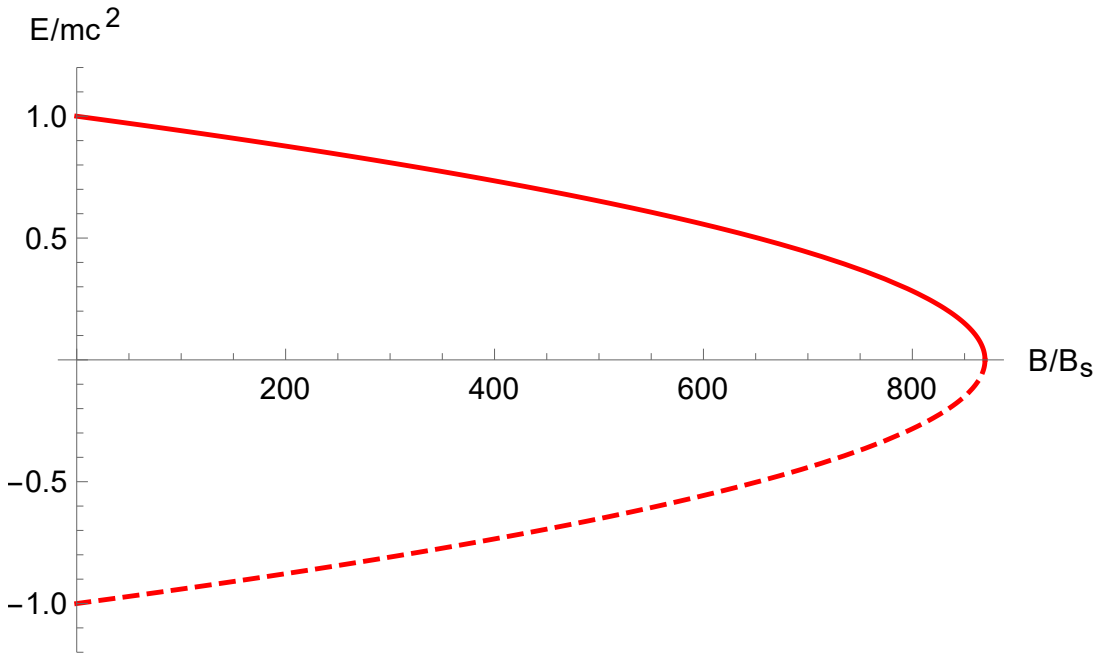


Figure 2.2: The $n = 0$, $s = 1/2$ ground state for a KGP electron given by Eq. (2.16) with $g/2 - 1 = \alpha/2\pi$ in a homogeneous magnetic field. We consider the particle with no $z$-direction momentum. The particle state (solid red) and antiparticle (dashed red) are presented.

relevant consequences to astrophysics.

Figure 2.3 shows analogous reduction in particle/antiparticle energy gap for the DP equation. In this case the vanishing point happens at a larger magnetic field strength. This time the solutions continue past this point, but require allowing the states to cross into the opposite continua which we consider nonphysical. We are not satisfied with either model's behavior though the KGP description is preferable. However, it is undesirable that both KGP and DP solutions loose physical meaning and vacuum stability in strong magnetic fields.

### 2.3.2 High-Z hydrogen-like atoms

For the case of $g = 2$ hydrogen-like systems with large $Z$ nuclei, there is extensive background related to the long study of the solutions of the Dirac equation (Rafelski et al., 1978; Greiner et al., 2012a; Rafelski et al., 2017). For $g \neq 2$ and $1/r$ singular

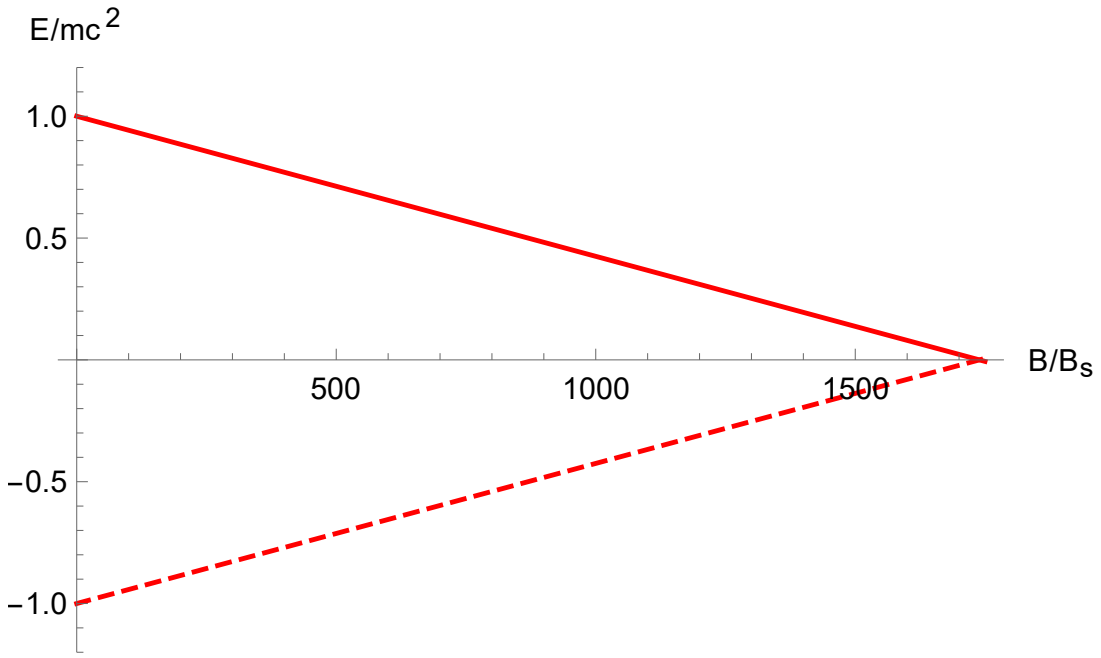


Figure 2.3: The $n = 0$, $s = 1/2$ ground state for a DP electron given by Eq. (2.21b) with $g/2 - 1 = \alpha/2\pi$ in a homogeneous magnetic field. We consider the particle with no $z$-direction momentum. The particle state (solid red) and antiparticle (dashed red) are presented.

potential we refer back to the exact expression for the KGP energy levels in Eq. (2.29). In the situation of critical electric fields, states lose self-adjointness for large $Z$ in both the Dirac $g=2$ case (Gesztesy et al., 1985) and for KGP $g\neq 2$. Thaller (2013) notes that the DP-Coulomb solutions retain self-adjointness via 'diving' states. For KGP $|g| < 2$, states vanish similar to Dirac energy levels for the $1/r$ singular potential, but if $|g|>2$ there is merging of particle to particle states (and antiparticle to antiparticle) for states of the same total angular momentum quantum number $j$, but opposite spin orientations.

This merging state behavior can be seen in Figure 2.4, which shows the meeting of the $1S_{1/2}$ and $2P_{1/2}$ states when $|g| > 2$. For $|g| < 2$ there is no state merging, but the solution is discontinuous in the sense that even for $1S_{1/2}$ we see a maximum allowed value of $Z$ at a finite energy. This is reminiscent of the Dirac $g=2$ behavior we are familiar with for the $2P_{1/2}$ state (see upper dashed blue line in Figure 2.4)

and many other $g=2$ eigenstates. We know from study of numerical solutions of the Dirac equation that the regularization of the Coulomb potential by a finite nuclear size removes this singular behavior. It remains to be seen how this exactly works in the context of the KGP equation allowing for the magnetic anomaly.

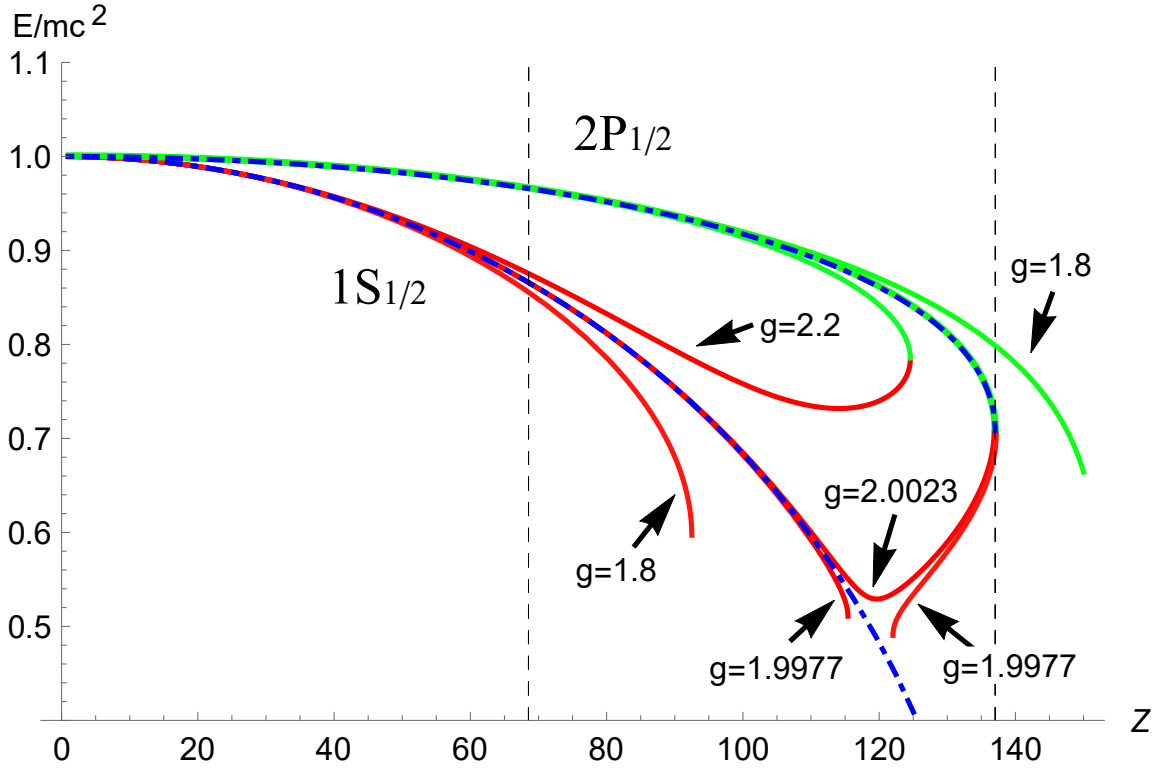


Figure 2.4: The KGP $1S_{1/2}$ (lower red curves) and $2P_{1/2}$ (upper green curves) energy levels for $g$-factor values $g=\{1.8,\ 1.9977,\ 2.0023,\ 2.2\}$ are shown for large $Z$ hydrogen-like atoms. The curves for the Dirac $g=2$ case for (lower dashed blue) $1S_{1/2}$ and (upper dashed blue) $2P_{1/2}$ are also presented.

Thaller (2013) presented numerically computed DP equation energy levels for large $Z$ hydrogen like atoms. These numerical solutions involve crossings in energy levels between states with the same total angular quantum number $j$, but differing spin orientations such as $1S_{1/2}$ and $2P_{1/2}$; these states also have the behavior of diving into the antiparticle lower continuum even for $1/r$-potential. These features are not present for the KGP-Coulomb solution. However, there is a similarity between the numerical solutions of the DP equation and our analytical KGP solutions, because

for $|g| > 2$ the merging states as described above correspond to the crossing states in the DP solution.

The DP equation also allows for the so-called 'super-positronium' states as described by Barut and Kraus (1975, 1976). Such states represent resonances due to the magnetic interaction that reside incredibly close to the center of the atom i.e $\sqrt{\langle r^2 \rangle} \approx a\alpha\hbar/mc$, but this feature is absent from the KGP formation of the Coulomb problem as all KGP-Coulomb wave functions which can be normalized can be successfully matched to their Dirac ($g=2$) companions.

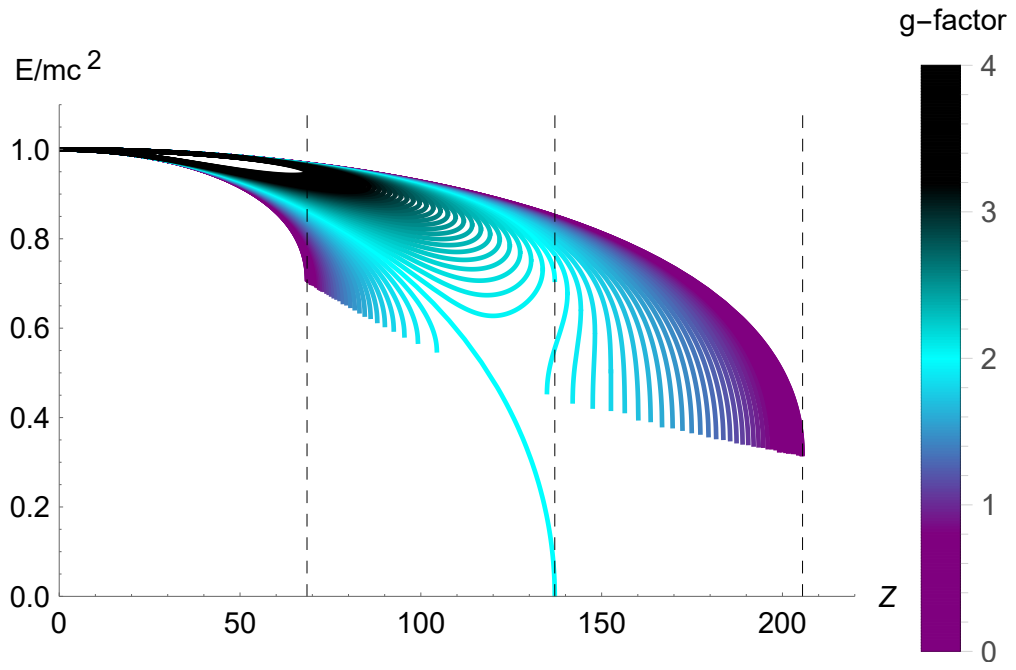


Figure 2.5: The KGP $1S_{1/2}$ and $2P_{1/2}$ states are plotted for hydrogen-like energies for $220 > Z > 0$. The spread of lines corresponds to a spread of $g$-factor values: $4 > g > 0$. Integer multiples of $Z = 137/2$ are marked with vertical dashed lines. The separation between any two adjacent curves is $|g_i - g_{i+1}| = 0.05$. The unique curve which dives towards and stops at the boundary $E = 0$ is the Dirac $g = 2$ ground state.

Because analytical solutions of the DP-Coulomb problem are not available, unlike our results for KGP, it is hard to pinpoint precisely the origin of the diving and

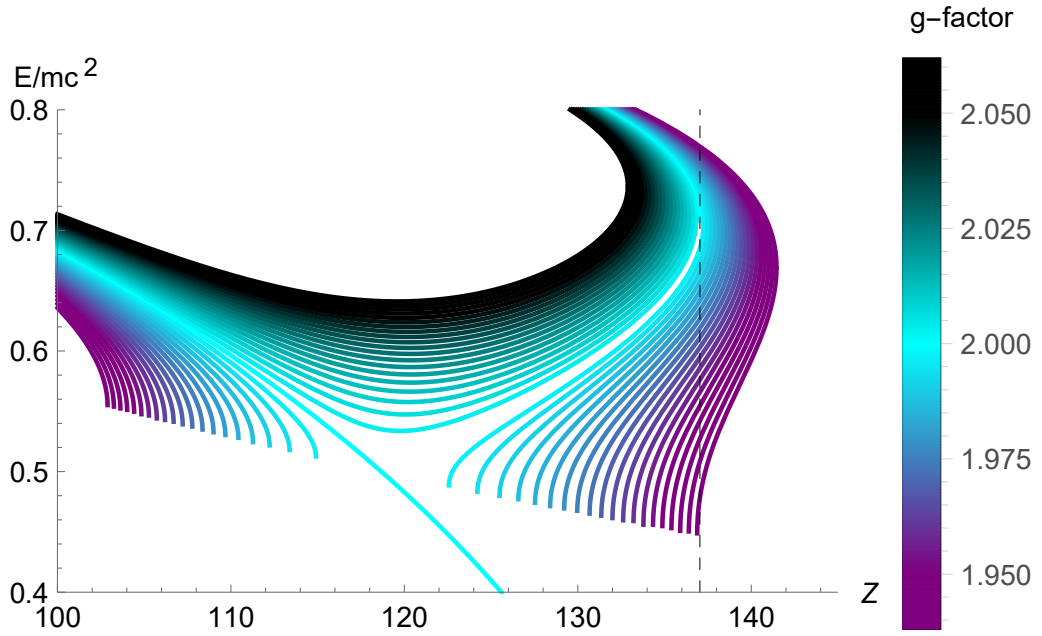


Figure 2.6: A close up of the KGP $1S_{1/2}$ and $2P_{1/2}$ states between $2.0625 > g > 1.9375$. The separation between any two adjacent curves is $|g_i - g_{i+1}| = 0.003125$. The value $Z = 137$ is marked with a vertical dashed line.

crossing state behavior. However, we can hypothesize that the problems arise due to the pathological structure of DP equation where the magnetic anomaly rather than full magnetic moment appears. On the other hand KGP framework for large $Z$ shows interesting and well-behaved analytical behavior.

We further can explore the $g$-dependency on the $1S_{1/2}$ and $2P_{1/2}$ states by plotting a spectrum of $g$-factor values as is done in Figure 2.5. Purple regions are where $g \to 0$ and the energies resembles the familiar Klein-Gordon case. As $g \to 0$, small changes in $g$-factor only lead to modest changes in the energies for large $Z$ systems. The black curves represent where $g \to 4$. A unique feature of $g > 2$ fermions is that after a certain point, certain states become *less* bound with increasing $Z$. These rising curves represent spin anti-aligned $-\lambda$ levels which become nonphysical (e.g the slope becomes vertical) and merge with their spin aligned $+\lambda$ counterparts precisely where

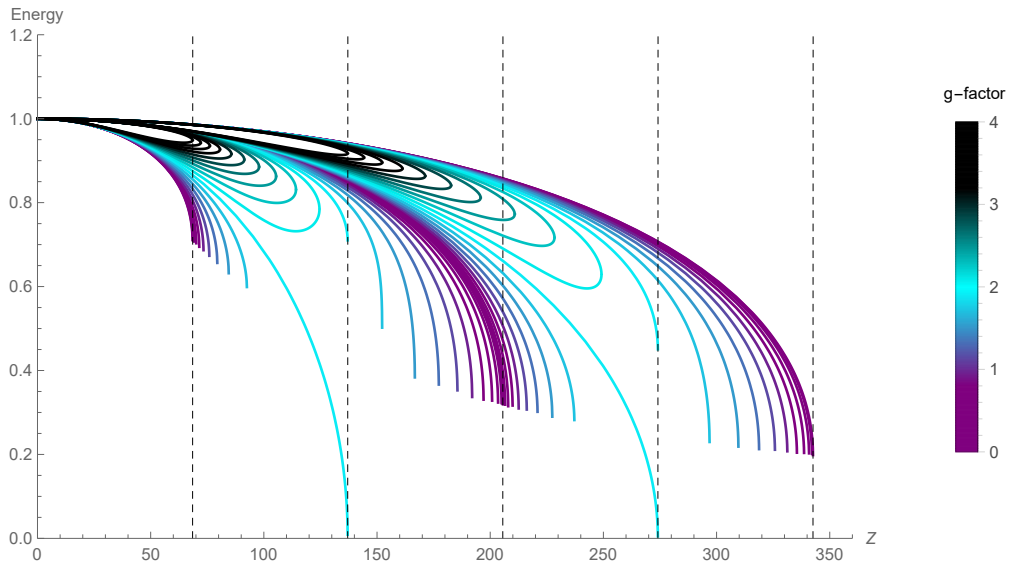


Figure 2.7: Energy eigenvalues for $\pm\lambda$. Curves are plotted for $j = 1/2, 3/2, 5/2$ with the relativistic principle quantum number $n_r = 0$. (dashed vertical) These lines indicate integer multiples of $\frac{137}{2}$.

those states also become nonphysical.

The cyan curves in Figure 2.5 are where $g \approx 2$ and the states resemble the Dirac case. At exactly $g = 2$ there is a unique behavior where the $1S_{1/2}$ state dashes downward and terminates at $Z = 1/\alpha$. This path is unique and does not occur for any $g \neq 2$. Additionally, the $g = 2$ state does not smoothly connect with the $g \approx 2$ solutions for large $Z$ hydrogen-like atoms. This is more visible in Figure 2.6 (note the same purple-cyan-black color scheme is used but for different $g$-factor values) which plots a variety of $g$-factor values near $g \approx 2$. More specifically, small changes in $g$-factor lead to large deviations in the energies which is represented by the lack of dense lines near $g = 2$ indicating the "cusp-like" nature of the Dirac case for very small anomalies.

The pattern of merging states with the same angular momentum first discussed

in Figure 2.4 repeats itself for higher values of $j$ total angular momentum. We show this explicitly in Figure 2.7 where

## 2.4 Special topics related to Klein-Gordon-Pauli

### 2.4.1 Combination of mass and magnetic moment

While we've thus far focused on the Dirac-Pauli and Klein-Gordon-Pauli models for magnetic dipole moments, the non-uniqueness of spin dynamics allows us to invent further non-linear EM models which all in the non-relativistic limit yield the non-relativistic QM magnetic dipole Hamiltonian. One such extension to quantum spin dynamics is to note the close relationship mass and magnetic moment share in the KGP formalism. We can write a unified dipole-mass as

$$\boxed{\widetilde{m}(\boldsymbol{E},\boldsymbol{B}) = m + \mu\frac{\sigma_{\alpha\beta}F^{\alpha\beta}}{2c^2}}\,, \tag{2.60}$$

which satisfies the wave equation

$$\left((i\hbar\partial_\mu - eA_\mu)^2 - \widetilde{m}^2(\boldsymbol{E},\boldsymbol{B})c^2\right)\Psi = 0\,, \tag{2.61}$$

$$\left((i\hbar\partial_\mu - eA_\mu)^2 - \left(mc + \mu\frac{\sigma^{\alpha\beta}F_{\alpha\beta}}{2c}\right)^2\right)\Psi = 0\,. \tag{2.62}$$

This modified KGP formulation then requires spin sensitive mass and an explicit electromagnetic component to the charged lepton mass. As informed by classical mechanics, charged particles should be understood to derive at least some of their mass from the mass-energy of their electromagnetic fields. Eq. (2.63) results in higher order vertex diagrams coupling fermions to photons.

The approach in Eq. (2.60) is superficially similar to the model proposed by Frenkel (1926) in classical mechanics by giving the particle a spin dependent mass of the form $m \sim \Sigma_{\mu\nu}F^{\mu\nu}$ where $\Sigma_{\mu\nu}$ is the covariant generalization of the classical magnetic and electric dipole. Eq. (2.62) is however distinct in that the mass is allowed off-diagonal components in spinor space (a subspace which doesn't exist classically). The dipole-

mass Eq. (2.60) is off-diagonal in spinor space in the Dirac representation and no longer commutes likes a scalar.

Eq. (2.60) also differs from the regular KGP equation by the presence of an additional quadratic interaction which we can evaluate using Eq. (1.30) in the Dirac representation as

$$\delta V = -\frac{\mu^2}{4}\left(\gamma_\alpha\gamma_\beta F^{\alpha\beta}\right)^2 = \mu^2 \begin{pmatrix} i\boldsymbol{\sigma}\cdot\boldsymbol{E}/c & -\boldsymbol{\sigma}\cdot\boldsymbol{B} \\ -\boldsymbol{\sigma}\cdot\boldsymbol{B} & i\boldsymbol{\sigma}\cdot\boldsymbol{E}/c \end{pmatrix}\begin{pmatrix} i\boldsymbol{\sigma}\cdot\boldsymbol{E}/c & -\boldsymbol{\sigma}\cdot\boldsymbol{B} \\ -\boldsymbol{\sigma}\cdot\boldsymbol{B} & i\boldsymbol{\sigma}\cdot\boldsymbol{E}/c \end{pmatrix}, \quad (2.63)$$

$$\delta V = \mu^2 \begin{pmatrix} \boldsymbol{B}^2 - \boldsymbol{E}/c^2 & -i\boldsymbol{E}\cdot\boldsymbol{B} \\ -i\boldsymbol{E}\cdot\boldsymbol{B} & \boldsymbol{B}^2 - \boldsymbol{E}/c^2 \end{pmatrix} = 2\mu^2 \begin{pmatrix} \mathcal{S} & -i\mathcal{P} \\ -i\mathcal{P} & \mathcal{S} \end{pmatrix}. \quad (2.64)$$

We define the invariants of the electromagnetic field tensor $F^{\alpha\beta}$ in Eq. (2.64) letting us write the above more compactly as

$$\mathcal{S} = \frac{1}{2}(\boldsymbol{B}^2 - \boldsymbol{E}^2/c^2)\,, \qquad \mathcal{P} = \boldsymbol{E}\cdot\boldsymbol{B}/c\,, \qquad \delta V = 2\mu^2\left(\mathcal{S} - i\gamma^5\mathcal{P}\right). \quad (2.65)$$

We note that $\sigma_{\alpha\beta}F^{\alpha\beta}/2$ can also be written in terms of its four eigenvalues

$$\lambda_1 = +\mathcal{S} + i\mathcal{P}\,, \qquad \lambda_2 = +\mathcal{S} - i\mathcal{P}\,, \qquad \lambda_3 = -\mathcal{S} + i\mathcal{P}\,, \qquad \lambda_4 = -\mathcal{S} - i\mathcal{P}\,. \quad (2.66)$$

This represents simply only one possible non-linear extension to electromagnetism in relativistic quantum mechanics of which there are a family of extensions (Foldy, 1952).

For the homogeneous magnetic field Eq. (2.62) can be solved in much the same way as the KGP equation in Section 2.1. One obtains energy eigenvalues by noting the simple shift that occurs in the mass of $m^2 \to m^2 + \mu^2 B^2$ quadratic in the magnetic field. The resulting energy levels are

$$E_{n,s}(\boldsymbol{B}) = \sqrt{m_e^2c^4 + \mu^2B^2 + p_3^2c^2 + 2e\hbar c^2 B\left(n + \frac{1}{2}\right) - 2\mu B m_e c^2 s} \quad (2.67)$$

An interesting feature is that in ultra-high magnetic fields ($B >> B_s$), Eq. (2.67)

approximates

$$E \approx \mu B \, . \tag{2.68}$$

This is not dissimilar to the non-relativistic case where the magnetic energy is simply proportional to the magnetic field.

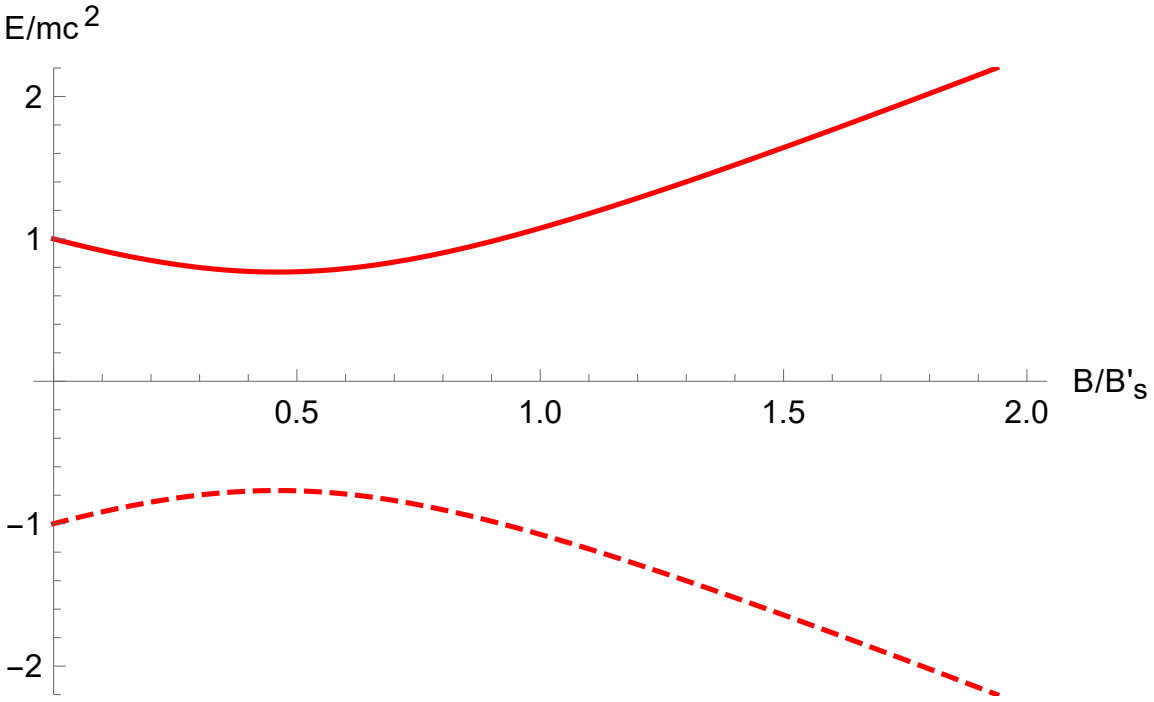


Figure 2.8: The $n = 0$, $s = 1/2$ ground state for a IKGP proton given by Eq. (2.67) with $g = 5.58$ in a homogeneous magnetic field. The magnetic minimum is well visible for particles with larger anomalous moment such as proton. We consider the particle with no $z$-direction momentum. The particle state (solid red) and antiparticle (dashed red) are presented. The magnetic field scale is $B'_S = (m_p^2/m_e^2)B_S$.

The most striking feature is that the ground state remains physical for all values of magnetic field when an anomalous moment is included. The self-adjointness of the system is not lost for some critical magnetic field strength. It can be then thought that the magnetic field provides a stabilizing influence on the system. Rather, there

exists a "magnetic minimum" located for $n = 0, s = 1/2$ at

$$B_{\min} = \frac{4mc^2}{g^2\mu_B}a \ , \tag{2.69}$$

which for the electron is

$$B^e_{\min} = \frac{8a_e}{g_e^2}B_S = 1.02126 \times 10^{11} \text{ G} \ . \tag{2.70}$$

The minimum for a proton is in comparison

$$B^p_{\min} = \frac{8a_p}{g_p^2}\frac{m_p^2}{m_e^2}B_s = 6.841 \times 10^{19} \text{ G} \ , \tag{2.71}$$

which can be seen in Figure 2.8. Here it is understood that for the calculation of the proton's magnetic minimum, the nuclear mass and magneton was used rather than the electron Bohr magneton. For large enough g-factor, excited states may also contain a minimum, but for any nonzero anomalous moment the ground state always does.

### 2.4.2 Extensions to non-Albelian fields

Briefly, we would like to comment on the g-factor of the quarks which unlike the leptons participate in the strong color interaction of quantum chromodynamics (QCD). Since color charges follows a more complex $SU(3)$ group structure unlike the more straight forward $U(1)$ of electromagnetism, the "color magnetism" of QCD requires more than just the analogous Pauli term to describe color dipole moments owing due to the fact that QCD has non-Abelian (non-commuting) gluon gauge fields $\mathcal{A}^\alpha$.

The quarks, like the leptons, should obey the quantum mechanical analogue of the energy-momentum relation seen in Eq. (1.57) with the only theoretical difference being a modified covariant derivative. The covariant derivative, written in terms of kinetic momentum, should appear as

$$\text{EM} + \text{QCD}: \qquad i\hbar\widetilde{\nabla} = \pi^\alpha = p^\alpha - q_{\text{EM}}A^\alpha - q_{\text{QCD}}\mathcal{A}^\alpha \ , \tag{2.72}$$

where $q_{\rm EM}$ is the electric charge of the quarks $q_{\rm EM}/e \in \pm 1/3, \pm 2/3$ and $q_{\rm QCD}$ is the color charge coupling strength. In many texts the symbol $g_s$ is used for the color coupling strength, but we circumvent that notation to avoid confusion with $g$-factor.

We follow the conventions in Greiner et al. (2006). The eight $3 \times 3$ Gell-Mann matrices $\lambda^a$ are embedded into each independent field as

$$\mathcal{A}^\alpha \equiv \frac{1}{2}\lambda^a \mathcal{A}^\alpha_a \,, \qquad a \in 1 \ldots 8 \,, \qquad [\lambda^a, \lambda^b] = \frac{i}{2} f^{abc} \lambda^c \,, \tag{2.73}$$

where $\mathcal{A}^\alpha_a$ are the individual fields for each gluon species in a given representation and $f^{abc}$ is the $SU(3)$ antisymmetric structure function. The non-commuting behavior of the Gell-Mann matrices captures the non-Abelian structure of the gauge fields. The gluon field strength tensor $\mathcal{G}^{\alpha\beta}$ is then

$$\mathcal{G}^{\alpha\beta} = \partial^\alpha \mathcal{A}^\beta - \partial^\beta \mathcal{A}^\alpha + \frac{i}{\hbar} q_{\rm QCD} \left[\mathcal{A}^\alpha, \mathcal{A}^\beta\right] \,, \tag{2.74}$$

$$\left[\mathcal{A}^\alpha, \mathcal{A}^\beta\right] = \frac{1}{4}\mathcal{A}^\alpha_a \mathcal{A}^\beta_b \left[\lambda^a, \lambda^b\right] = \frac{i}{8}\mathcal{A}^\alpha_a \mathcal{A}^\beta_b f^{abc} \lambda_c \,. \tag{2.75}$$

Following the same procedure in Section 1.2.2, we can generalize the energy-momentum relation and obtain the EM+QCD variant of the KGP equation for quarks. We find that the resulting quark-KGP equation is

$$\left(\eta_{\alpha\beta}\pi^\alpha \pi^\beta - \frac{q_{\rm EM}\hbar}{2}\sigma_{\alpha\beta}F^{\alpha\beta} - \frac{q_{\rm QCD}\hbar}{2}\sigma_{\alpha\beta}\mathcal{G}^{\alpha\beta}\right)\Psi = m_q^2 c^2 \Psi_q \,, \tag{2.76}$$

which mirrors the electromagnetic case except for the extension of a chromomagnetic Pauli term. We note that $m_q$ is the quark mass and that the field $\Psi_q$ is a color triplet of spinors for: red, green, blue:

$$\Psi_q = \begin{pmatrix} \Psi_r \\ \Psi_g \\ \Psi_b \end{pmatrix} \,. \tag{2.77}$$

As only the non-commuting portion of Eq. (2.76) (written explicitly in Eq. (2.75)) is off-diagonal in color, this means that the additional non-commuting chromomagnetic

term acts as a transition matrix between different quark colors.

This method (based on the commutator of the kinetic momentum) suggests that the color and electromagnetic $g$-factors both have a natural value of $g_{\rm EM} = g_{\rm QCD} = 2$. We can generalize Eq. (2.76) to allow for arbitrary EM and QCD dipole moments $g_{\rm EM}$ and $g_{\rm QCD}$ respectively as

$$\boxed{\left(\eta_{\alpha\beta}\pi^{\alpha}\pi^{\beta} - \frac{g_{\rm EM}}{2}\frac{q_{\rm EM}\hbar}{2}\sigma_{\alpha\beta}F^{\alpha\beta} - \frac{g_{\rm QCD}}{2}\frac{q_{\rm QCD}\hbar}{2}\sigma_{\alpha\beta}\mathcal{G}^{\alpha\beta}\right)\Psi = m_q^2c^2\Psi}. \tag{2.78}$$

While in electromagnetism, DP and KGP approaches only differ in the presence of strong EM fields and are otherwise identical in the weak field limit, this cannot be equally said in QCD. The perturbative limit which justifies the DP approach for leptons in QED is possible due to the small value of the fine structure constant which is not true in QCD. Only for high momentum interactions (such as those present in quark-gluon-plasma (QGP) or in energetic collisions) is the perturbative approach applicable.

The dipole characteristics of the top-quark is of particular interest (Labun and Rafelski, 2013; Vryonidou and Zhang, 2018) because of top-quark's strong coupling to the Higgs and potential BSM physics, though current studies focus on a DP approach to chromomagnetism (Zhang and Willenbrock, 2011; Zhang, 2012; Buarque Franzosi and Zhang, 2015). There is also the added complexity of both the chromomagnetic and magnetic $g$-factors differing from the natural value independently of one another $g_{\rm EM} \neq g_{\rm QCD} \neq 2$. Further study of the KGP approach to chromomagnetism should be pursued. To our knowledge, there is no formulation of Eq. (2.78) as a field theory as discussed in Section 1.2.1 for charged leptons.

## 2.5 Classical relativistic spin dynamics

We turn away from quantum mechanical approaches to briefly inspect the classical analogue of spin dynamics. Considering the Poincaré group of space-time symmetry transformations (Weinberg, 2005; Greiner and Müller, 2012), it was established by Wigner that elementary particles are representations of the group and can be

characterized by eigenvalues of two the Poincaré group's two Casimir operators:

$$C_1 \equiv p_\mu p^\mu = p^2 = m^2 c^2 \,, \tag{2.79}$$

$$C_2 \equiv w_\mu w^\mu = w^2 \,, \qquad w_\alpha = \frac{1}{2}\varepsilon_{\alpha\beta\mu\nu} M^{\beta\mu} p^\nu \,, \tag{2.80}$$

where $w^\alpha$ is the Pauli-Lubanski pseudo-vector. Here $M^{\alpha\beta}$ is the relativistic tensor expression for the angular momentum defined via

$$M^{\alpha\beta} = x^\alpha p^\beta - x^\beta p^\alpha + S^{\alpha\beta} \tag{2.81}$$

where $S^{\alpha\beta}$ is the spin angular momentum tensor. The spin tensor $S^{\alpha\beta}$ can be understood via the classical (Cl.) four-spin defined in the rest frame for a massive particle as

$$s^\alpha = (0, \boldsymbol{s}) \,, \qquad s_\alpha s^\alpha = -\boldsymbol{s}_{\text{Cl.}}^2 \,, \qquad s_\alpha = \frac{1}{2mc}\varepsilon_{\alpha\beta\mu\nu} S^{\beta\mu} p^\nu \,, \tag{2.82}$$

where $\boldsymbol{s}_{\text{Cl.}}$ is the classical Euclidean three-spin (not to be confused with the quantum operator $\boldsymbol{s}$). We also note that to make the units correct, the Pauli-Lubanski pseudo-vector and the four-spin are proportional in the rest frame by a factor of $\sqrt{C_1} = mc$. Quantum mechanically (Ohlsson, 2012) $S^{\alpha\beta}$ appears as $\sim \sigma^{\alpha\beta}$ which we've already identified as the spin tensor in Dirac theory defined via the $\gamma^\alpha$ matrices.

### 2.5.1 Covariant magnetic potential and modified Lorentz force

We are interested in elementary particles with electric charge $e$, and elementary magnetic dipole charge $d = \mu/|\boldsymbol{s}_{\text{Cl.}}|$. Therefore the covariant dynamics must be extended beyond the Lorentz force to incorporate the Stern–Gerlach (SG) force. To achieve a suitable generalization we introduce (Rafelski et al., 2018) the covariant magnetic potential

$$B_\alpha(x, s) \equiv F^*_{\alpha\beta} s^\beta \tag{2.83}$$

As $s_\alpha$ is a pseudo-vector; the product in Eq. (2.83) results in a polar 4-vector $B_\alpha$. We note that the magnetic dipole potential $B_\alpha$ by construction in terms of the antisymmetric field pseudo-vector $F^*_{\alpha\beta}$ satisfies

$$\partial_\alpha B^\alpha = 0\,, \qquad s\cdot B = 0 \rightarrow B\cdot\frac{ds}{d\tau} + s\cdot\frac{dB}{d\tau}\,, \tag{2.84}$$

where $\tau$ is the proper time.

The zeroth component of the covariant potential in the rest frame Eq. (2.83) reproduces the classical magnetic dipole energy given by

$$U_{\text{Mag.}} = dB^0 = dF^{0\beta}s_\beta = -\boldsymbol{\mu}_{\text{Cl.}}\cdot\boldsymbol{B}\,, \qquad \boldsymbol{\mu}_{\text{Cl.}} = \mu\frac{\boldsymbol{s}_{\text{Cl.}}}{|\boldsymbol{s}_{\text{Cl.}}|}\,. \tag{2.85}$$

We can then define a covariant magnetic field tensor from the potential Eq. (2.83) which generalizes the Lorentz force as

$$G^{\alpha\beta} = \partial^\alpha B^\beta - \partial^\beta B^\alpha = G^{\alpha\beta} = \partial^\alpha F^{*\beta\gamma}s_\gamma - \partial^\beta F^{*\alpha\gamma}s_\gamma\,, \tag{2.86}$$

$$\frac{dp^\alpha}{d\tau} = eF^{\alpha\beta}u_\beta + dG^{\alpha\beta}u_\beta\,, \tag{2.87}$$

where $u_\alpha$ is the four-velocity and as previously stated, $e$ and $d$ are the electric and dipole charges. While the first term in Eq. (2.87) is the standard Lorentz force, the second term is a covariant formulation of the SG force.

Because the spin precession is sensitive to the force on a particle, the presence of a SG force will induce precession terms which are second order in spin. The torque on the magnetic moment of the particle can be determined via the properties of the four-spin. Namely $s^\alpha$ is orthogonal (Schwinger, 1974) to the four-velocity yielding

$$u\cdot\frac{ds}{d\tau} + \frac{du}{d\tau}\cdot s \tag{2.88}$$

The spin torque equations can be obtained (Bargmann et al., 1959) by inserting the Lorentz force (in our case the modified Lorentz force) that corresponds to Eq. (2.87)

yielding

$$\begin{aligned}\frac{\mathrm{d}s^{\mu}}{\mathrm{d}\tau} &= (1+\tilde{a})\frac{e}{m}F^{\mu\nu}s_{\nu} - \tilde{a}\frac{e}{m}u^{\mu}\left(u_{\alpha}F^{\alpha\beta}s_{\beta}\right)/c^{2} \\ &\quad + (1+\tilde{b})\frac{d}{m}G^{\mu\nu}s_{\nu} - \tilde{b}\frac{d}{m}u^{\mu}\left(u_{\alpha}G^{\alpha\beta}s_{\beta}\right)/c^{2}\,. \end{aligned} \tag{2.89}$$

The constants $\tilde{a}$ and $\tilde{b}$ are arbitrary allowing for extra terms not forbidden by special relativity. With $d = 0$, Eq. (2.89) are known as the Thomas-Bargmann-Michel-Telegdi (TMBT) equations. In the standard derivation of relativistic spin precession, in the TBMT equation, the $\tilde{a}$ constant is associated with the anomalous magnetic moment.

In allowing for spin precession sourced by a Stern-Gerlach dipole force, an additional constant $\tilde{b}$ must be introduced. The terms in Eq. (2.86) involving the $G$ tensor are spin precession directly originating from dipole forces. In homogeneous electromagnetic fields, Eq. (2.86) reduces to the standard TBMT equation. These dynamical torque equations have found use in describing neutral and charged systems classically (Formanek et al., 2021, 2019) and inspired further efforts to improve covariant dynamics (Formanek, 2020).

# CHAPTER 3

## Dynamic neutrino flavor mixing through transition moments

We propose that neutrino flavors are remixed when exposed to strong EM fields travelling as a superposition distinct from the vacuum propagation of free neutrinos. Neutrino mixing is an important topic for studying BSM physics as flavor mixing only occurs in the presence of massive neutrinos allowing for the misalignment between the flavor basis which participates in left-chiral $SU(2)_L$ weak interactions and the mass basis which are the propagating neutrino states.

An anomalous magnetic moment (AMM) can be introduced into the neutrino effective Lagrangian via a Pauli term; see Chapter 1. We narrow our analysis for Majorana neutrinos which are allowed only transition magnetic moments which couple different flavors electromagnetically, but do not violate CPT symmetry. Transition moments however break lepton number conservation.

### 3.1 Electromagnetic characteristics of neutrinos

We study the connection between Majorana neutrino transition magnetic dipole moments (Fujikawa and Shrock, 1980; Shrock, 1980, 1982) and neutrino flavor oscillation. Neutrino electromagnetic (EM) properties have been considered before (Schechter and Valle, 1981; Giunti and Studenikin, 2015; Popov and Studenikin, 2019; Chukhnova and Lobanov, 2020) including the effect of oscillation (Lim and Marciano, 1988; Akhmedov, 1988; Pal, 1992; Elizalde et al., 2004; Akhmedov and Martínez-Miravé, 2022) in magnetic fields. The influence of transition magnetic moments on solar neutrinos is expected (Martínez-Miravé, 2023), but difficult to measure due to the lack of knowledge of solar magnetism near the core.

The case of transition moments has the mathematical characteristics of an off-diagonal mass which is distinct from normal direct dipole moment behavior. EM

field effects are also distinct from weak interaction remixing within matter, *i.e.* the Mikheyev-Smirnov-Wolfenstein effect (Wolfenstein, 1978; Mikheyev and Smirnov, 1985; Smirnov, 2003).

The size of the neutrino magnetic dipole moment can be constrained as follows: The lower bound is found by higher order standard model interactions with the minimal extension of neutrino mass $m_\nu$ included (Fujikawa and Shrock, 1980; Shrock, 1980, 1982). The upper bound is derived from reactor, solar and astrophysical experimental observations (Giunti et al., 2016; Canas et al., 2016; Studenikin, 2016; Aristizabal Sierra et al., 2022). The bounds are expressed in terms of the electron Bohr magneton $\mu_B$ as

$$\frac{e\hbar G_F m_\nu c^2}{8\pi^2\sqrt{2}} \sim 10^{-20}\mu_B < \mu_\nu^{\rm eff} < 10^{-10}\mu_B\,, \qquad \mu_B = \frac{e\hbar}{2m_e} \tag{3.1}$$

where $G_F$ is the Fermi constant and $\mu_\nu^{\rm eff}$ is the effective and characteristic size of the neutrino magnetic moment. In Eq. (3.1), the lower bound was estimated using a characteristic mass of $m_\nu \sim 0.1$ eV. From cosmological studies, the sum of neutrino masses is estimated (Aghanim et al., 2020) to be $\sum_i m_i < 0.12$ eV; the effective electron (anti)neutrino mass is bounded (Aker et al., 2022) by $m_e^\nu < 0.8$ eV.

## 3.2 Neutrino flavor mixing and electromagnetic fields

Oscillation of neutrino flavors observed in experiment is in general interpreted as being due to a difference in neutrino mass and flavor eigenstates. This misalignment between the two representations is described as rotation of the neutrino flavor $N$-vector where $N = 3$ is the observed number of generations. The unitary mixing matrix $V_{\ell k}$ allows for the change of basis between mass ($k$) and flavor ($\ell$) eigenstates via the transform

$$\nu_\ell = V_{\ell k}\nu_k \;\rightarrow\; \begin{pmatrix}\nu_e\\ \nu_\mu\\ \nu_\tau\end{pmatrix} = \begin{pmatrix}V_{e1} & V_{e2} & V_{e3}\\ V_{\mu 1} & V_{\mu 2} & V_{\mu 3}\\ V_{\tau 1} & V_{\tau 2} & V_{\tau 3}\end{pmatrix}\begin{pmatrix}\nu_1\\ \nu_2\\ \nu_3\end{pmatrix}\,, \tag{3.2}$$

where $\nu_\ell$ is the neutrino four-spinor written in the flavor basis while in the mass basis we use $\nu_k$ with $k \in 1, 2, 3$.

The parameterization of the components of the mixing matrix depends on the Dirac or Majorana-nature of the neutrinos. First we recall the Dirac neutrino mixing matrix $U_{\ell k}$ in the standard parameterization (Schwartz, 2014)

$$U_{\ell k} = \begin{pmatrix} c_{12}c_{13} & s_{12}c_{13} & s_{13}e^{-i\delta} \\ -s_{12}c_{23} - c_{12}s_{13}s_{23}e^{i\delta} & c_{12}c_{23} - s_{12}s_{13}s_{23}e^{i\delta} & c_{13}s_{23} \\ s_{12}s_{23} - c_{12}s_{13}c_{23}e^{i\delta} & -c_{12}s_{23} - s_{12}s_{13}c_{23}e^{i\delta} & c_{13}c_{23} \end{pmatrix} , \tag{3.3}$$

where $c_{ij} = \cos(\theta_{ij})$ and $s_{ij} = \sin(\theta_{ij})$. In this convention, the three mixing angles $(\theta_{12}, \theta_{13}, \theta_{23})$ are understood to be the Euler angles for generalized rotations and $\delta$ is the CP-violating complex phase.

For the Majorana case we must allow a greater number of complex phases: Majorana neutrinos allow up to two additional complex phases $\rho$ and $\sigma$ which along with $\delta$ participate in CP-violation. A parameterization is achieved by introducing an additional phase matrix $P_{kk'}$

$$V_{\ell k} = U_{\ell k'} P_{k' k} \, , \tag{3.4}$$

$$P_{kk'} = \mathrm{diag}(e^{i\rho}, e^{i\sigma}, 1) \, . \tag{3.5}$$

The mixing matrix $V_{\ell k}$ defined in Eq. (3.4) can then be used to transform the symmetric mass matrix $M_{\ell\ell'}$ from the flavor basis into the diagonal mass basis

$$M_{\ell\ell'} = \begin{pmatrix} m^\nu_{ee} & m^\nu_{e\mu} & m^\nu_{e\tau} \\ m^\nu_{e\mu} & m^\nu_{\mu\mu} & m^\nu_{\mu\tau} \\ m^\nu_{e\tau} & m^\nu_{\mu\tau} & m^\nu_{\tau\tau} \end{pmatrix} , \qquad M^{\mathrm{T}}_{\ell\ell'} = M_{\ell\ell'} \, , \tag{3.6}$$

$$V^{\mathrm{T}}_{\ell k} M_{\ell\ell'} V_{\ell' k'} = M_{kk'} = m_k \delta_{kk'} = \mathrm{diag}(m_1, m_2, m_3) \, . \tag{3.7}$$

We note the Majorana mass matrix is symmetric due to the anticommuting nature of the neutrino fields $\bar{\nu}\nu = -\nu^{\mathrm{T}}\bar{\nu}^{\mathrm{T}}$ and is in general complex (Adhikary et al., 2013;

Giunti and Kim, 2007) though it will be taken to be fully real in this work. There are many interesting models for mass matrices which were pioneered by Fritzsch and Xing (1996, 1998, 2000); Xing (2001) in the leptonic sector. The masses $m_k$ are taken to be real and positive labelling the free propagating states of the three neutrinos.

### 3.2.1 Effective Majorana neutrino Lagrangian

Given the mass matrix defined in Eq. (3.6), the Majorana mass term in the Lagrangian can be written in the flavor basis as

$$-\mathcal{L}^{\text{Maj.}}_{\text{mass}} = \frac{1}{2}\bar{\nu}_\ell M_{\ell\ell'}\nu_{\ell'} = -\frac{1}{2}\nu^{\text{T}}_{L,\ell}C^\dagger M_{\ell\ell'}\nu_{L,\ell'} + \text{h.c.}\,, \tag{3.8}$$

where the Majorana fields are written as $\nu = \nu_L + C(\bar{\nu}_L)^{\text{T}}$. The field $\nu_L$ refers to left-handed Weyl four-component spinors. Charged conjugated fields are written as $\nu^c = C(\bar{\nu})^{\text{T}}$. The charge conjugation operator $C$ is defined in the usual way in Itzykson and Zuber (1980); p.692.

Given these conventions, we can extend our consideration to include the electromagnetic interaction of neutrinos which is possible if neutrinos are equipped with a magnetic moment matrix $\mu_{\ell\ell'}$. We allow for a fixed *external* electromagnetic field tensor $F^{\alpha\beta}_{\text{ext}}(x^\mu)$ which imparts a force on the neutrino fields. We emphasize that $F^{\alpha\beta}_{\text{ext}}$ is not dynamical in our formulation and consists of real functions over four-position and not field operators.

We generalize the AMM Pauli Lagrangian in Eq. (1.31) to account for the Majorana fields in the flavor basis as

$$-\mathcal{L}^{\text{Maj.}}_{\text{AMM}} = \frac{1}{2}\bar{\nu}_\ell\left(\mu_{\ell\ell'}\frac{1}{2}\sigma_{\alpha\beta}F^{\alpha\beta}_{\text{ext}}\right)\nu_{\ell'} = -\frac{1}{2}\nu^{\text{T}}_{L,\ell}C^\dagger\left(\mu_{\ell\ell'}\frac{1}{2}\sigma_{\alpha\beta}F^{\alpha\beta}_{\text{ext}}\right)\nu_{L,\ell'} + \text{h.c.} \tag{3.9}$$

The operator $\sigma_{\alpha\beta}$ is the $4\times4$ spin tensor defined in Eq. (1.26). We would like to point out some interesting features of the Pauli term most notably that the spin tensor itself is not Hermitian with

$$\sigma^\dagger_{\alpha\beta} = \gamma_0\sigma_{\alpha\beta}\gamma_0\,. \tag{3.10}$$

However, the conjugate of the Lagrangian term in Eq. (3.9)

$$\left(\nu^\dagger\gamma_0\sigma_{\alpha\beta}F_{\rm ext}^{\alpha\beta}\nu\right)^\dagger = \nu^\dagger\sigma_{\alpha\beta}^\dagger F_{\rm ext}^{\alpha\beta}\gamma_0\nu = \nu^\dagger\gamma_0\sigma_{\alpha\beta}F_{\rm ext}^{\alpha\beta}\nu\,, \tag{3.11}$$

is Hermitian. More about the spin tensor's properties will be elaborated on in Section 3.1.

The Majorana magnetic moment matrix acts in flavor space. It satisfies the following constraints (Giunti and Studenikin, 2015) for CPT symmetry reasons and the anticommuting nature of fermions

$$\mu_{\ell\ell'}^\dagger = \mu_{\ell\ell'}\,, \qquad \mu_{\ell\ell'}^{\rm T} = -\mu_{\ell\ell'}\,, \tag{3.12}$$

*i.e.* the AMM matrix $\mu_{\ell\ell'}$ is Hermitian and fully anti-symmetric. This requires that the transition magnetic moment elements are purely imaginary while all diagonal AMM matrix elements vanish

$$\mu_{\ell\ell'} = \begin{pmatrix} \mu_{ee} & \mu_{e\mu} & \mu_{e\tau} \\ \mu_{\mu e} & \mu_{\mu\mu} & \mu_{\mu\tau} \\ \mu_{\tau e} & \mu_{\tau\mu} & \mu_{\tau\tau} \end{pmatrix} \xrightarrow{\text{Majorana}} \mu_{\ell\ell'} = \begin{pmatrix} 0 & i\mu_{e\mu} & -i\mu_{e\tau} \\ -i\mu_{e\mu} & 0 & i\mu_{\mu\tau} \\ i\mu_{e\tau} & -i\mu_{\mu\tau} & 0 \end{pmatrix}. \tag{3.13}$$

We can combine the mass term in Eq. (3.8) and AMM contribution in Eq. (3.9) into a single effective Lagrangian

$$\mathcal{L}_{\rm eff}^{\rm Maj.} = \mathcal{L}_{\rm kinetic}^{\rm Maj.} + \mathcal{L}_{\rm mass}^{\rm Maj.} + \mathcal{L}_{\rm AMM}^{\rm Maj.}\,, \tag{3.14}$$

$$\mathcal{L}_{\rm eff}^{\rm Maj.} = \mathcal{L}_{\rm kinetic}^{\rm Maj.} - \frac{1}{2}\bar{\nu}_\ell\left(M_{\ell\ell'} + \mu_{\ell\ell'}\frac{1}{2}\sigma_{\alpha\beta}F_{\rm ext}^{\alpha\beta}\right)\nu_{\ell'}\,. \tag{3.15}$$

Eq. (3.15) is our working Lagrangian. For later convenience we define the generalized mass-dipole matrix $\mathcal{M}_{\ell\ell'}$ present in Eq. (3.15) as

$$\mathcal{M}_{\ell\ell'}(\boldsymbol{E},\boldsymbol{B}) \equiv M_{\ell\ell'} + \mu_{\ell\ell'}\frac{1}{2}\sigma_{\alpha\beta}F_{\rm ext}^{\alpha\beta}\,, \qquad \mathcal{M}_{\ell\ell'}^\dagger = \gamma_0\mathcal{M}_{\ell\ell'}\gamma_0\,. \tag{3.16}$$

As neutrinos must propagate as energy eigenstates, our objective is to find the eigen-

values of Eq. (3.15) rather than Eq. (3.7). As the mass eigenvalues are modified by the presence the EM interactions $m \to \widetilde{m}(\boldsymbol{E}, \boldsymbol{B})$ so will the mixing matrix, leading to modifications of Eq. (3.4). These electromagnetic components then facilitate time-dependant oscillation among the free-particle mass eigenstates (Giunti and Studenikin, 2015).

Additionally we may consider matter effects via the weak interaction. Electron (anti)neutrinos passing through matter preferentially interact via weak charge-current (via the $W^{\pm}$ boson) with electrons which make up the bulk of charged leptons in most matter. The neutral-current (via the $Z_0$ boson) however affects all flavors and couples to the neutrons within the medium as the electron and proton contributions cancel in charge neutral matter. This can be represented, MSW effect aside, as the weak charge-current $V_{CC}$ and neutral-current $V_{NC}$ effective potentials (Pal, 1992; Greiner and Müller, 2009) which contribute to the action as

$$\mathcal{L}^{\text{Maj.}}_{\text{matter}} = \bar{\nu}_\ell(\gamma_0 V_{\ell\ell'})\nu_{\ell'}\,, \qquad V_{\ell\ell'} = \begin{pmatrix} V_{CC}+V_{NC} & 0 & 0 \\ 0 & V_{NC} & 0 \\ 0 & 0 & V_{NC} \end{pmatrix}, \tag{3.17}$$

$$V_{CC} = \sqrt{2}G_F\hbar^2c^2n_e\,, \qquad V_{NC} = -\frac{1}{2}\sqrt{2}G_F\hbar^2c^2n_n\,. \tag{3.18}$$

The coefficient $G_F$ is the Fermi constant, $n_e$ is the number density of electron matter and $n_n$ is the number density of neutrons within the medium. We note that $V_{\ell\ell'}\gamma_0$ behaves like the zeroth component of a vector-potential. As written, Eq. (3.17) is approximately true for non-relativistic matter.

### 3.2.2 Chiral properties of the relativistic Pauli dipole

While the Pauli dipole was introduced and discussed in Section 1.1.2, we will further elaborate on details directly relevant to neutrinos. The electromagnetic dipole behavior of the neutrino depends on mathematical properties of the tensor product $\sigma_{\alpha\beta}F^{\alpha\beta}_{\text{ext}}$. We prefer to work in the Weyl (chiral) spinor representation where the EM contribution is diagonal in spin space. Therefore we evaluate the product $\sigma_{\alpha\beta}F^{\alpha\beta}_{\text{ext}}$ in

the Weyl representation following Feynman and Gell-Mann (1958) yielding

$$-\frac{1}{2}\sigma_{\alpha\beta}F^{\alpha\beta}_{\rm ext} = \begin{pmatrix} \boldsymbol{\sigma}\cdot(\boldsymbol{B}+i\boldsymbol{E}/c) & 0 \\ 0 & \boldsymbol{\sigma}\cdot(\boldsymbol{B}-i\boldsymbol{E}/c) \end{pmatrix} \equiv \begin{pmatrix} \boldsymbol{\sigma}\cdot\boldsymbol{f}_+ & 0 \\ 0 & \boldsymbol{\sigma}\cdot\boldsymbol{f}_- \end{pmatrix}, \tag{3.19}$$

where we introduced the complex electromagnetic field form $\boldsymbol{f}_\pm = \boldsymbol{B} \pm i\boldsymbol{E}/c$ showing sensitivity to both magnetic and electric fields. The eigenvalues of Eq. (3.19) were also discussed in Section 2.4.1. As this expression is diagonal in the Weyl representation, it does not exchange handedness when acting upon a state. This is explicitly understood by the fact that Eq. (3.19) commutes with $\gamma^5$. Since left and right-handed neutrinos are not remixed by magnetic moments, sterile right-handed neutrinos do not need to be introduced. We can also see explicitly in Eq. (3.19) its non-Hermitian character, see Eq. (3.15), of the EM spin-field coupling. Specifically this is mirrored in the complex field's $\boldsymbol{f}_\pm$ relation to its complex conjugate $(\boldsymbol{f}_\pm)^* = \boldsymbol{f}_\mp$. The complex EM fields have a Hermitian ($\boldsymbol{B}$) and anti-Hermitian ($i\boldsymbol{E}$) part.

Taking the product of $\boldsymbol{f}_\pm$ with its complex conjugate we find

$$\frac{1}{2}\left(\boldsymbol{\sigma}\cdot\boldsymbol{f}_\pm\right)\left(\boldsymbol{\sigma}\cdot\boldsymbol{f}_\mp\right) = T^{00}_{\rm ext} \mp \sigma_i T^{0i}_{\rm ext}\,, \tag{3.20}$$

where we recognize the stress-energy tensor $T^{\alpha\beta}_{\rm ext}$ component $T^{00}_{\rm ext}$ for field energy density and $T^{0i}_{\rm ext}$ momentum density respectively

$$T^{00}_{\rm ext} = \frac{1}{2}\left(B^2 + E^2/c^2\right), \qquad T^{0i}_{\rm ext} = \frac{1}{c}\varepsilon_{ijk}E_jB_k\,. \tag{3.21}$$

As we will see in Section 3.3, Eq. (3.20) will appear in the EM-mass eigenvalues of our effective Lagrangian Eq. (3.14). Using the identity in Eq. (3.19) and Eq. (3.20) we also find the interesting relationship

$$\frac{1}{2}\left(\frac{1}{2}\sigma_{\alpha\beta}F^{\alpha\beta}_{\rm ext}\right)\left(\frac{1}{2}\sigma_{\alpha\beta}F^{\alpha\beta}_{\rm ext}\right)^\dagger = \gamma_0\left(T^{00}_{\rm ext}\gamma_0 + T^{0i}_{\rm ext}\gamma_i\right). \tag{3.22}$$

Now that we have elaborated on the relevant EM field identities, we turn back to the magnetic dipole and flavor rotation problem.

### 3.3 Electromagnetic-flavor mixing for two generations

Considering experimental data on neutrino oscillations, it is understood that either the two lighter (normal hierarchy) or the two heavier (inverted hierarchy) neutrino states are close together in mass. If the electromagnetic properties of the neutrino do indeed lead to flavor mixing effects, then it is likely the closer pair of neutrino mass states that are most sensitive to the phenomenon we explore. In the spirit of Bethe (1986), we therefore explore the $N = 2$ two generation $(\nu_e, \nu_\mu)$ toy model.

Following the properties established in Eq. (3.12) and Eq. (3.16) we write down the two generation mass and dipole matrices as

$$M_{\ell\ell'} = \begin{pmatrix} m_e^\nu & \delta m \\ \delta m & m_\mu^\nu \end{pmatrix}, \qquad \mu_{\ell\ell'} = \begin{pmatrix} 0 & i\delta\mu \\ -i\delta\mu & 0 \end{pmatrix}. \tag{3.23}$$

The AMM coupling $\delta\mu$ is taken to be real with a pure imaginary coefficient. While the mass elements $(m_e^\nu, m_\mu^\nu, \delta m)$ are generally complex, we choose in our toy model for them to be fully real

$$m_e^\nu = (m_e^\nu)^*, \qquad m_\mu^\nu = (m_\mu^\nu)^*, \qquad \delta m = \delta m^*, \tag{3.24}$$

making the mass matrix $M_{\ell\ell'}$ Hermitian. This allows us to more easily evaluate and emphasize the EM contributions to mixing rather than complications arising from the mass matrix.

Using Eq. (3.23) and Eq. (3.24), we write the mass-dipole matrix in Eq. (3.16) in terms of $2 \times 2$ flavor components as

$$\mathcal{M}_{\ell\ell'} = \begin{pmatrix} m_e^\nu & \delta m + i\delta\mu\sigma_{\alpha\beta}F_{\rm ext}^{\alpha\beta}/2 \\ \delta m - i\delta\mu\sigma_{\alpha\beta}F_{\rm ext}^{\alpha\beta}/2 & m_\mu^\nu \end{pmatrix}, \qquad \mathcal{M}_{\ell\ell'}^\dagger = \gamma_0\mathcal{M}_{\ell\ell'}\gamma_0\,. \tag{3.25}$$

As noted before, this matrix is not Hermitian due to the inclusion of the spin tensor, therefore it is not guaranteed to satisfy an algebraic eigenvalue equation in its present form which is a requirement for well behaved masses.

This can be remedied by recalling that any arbitrary complex matrix can be diagonalized into its real eigenvalues $\lambda_j$ by the biunitary transform

$$W^{\dagger}_{\ell j}\mathcal{M}_{\ell\ell'}Y_{\ell' j'} = \lambda_j \delta_{jj'}\,, \tag{3.26}$$

where $Y_{\ell j}$ and $W_{\ell j}$ are both unitary matrices. Taking the complex conjugate of Eq. (3.26), we arrive at

$$(W^{\dagger}_{\ell j}\mathcal{M}_{\ell\ell'}Y_{\ell' j'})^{\dagger} = Y^{\dagger}_{\ell j'}\gamma_0\mathcal{M}_{\ell\ell'}\gamma_0 W_{\ell' j} = \lambda_j\delta_{jj'}\,, \tag{3.27}$$

$$Y_{\ell j} = \gamma_0 W_{\ell j} \rightarrow W^{\dagger}_{\ell j}\mathcal{M}_{\ell\ell'}\gamma_0 W_{\ell' j'} = \lambda_j\delta_{jj'}\,. \tag{3.28}$$

As $Y_{\ell j}$ and $W_{\ell j}$ are related by a factor of $\gamma_0$ based on the conjugation properties of Eq. (3.25), this lets us eliminate $Y_{\ell j}$ and diagonalize using a single unitary matrix $W_{\ell j}$. The related matrix $\mathcal{M}_{\ell\ell'}\gamma_0$ is Hermitian

$$(\mathcal{M}_{\ell\ell'}\gamma_0)^{\dagger} = \mathcal{M}_{\ell\ell'}\gamma_0\,, \tag{3.29}$$

and also equivalent to the root of the Hermitian product of Eq. (3.25)

$$(\mathcal{M}\mathcal{M}^{\dagger})_{\ell\ell'} = ((\mathcal{M}\gamma_0)(\mathcal{M}\gamma_0))_{\ell\ell'}\,. \tag{3.30}$$

Therefore a suitable unitary transformation $W_{\ell j}$ rotates flavor $\ell$-states into magnetized mass $j$-states. The eigenvalues $\lambda_j^2$ of $(\mathcal{M}\mathcal{M}^{\dagger})_{\ell\ell'}$ are the squares of both signs of the eigenvalues of $\mathcal{M}_{\ell\ell'}\gamma_0$. We write this property (with flavor indices suppressed) as

$$W^{\dagger}(\mathcal{M}\mathcal{M}^{\dagger})W = W^{\dagger}(\mathcal{M}\gamma_0)WW^{\dagger}(\mathcal{M}\gamma_0)W = \mathrm{diag}(\lambda_1^2, \lambda_2^2)\,. \tag{3.31}$$

We associate $\lambda_j = \widetilde{m}_j(\boldsymbol{E}, \boldsymbol{B})$ with $j \in 1, 2$ as the effective EM-mass states which are field dependant in this basis.

### 3.3.1 Separating electromagnetic-mass mixing into two rotations

The matrix $W_{\ell j}$ mixes flavor states into a new basis distinct from the free-particle case however this rotation must smoothly connect with the free-particle case in the limit that the electromagnetic fields go to zero. We proceed to evaluate $W_{\ell j}$ breaking the rotation into two separate unitary transformations:

a. Rotation matrix $V^{\dagger}_{\ell k}(\ell \to k)$ converting from flavor to free-particle mass

b. Rotation matrix $Z^{\text{ext}\dagger}_{kj}(k \to j)$ converting from free-particle mass to EM-mass

Guided by Eq. (3.2) we write

$$\nu_j = W^{\dagger}_{\ell j}\nu_\ell = Z^{\text{ext}\dagger}_{kj}V^{\dagger}_{\ell k}\nu_\ell \,. \tag{3.32}$$

In the limit that the EM fields go to zero, the electromagnetic rotation becomes unity $Z^{\text{ext}}_{kj} \to \delta_{kj}$ thereby ensuring the EM-mass basis and free-particle mass basis become equivalent. The rotation $Z^{\text{ext}}_{kj}$ can then be interpreted as the external field forced rotation. While our argument above is done explicitly for the two generation case, it can be generalized to accommodate three generations of neutrinos as well.

According to Eq. (3.7), the mass matrix in Eq. (3.23) can be diagonalized in the two generation case by a one parameter unitary mixing matrix $V_{\ell k}$ given by

$$V_{\ell k}(\theta) = \begin{pmatrix} \cos\theta & \sin\theta \\ -\sin\theta & \cos\theta \end{pmatrix} . \tag{3.33}$$

For a real Hermitian $2 \times 2$ mass matrix, the rotation matrix $V_{\ell k}$ is real and only depends on the angle $\theta$. The explicit form of the EM-field related rotation $Z^{\text{ext}}_{kj}$ introduced in Eq. (3.32) is

$$Z^{\text{ext}}_{kj}(\omega,\phi) = \begin{pmatrix} \cos\omega & e^{i\phi}\sin\omega \\ -e^{-i\phi}\sin\omega & \cos\omega \end{pmatrix} , \qquad W_{\ell j}(\theta,\omega,\phi) = V_{\ell k}(\theta)Z^{\text{ext}}_{kj}(\omega,\phi) \,, \tag{3.34}$$

where $Z^{\text{ext}}_{kj}$ depends on the real angle $\omega$ and complex phase $\phi$. The full rotation $W_{\ell j}$ therefore depends on three parameters when broken into free-particle rotation and

EM rotation.

The eigenvalues of the original Hermitian mass matrix in Eq. (3.23) are given by

$$m_{1,2} = \frac{1}{2}\left(m_e^\nu + m_\mu^\nu \mp \sqrt{|\Delta m_0|^2 + 4\delta m^2}\right), \qquad |\Delta m_0| = |m_\mu^\nu - m_\mu^e|\,. \tag{3.35}$$

We assign $m_1$ to the lower mass $(-)$ root and $m_2$ with the larger mass $(+)$ additive root. The rotation angle $\theta$ in Eq. (3.33) is then given by

$$\sin 2\theta = \sqrt{\frac{4\delta m^2}{|\Delta m_0|^2 + 4\delta m^2}}\,, \qquad \cos 2\theta = \sqrt{\frac{|\Delta m_0|^2}{|\Delta m_0|^2 + 4\delta m^2}}\,. \tag{3.36}$$

In our toy model, the off-diagonal imaginary transition magnetic moment $\mu_{\ell\ell'}$ commutes with the real valued mixing matrix $V_{\ell k}$ and the following relations hold

$$V_{\ell k}^\dagger \mu_{\ell\ell'} V_{\ell' k'} = (V^\dagger V)_{k\ell'}\mu_{\ell' k'} = \mu_{kk'} = \begin{pmatrix} 0 & i\delta\mu \\ -i\delta\mu & 0 \end{pmatrix}. \tag{3.37}$$

We see that the Majorana transition dipoles in our model are off-diagonal in both flavor and mass basis. Therefore the real parameter unitary matrix in Eq. (3.37) cannot rotate a pure imaginary matrix at least in the two generation case. We apply the rotation in Eq. (3.33) to Eq. (3.29) yielding

$$V_{\ell k}^\dagger(\mathcal{M}_{\ell\ell'}\gamma_0)V_{\ell' k'} = V_{\ell k}^\dagger M_{\ell\ell'}\gamma_0 V_{\ell' k'} + V_{\ell k}^\dagger(\mu_{\ell\ell'}\sigma_{\alpha\beta}\gamma_0 F_{\rm ext}^{\alpha\beta}/2)V_{\ell' k'}\,, \tag{3.38}$$

$$V_{\ell k}^\dagger(\mathcal{M}_{\ell\ell'}\gamma_0)V_{\ell' k'} = \begin{pmatrix} m_1\gamma_0 & i\delta\mu\sigma_{\alpha\beta}\gamma_0 F_{\rm ext}^{\alpha\beta}/2 \\ -i\delta\mu\sigma_{\alpha\beta}\gamma_0 F_{\rm ext}^{\alpha\beta}/2 & m_2\gamma_0 \end{pmatrix} \equiv \begin{pmatrix} \mathcal{A} & i\mathcal{C} \\ -i\mathcal{C} & \mathcal{B} \end{pmatrix}, \tag{3.39}$$

where we have defined implicitly the Hermitian elements $(\mathcal{A}, \mathcal{B}, \mathcal{C})$. Applying now both rotations to Eq. (3.29) yields

$$W_{\ell j}^\dagger(\mathcal{M}_{\ell\ell'}\gamma_0)W_{\ell' j'} = Z^{\rm ext\dagger}\begin{pmatrix} \mathcal{A} & i\mathcal{C} \\ -i\mathcal{C} & \mathcal{B} \end{pmatrix} Z^{\rm ext} = \lambda_j\delta_{jj'}\,. \tag{3.40}$$

Eq. (3.40) is therefore the working matrix equation which needs to be solved to identify

the EM rotation parameters. As discussed before, this means that the rotation angle $\omega$ and phase $\phi$ are in general functions of electromagnetic fields.

### 3.3.2 Effective electromagnetic-mass eigenvalues

We will now solve for the rotation parameters necessary to define the EM-mass basis which acts as a distinct propagating basis for neutrinos in external fields. Considering that the $j$-columns vectors $\boldsymbol{v}^{(j)}$ of $Z^{\rm ext}_{kj}$ as eigenvectors for each eigenvalue $\lambda_j$

$$Z^{\rm ext}_{kj} = v^{(j)}_k = \begin{pmatrix} \boldsymbol{v}^1 & \boldsymbol{v}^2 \end{pmatrix} , \tag{3.41}$$

Eq. (3.40) has the meaning of an eigenvalue equation

$$\begin{pmatrix} \mathcal{A} & i\mathcal{C} \\ -i\mathcal{C} & \mathcal{B} \end{pmatrix} Z^{\rm ext} = Z^{\rm ext} \begin{pmatrix} \lambda_1 & 0 \\ 0 & \lambda_2 \end{pmatrix} \rightarrow \begin{pmatrix} \mathcal{A} & i\mathcal{C} \\ -i\mathcal{C} & \mathcal{B} \end{pmatrix} \boldsymbol{v}^{(j)} = \lambda_j \boldsymbol{v}^{(j)} . \tag{3.42}$$

Given the eigenvalue equation defined in Eq. (3.42), the effective EM-masses are then solutions to the characteristic polynomial

$$(\mathcal{A} - \lambda_j \gamma_0)(\mathcal{B} - \lambda_j \gamma_0) - \mathcal{C}^2 = 0 , \tag{3.43}$$

which we obtained by taking the determinant of Eq. (3.42) over flavor but not spin space. It is useful to define the following identities for the off-diagonal element

$$\mathcal{C}^2 = \delta\mu^2 \left(\frac{1}{2}\sigma_{\alpha\beta}F^{\alpha\beta}_{\rm ext}\right)\left(\frac{1}{2}\sigma_{\alpha\beta}F^{\alpha\beta}_{\rm ext}\right)^\dagger = 2\delta\mu^2\gamma_0\left(T^{00}_{\rm ext}\gamma_0 + T^{0i}_{\rm ext}\gamma_i\right) , \tag{3.44}$$

and for the diagonal elements

$$(\mathcal{B} - \mathcal{A})^2 = |m_2 - m_1|^2 = |\Delta m|^2 , \qquad (\mathcal{A} + \mathcal{B})\gamma_0 = m_1 + m_2 . \tag{3.45}$$

Eq. (3.44) was obtained using the expression in Eq. (3.22). Because of the spinor behavior of each element, the eigenvalues are obtained with $\gamma_0$ coefficients. Eq. (3.43)

therefore has the roots $\lambda_{1,2} = \widetilde{m}_{1,2}(\boldsymbol{E},\boldsymbol{B})$

$$\widetilde{m}_{1,2}(\boldsymbol{E},\boldsymbol{B}) = \frac{1}{2}\left(m_1+m_2 \mp \sqrt{|\Delta m|^2+8\delta\mu^2\gamma_0\left(T^{00}_{\rm ext}\gamma_0 + T^{0i}_{\rm ext}\gamma_i\right)}\right), \tag{3.46}$$

$$\boxed{\widetilde{m}_{1,2}(\boldsymbol{E},\boldsymbol{B}) = \frac{m_1+m_2}{2} \mp \frac{1}{2}\sqrt{|\Delta m|^2+8\delta\mu^2\gamma_0\left(\gamma_0\frac{1}{2}\left(B^2+\frac{E^2}{c^2}\right)+\boldsymbol{\gamma}\cdot\left(\frac{\boldsymbol{E}}{c}\times\boldsymbol{B}\right)\right)}} \tag{3.47}$$

The EM-mass eigenstates $\widetilde{m}(\boldsymbol{E},\boldsymbol{B})$ depends on the energy density $T^{00}_{\rm ext}$ of the EM field and the spin projection along the EM momentum density $T^{0i}_{\rm ext}$. However the coefficient $\delta\mu^2$ is presumed to be very small, therefore the EM contribution only manifests in strong EM fields or where the free-particle case has very nearly or exactly degenerate masses, $\Delta m \to 0$. When the the electromagnetic fields go to zero, the EM-masses in Eq. (3.47) reduce as expected to the free-particle result.

The complex phase in Eq. (3.34) has the value $\phi = \pi(n-1/2)$ with $n \in 0, \pm1, \pm2...$ making the complex exponential in Eq. (3.34) pure imaginary. Curiously, the phase is not field dependant, but tied to the fact that the Majorana moments are pure imaginary quantities. Complex phases in mixing matrices are generally associated with CP violation such as the Dirac phase $\delta$ in Eq. (3.3) which suggests that CP violation in the neutrino sector can be induced in the presence of external EM fields. Some implications of CP violation from transition moments are discussed in Nieves (1982). Analysis of the three generation case is required to show this explicitly, but we postulate that the constant valued complex phases would be replaced with field dependant quantities $\delta \to \delta(\boldsymbol{E},\boldsymbol{B})$.

We note that the solution in Eq. (3.47) actually contain four distinct EM-mass eigenstates $\widetilde{m}^s_j(\boldsymbol{E},\boldsymbol{B})$ with the lower ($j = 1$) and upper ($j = 2$) masses and the additional spin splitting from the alignment ($s = +1$) or anti-alignment ($s = -1$) of the neutrino spin with the momentum density of the external EM field. Spin splitting vanishes for the pure electric or magnetic field cases. For good spin eigenstates $s \in \pm1$,

we can rewrite Eq. (3.44) with EM fields explicitly as

$$\mathcal{C}_s^2(\boldsymbol{E},\boldsymbol{B}) = 2\delta\mu^2\left(\frac{1}{2}(B^2+E^2/c^2)+s|\boldsymbol{E}/c\times\boldsymbol{B}|\right). \tag{3.48}$$

The above expression within the square is positive definite, therefore Eq. (3.48) is always real. Spin splitting requires that we consider separate rotations for each spin state as the rotation angle $\omega_s$ depends on the spin quantum number

$$\sin 2\omega_s = \sqrt{\frac{4\mathcal{C}_s^2}{|\Delta m|^2+4\mathcal{C}_s^2}}\,, \qquad \cos 2\omega_s = \sqrt{\frac{|\Delta m|^2}{|\Delta m|^2+4\mathcal{C}_s^2}}\,. \tag{3.49}$$

The expressions in Eq. (3.49) are mathematically similar to that of the free-particle case written in Eq. (3.36) in the two flavor generation model with the off-diagonal mass being replaced with the EM dependant quantity $\mathcal{C}_s$.

### 3.4 Strong field (degenerate mass) and weak field limits

The rotation angles in Eq. (3.49) reveal two distinct limits where EM-masses are dominated by either:

a. Intrinsic mass splitting $\mathcal{C}_s \ll |\Delta m|^2$ with $\omega_s \to 0$

b. EM mass splitting $\mathcal{C}_s \gg |\Delta m|^2$ with $\omega_s \to \pi/4$

For the first case where the masses are not degenerate or the fields are weak, we obtain the expansion

$$\lim_{\mathcal{C}_s\ll|\Delta m|^2} \widetilde{m}^s_{1,2}(E,B) = \frac{1}{2}\left(m_1+m_2 \mp |\Delta m|\left(1+\frac{2\mathcal{C}_s^2}{|\Delta m|^2}+\ldots\right)\right), \tag{3.50}$$

which as stated before reduces to the free-particle case at lowest order.

In the opposite limit, where the masses are very nearly degenerate or fields are strong, the EM-mass eigenvalues in Eq. (3.47) can be approximated by the series

$$\lim_{\mathcal{C}_s\gg|\Delta m|^2} \widetilde{m}^s_{1,2}(E,B) = \frac{1}{2}\left(m_1+m_2 \mp 2\mathcal{C}_s\left(1+\frac{|\Delta m|^2}{8\mathcal{C}_s^2}+\ldots\right)\right) \tag{3.51}$$

For fully degenerate free-particle masses $m_1 = m_2$, this reduces to

$$\lim_{|\Delta m|^2 \to 0} \widetilde{m}^s_{1,2}(E, B) = m_1 \mp \mathcal{C}_s \,. \tag{3.52}$$

Eq. (3.52) indicates that for degenerate free-particle masses, the effective splitting $|\Delta m_{\rm EM}| \equiv \mathcal{C}_s$ between masses arises purely from the electromagnetic interaction of the neutrinos. We return to this interesting insight in our final comments.

Because of the bounds in Eq. (3.1) on the effective neutrino magnetic moment, we can estimate the field strength required for an external magnetic field to generate an electromagnetic mass splitting of $|\Delta m_{\rm EM}| = 10^{-3}$ eV which is a reasonable comparison to intrinsic splitting based on the experimental limits on neutrino masses. Using the upper limit for the neutrino effective moment of $\mu_\nu^{\rm eff} \sim 10^{-10}\mu_B$ we obtain

$$\left.\frac{\mathcal{C}_s}{\mu_\nu^{\rm eff}}\right|_{\vec{E}=0} = \frac{10^{-3}\,{\rm eV}}{10^{-10}\mu_B} \approx 1.7 \times 10^{11}\,{\rm T}\,. \tag{3.53}$$

This is near the upper bound of the magnetic field strength of magnetars (Kaspi and Beloborodov, 2017) which are of the order $10^{11}$ Tesla. In this situation, the EM contribution to the mass splitting rivals the estimated inherent splitting (Workman et al., 2022) of the two closer in mass neutrinos. Primordial magnetic fields (Grasso and Rubinstein, 2001) in the Early Universe may also present an environment for significant EM neutrino flavor mixing as both the external field strength and density of neutrinos would be very large (Rafelski et al., 2023a). The magnetic properties of neutrinos may also have contributed alongside the charged leptons in magnetization in the Early Universe (Steinmetz et al., 2023) prior to recombination.

While the above estimate was done with astrophysical systems in mind, we note that strong electrical fields should also produce EM-mass splitting. Therefore environments near to high $Z$-nuclei is also of interest (Bouchiat and Bouchiat, 1974, 1997; Safronova et al., 2018) as weak interactions violate parity. Should neutrinos have abnormally large transition magnetic dipole moments, then they should exhibit mass splitting from the neutrino's electromagnetic dipole interaction which may compete with the intrinsic mass differences of the free-particles.

# CHAPTER 4

## Matter-antimatter origin of cosmic magnetism

We investigate the hypothesis that the observed intergalactic magnetic fields (IGMF) are primordial in nature, predating the recombination epoch. Specifically, we explore the role of the extremely large electron-positron ($e^+e^-$) pair abundance in the temperature range of 2000 keV $> T >$ 20 keV which only disappeared after Big Bang nucleosynthesis (BBN). We review the status of cosmic magnetism in Section 4.1 which motivates our study. Section 4.4 describes the relativistic paramagnetism of the electron-positron gas. We then propose in Section 4.5.1 a model of self-magnetization caused by spin polarization within the individual species in the gas.

This chapter serves primarily as a review of our work in Steinmetz et al. (2023) and portions of Rafelski et al. (2023a) where we propose that the early universe electron-positron plasma was a highly magnetized environment. We will use natural units ($c = \hbar = k_B = 1$) unless otherwise noted.

**NOTE: The letter $\mu$ within this chapter will refer exclusively to charged chemical potential and *not* magnetic moment as before.**

### 4.1 Short survey of magnetism in the universe

Macroscopic domains of magnetic fields have been found in all astrophysical environments from compact objects (stars, planets, etc.); interstellar and intergalactic space; and surprisingly in deep extra-galactic void spaces. Considering the ubiquity of magnetic fields in the universe (Giovannini, 2018, 2004; Kronberg, 1994), we search for a common primordial mechanism initiate the diversity of magnetism observed today. In this chapter, IGMF will refer to experimentally observed intergalactic fields of any origin while primordial magnetic fields (PMF) refers to fields generated via early universe processes possibly as far back as inflation. The conventional elaboration of the

origins for cosmic PMFs are detailed in (Gaensler et al., 2004; Durrer and Neronov, 2013; Batista and Saveliev, 2021).

IGMF are notably difficult to measure and difficult to explain. The bounds for IGMF at a length scale of 1 Mpc are today (Neronov and Vovk, 2010; Taylor et al., 2011; Pshirkov et al., 2016; Jedamzik and Saveliev, 2019; Vernstrom et al., 2021)

$$10^{-8}\ \mathrm{G} > B_{\mathrm{IGMF}} > 10^{-16}\ \mathrm{G}\,. \tag{4.1}$$

We note that generating PMFs with such large coherent length scales is nontrivial (Giovannini, 2023) though currently the length scale for PMFs are not well constrained (Batista and Saveliev, 2021). Faraday rotation from distant radio active galaxy nuclei (AGN) (Pomakov et al., 2022) suggest that neither dynamo nor astrophysical processes would sufficiently account for the presence of magnetic fields in the universe today if the IGMF strength was around the upper bound of $B_{\mathrm{IGMF}} \simeq 30-60$ nG as found in Vernstrom et al. (2021). Such strong magnetic fields would then require that at least some portion of the IGMF arise from primordial sources that predate the formation of stars.

Magnetized baryon inhomogeneities which in turn would produce anisotropies in the cosmic microwave background (CMB) (Jedamzik and Abel, 2013; Abdalla et al., 2022). Jedamzik and Pogosian (2020) propose further that the presence of a magnetic field of $B_{\mathrm{PMF}} \simeq 0.1$ nG could be sufficient to explain the Hubble tension.

Our motivating hypothesis is outlined qualitatively in Figure 4.1 where PMF evolution is plotted over the temperature history of the universe. The descending blue band indicates the range of possible PMF strengths. The different epochs of the universe according to ΛCDM are delineated by temperature. The horizontal lines mark two important scales: (a) the Schwinger critical field strength given by

$$B_{\mathrm{C}} = \frac{m_e^2}{e} \simeq 4.41 \times 10^{13}\,\mathrm{G}\,. \tag{4.2}$$

where electrodynamics is expected to display nonlinear characteristics and (b) the upper field strength seen in magnetars of $\sim 10^{15}$ G. A schematic of magnetogenesis

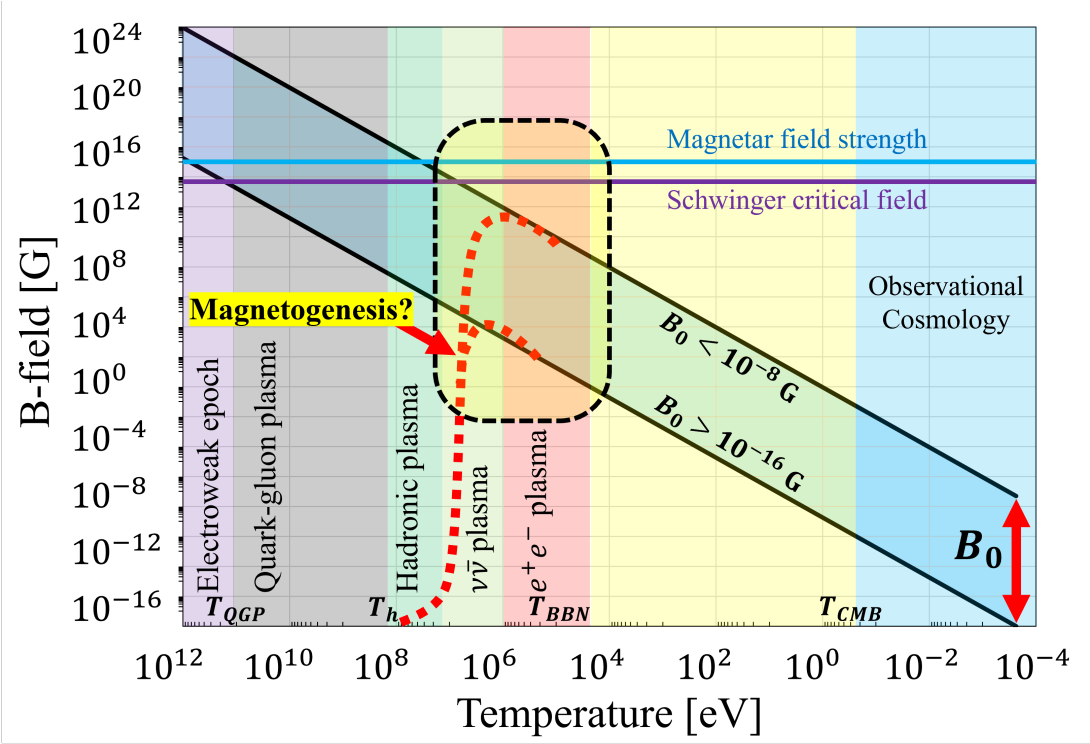


Figure 4.1: Qualitative plot of the primordial magnetic field strength over cosmic time. All figures are printed in temporal sequence in the expanding universe beginning with high temperatures (and early times) on the left and lower temperatures (and later times) on the right.

is drawn with the dashed red lines indicating spontaneous formation of the PMF within the early universe plasma itself. The $e^+e^-$ era is notably the final epoch where antimatter exists in large quantities in the cosmos (Rafelski et al., 2023a).

## 4.2 Electron-positron abundance

As the universe cooled below temperature $T = m_e$ (the electron mass), the thermal electron and positron comoving density depleted by over eight orders of magnitude. At $T_{\text{split}} = 20.3$ keV, the charged lepton asymmetry (mirrored by baryon asymmetry and enforced by charge neutrality) became evident as the surviving excess electrons persisted while positrons vanished entirely from the particle inventory of the universe due to annihilation.

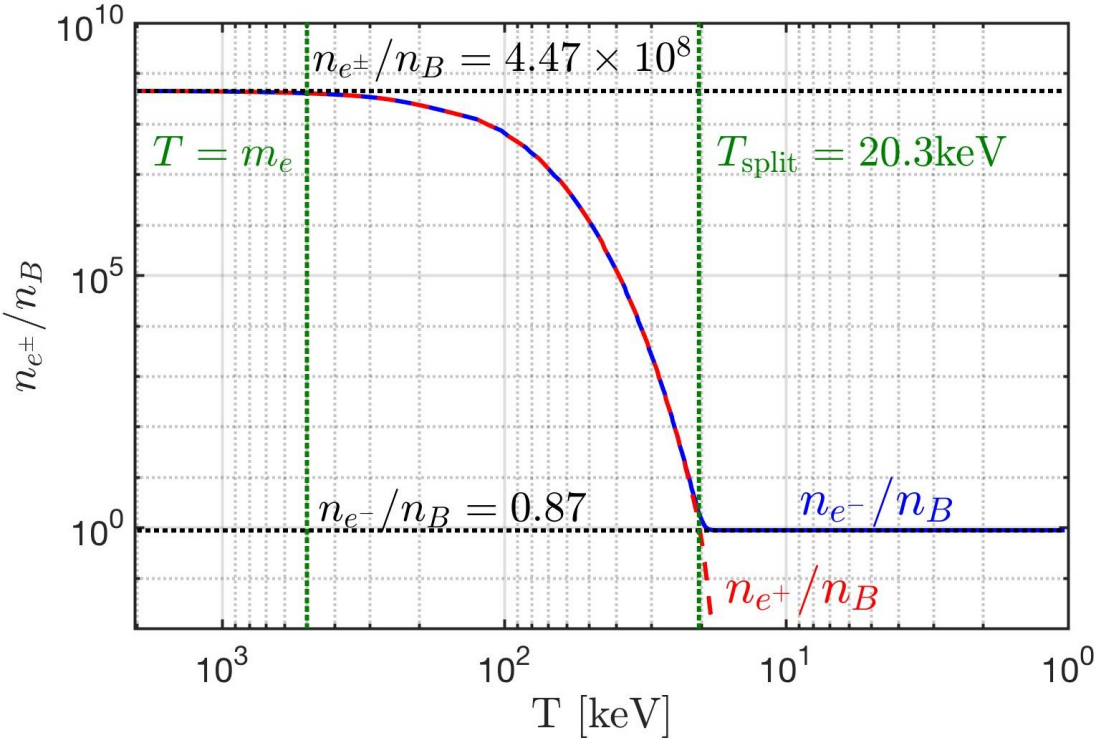


Figure 4.2: Number density of electron $e^-$ and positron $e^+$ to baryon ratio $n_{e^\pm}/n_B$ as a function of photon temperature in the universe. See text for further details. In this work we measure temperature in units of energy (keV) thus we set the Boltzmann constant to $k_B = 1$. Figure courtesy of Cheng Tao Yang.

The electron-to-baryon density ratio $n_{e^-}/n_B$ is shown in Figure 4.2 as the solid blue line while the positron-to-baryon ratio $n_{e^+}/n_B$ is represented by the dashed red line. These two lines overlap until the temperature drops below $T_{\rm split} = 20.3$ keV as positrons vanish from the universe marking the end of the $e^+e^-$ plasma and the dominance of the electron-proton ($e^-p$) plasma. The two vertical dashed green lines denote temperatures $T = m_e \simeq 511$ keV and $T_{\rm split} = 20.3$ keV. These results were obtained using charge neutrality and the baryon-to-photon content (entropy) of the universe; see details in Rafelski et al. (2023a). The two horizontal black dashed lines denote the relativistic $T \gg m_e$ abundance of $n_{e^\pm}/n_B = 4.47 \times 10^8$ and post-annihilation abundance of $n_{e^-}/n_B = 0.87$. Above temperature $T \simeq 85$ keV, the $e^+e^-$ primordial plasma density exceeded that of the Sun's core density $n_e \simeq 6 \times 10^{26}$ cm$^{-3}$ (Bahcall et al., 2001).

Conversion of the dense $e^+e^-$ pair plasma into photons reheated the photon background (Birrell et al., 2014) separating the photon and neutrino temperatures. The $e^+e^-$ annihilation and photon reheating period lasted no longer than an afternoon lunch break. Because of charge neutrality, the post-annihilation comoving ratio $n_{e^-}/n_B = 0.87$ (Rafelski et al., 2023a) is slightly offset from unity in Figure 4.2 by the presence of bound neutrons in $\alpha$ particles and other neutron containing light elements produced during BBN epoch.

The abundance of baryons is itself fixed by the known abundance relative to photons (Workman et al., 2022) and we employed the contemporary recommended value $n_B/n_\gamma = 6.09 \times 10^{-10}$. The resulting chemical potential needs to be evaluated carefully to obtain the behavior near to $T_{\rm split} = 20.3$ keV where the relatively small value of chemical potential $\mu$ rises rapidly so that positrons vanish from the particle inventory of the universe while nearly one electron per baryon remains. The detailed solution of this problem is found in Fromerth et al. (2012); Rafelski et al. (2023a) leading to the results shown in Figure 4.2.

## 4.3 Theory of thermal matter-antimatter plasmas

To evaluate magnetic properties of the thermal $e^+e^-$ pair plasma we take inspiration from Ch. 9 of Melrose's treatise on magnetized plasmas (Melrose, 2013). We focus on the bulk properties of thermalized plasmas in (near) equilibrium.

We consider a homogeneous magnetic field domain defined along the $z$-axis as

$$\boldsymbol{B} = (0,\, 0,\, B)\,, \tag{4.3}$$

with magnetic field magnitude $|\boldsymbol{B}| = B$. Following Chapter 2, we reprint the microscopic energy (Eq. (2.16) in different notation) of the charged relativistic fermion within a homogeneous magnetic field given by

$$E^n_{\sigma,s}(p_z, B) = \sqrt{m_e^2 + p_z^2 + eB\left(2n + 1 + \frac{g}{2}\sigma s\right)}\,, \tag{4.4}$$

where $n \in 0, 1, 2, \ldots$ is the Landau orbital quantum number, $p_z$ is the momentum parallel to the field axis and the electric charge is $e \equiv q_{e^+} = -q_{e^-}$. The index $\sigma$ in Eq. (4.4) differentiates electron ($e^-$; $\sigma = +1$) and positron ($e^+$; $\sigma = -1$) states. The index $s$ refers to the spin along the field axis: parallel ($\uparrow$; $s = +1$) or anti-parallel ($\downarrow$; $s = -1$) for both particle and antiparticle species.

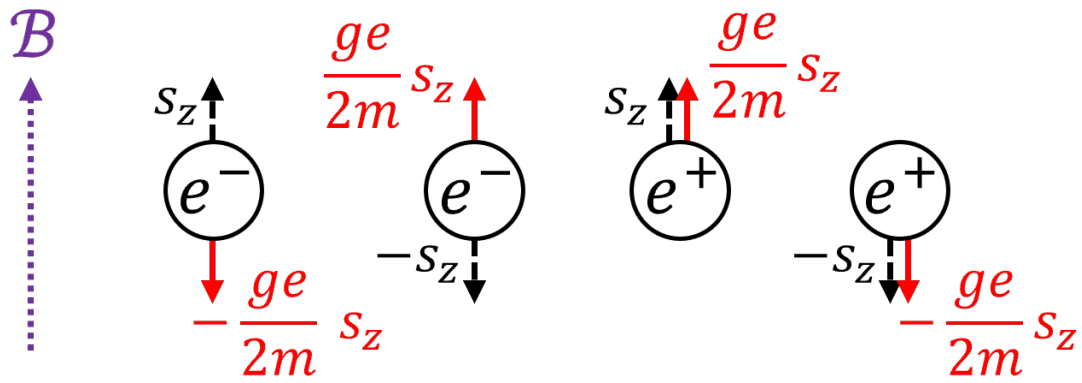


| | aligned: $s = +1$ | anti-aligned: $s = -1$ |
|---|---|---|
| electron: $\sigma = +1$ | $U_{\rm Mag} > 0$ | $U_{\rm Mag} < 0$ |
| positron: $\sigma = -1$ | $U_{\rm Mag} < 0$ | $U_{\rm Mag} > 0$ |

Figure 4.3: Organizational schematic of matter-antimatter ($\sigma$) and polarization ($s$) states with respect to the sign of the non-relativistic magnetic dipole energy $U_{\rm Mag}$ obtainable from Eq. (4.4).

The reason Eq. (4.4) distinguishes between electrons and positrons is to ensure the correct non-relativistic limit for the magnetic dipole energy is reached. Following the conventions found in Tiesinga et al. (2021), we set the gyro-magnetic factor $g \equiv g_{e^+} = -g_{e^-} > 0$ such that electrons and positrons have opposite $g$-factors and opposite magnetic moments relative to their spin; see Figure 4.3.

We recall the conventions established in Section 1.3. Conservation of magnetic flux requires that the magnetic field through a comoving surface $L_0^2$ remain unchanged. The magnetic field strength under expansion (Durrer and Neronov, 2013) starting at some initial time $t_0$ is then given by

$$B(t) = B_0 \frac{a_0^2}{a^2(t)} \rightarrow B(z) = B_0 \, (1+z)^2 \ , \tag{4.5}$$

where $B_0$ is the comoving value obtained from the contemporary value of the magnetic field today. Magnetic fields in the cosmos generated through mechanisms such as dynamo or astrophysical sources do not follow this scaling (Pomakov et al., 2022). It is only in deep intergalactic space where matter density is low are magnetic fields preserved (and thus uncontaminated) over cosmic time.

From Eq. (1.67) and Eq. (4.5) there emerges a natural ratio of interest which is conserved over cosmic expansion

$$b \equiv \frac{eB(t)}{T^2(t)} = \frac{eB_0}{T_0^2} \equiv b_0 = \text{ const.} \tag{4.6}$$

$$10^{-3} > b_0 > 10^{-11}\,, \tag{4.7}$$

given in natural units ($c = \hbar = k_B = 1$). We computed the bounds for this cosmic magnetic scale ratio by using the present day IGMF observations given by Eq. (4.1) and the present CMB temperature $T_0 = 2.7$ K $\simeq 2.3 \times 10^{-4}$ eV (Aghanim et al., 2020).

### 4.3.1 Eigenstatess of magnetic moment in cosmology

As statistical properties depend on the characteristic Boltzmann factor $E/T$, another interpretation of Eq. (4.6) in the context of energy eigenvalues (such as those given in Eq. (4.4)) is the preservation of magnetic moment energy relative to momentum under adiabatic cosmic expansion. The Boltzmann statistical factor is given by

$$x \equiv \frac{E}{T}\,. \tag{4.8}$$

We can explore this relationship for the magnetized system explicitly by writing out Eq. (4.8) using the KGP energy eigenvalues written in Eq. (4.4) as

$$x^n_{\sigma,s} = \frac{E^n_{\sigma,s}}{T} = \sqrt{\frac{m_e^2}{T^2} + \frac{p_z^2}{T^2} + \frac{eB}{T^2}\left(2n + 1 + \frac{g}{2}\sigma s\right)}\,. \tag{4.9}$$

Introducing the expansion scale factor $a(t)$ via Eq. (1.67), Eq. (4.5) and Eq. (4.6).

The Boltzmann factor can then be written as

$$x^n_{\sigma,s}(a(t)) = \sqrt{\frac{m_e^2}{T^2(t_0)}\frac{a(t)^2}{a_0^2} + \frac{p_{z,0}^2}{T_0^2} + \frac{eB_0}{T_0^2}\left(2n+1+\frac{g}{2}\sigma s\right)}\,. \tag{4.10}$$

This reveals that only the mass contribution is dynamic over cosmological time. The constant of motion $b_0$ defined in Eq. (4.6) is seen as the coefficient to the Landau and spin portion of the energy. For any given eigenstate, the mass term drives the state into the non-relativistic limit while the momenta and magnetic contributions are frozen by initial conditions.

As a point of comparison, the Boltzmann factor for the DP energy eigenvalues are given by

$$x^n_{\sigma,s}|_{\rm DP} = \sqrt{\left(\sqrt{\frac{m_e^2}{T^2} + \frac{eB}{T^2}\left(2n+1+\sigma s\right)} + \frac{eB}{2m_eT}\left(\frac{g}{2}-1\right)\sigma s\right)^2 + \frac{p_z^2}{T^2}}\,, \tag{4.11}$$

which scales during FLRW expansion as

$$x^n_{\sigma,s}(a(t))|_{\rm DP} = \sqrt{\left(\sqrt{\frac{m_e^2}{T_0^2}\frac{a(t)^2}{a_0^2} + \frac{eB_0}{T_0^2}\left(2n+1+\sigma s\right)} + \frac{eB_0}{2m_eT_0}\frac{a_0}{a(t)}\left(\frac{g}{2}-1\right)\sigma s\right)^2 + \frac{p_{z,0}^2}{T_0^2}}\,. \tag{4.12}$$

While the above expression is rather complicated, we note that the KGP Eq. (4.10) and DP Eq. (4.11) Boltzmann factors both reduce to the Schödinger-Pauli limit as $a(t) \to \infty$ thereby demonstrating that the total magnetic moment is protected under the adiabatic expansion of the universe.

Higher order non-minimal magnetic contributions which can be introduced to the energies such as $\sim \mu_B^2 B^2/T^2$ are then suppressed over cosmological time driving the system into minimal electromagnetic coupling with the exception of the anomalous magnetic moment. It is interesting to note that cosmological expansion serves to 'smooth out' the characteristics of more complex BSM electrodynamics erasing them from a statistical perspective in favor of the minimal or minimal-like dynamics.

### 4.3.2 Magnetized fermion partition function

To obtain a quantitative description of the above evolution, we study the bulk properties of the relativistic charged/magnetic gasses in a nearly homogeneous and isotropic primordial universe via the thermal Fermi-Dirac or Bose distributions.

The grand partition function for the relativistic Fermi-Dirac ensemble is given by the standard definition

$$\ln \mathcal{Z}_{\rm total} = \sum_{\alpha} \ln \left( 1 + \Upsilon_{\alpha_1 \ldots \alpha_m} \exp\left( -\frac{E_\alpha}{T} \right) \right) , \qquad \Upsilon_{\alpha_1 \ldots \alpha_m} = \lambda_{\alpha_1} \lambda_{\alpha_2} \ldots \lambda_{\alpha_m} \quad (4.13)$$

where we are summing over the set all relevant quantum numbers $\alpha = (\alpha_1, \alpha_2, \ldots, \alpha_m)$. We note here the generalized the fugacity $\Upsilon_{\alpha_1 \ldots \alpha_m}$ allowing for any possible deformation caused by pressures effecting the distribution of any quantum numbers.

In the case of the Landau problem, there is an additional summation over $\widetilde{G}$ which represents the occupancy of Landau states (Greiner et al., 2012b) which are matched to the available phase space within $\Delta p_x \Delta p_y$. If we consider the orbital Landau quantum number $n$ to represent the transverse momentum $p_T^2 = p_x^2 + p_y^2$ of the system, then the relationship that defines $\widetilde{G}$ is given by

$$\frac{L^2}{(2\pi)^2} \Delta p_x \Delta p_y = \frac{eBL^2}{2\pi} \Delta n \, , \qquad \widetilde{G} = \frac{eBL^2}{2\pi} \, . \quad (4.14)$$

The summation over the continuous $p_z$ is replaced with an integration and the double summation over $p_x$ and $p_y$ is replaced by a single sum over Landau orbits

$$\sum_{p_z} \to \frac{L}{2\pi} \int_{-\infty}^{+\infty} dp_z \, , \qquad \sum_{p_x} \sum_{p_y} \to \frac{eBL^2}{2\pi} \sum_{n} , \quad (4.15)$$

where $L$ defines the boundary length of our considered volume $V = L^3$.

The partition function of the $e^+e^-$ plasma can be understood as the sum of four

gaseous species

$$\ln \mathcal{Z}_{e^+e^-} = \ln \mathcal{Z}^{\uparrow}_{e^+} + \ln \mathcal{Z}^{\downarrow}_{e^+} + \ln \mathcal{Z}^{\uparrow}_{e^-} + \ln \mathcal{Z}^{\downarrow}_{e^-} \,, \tag{4.16}$$

of electrons and positrons of both polarizations ($\uparrow\downarrow$). The change in phase space written in Eq. (4.15) modify the magnetized $e^+e^-$ plasma partition function from Eq. (4.13) into

$$\ln \mathcal{Z}_{e^+e^-} = \frac{eBV}{(2\pi)^2} \sum_{\sigma}^{\pm 1} \sum_{s}^{\pm 1} \sum_{n=0}^{\infty} \int_{-\infty}^{\infty} \mathrm{d}p_z \left[ \ln \left( 1 + \lambda_\sigma \xi_{\sigma,s} \exp \left( - \frac{E^n_{\sigma,s}}{T} \right) \right) \right] \tag{4.17}$$

$$\Upsilon_{\sigma,s} = \lambda_\sigma \xi_{\sigma,s} = \exp \frac{\mu_\sigma + \eta_{\sigma,s}}{T} \,, \tag{4.18}$$

where the energy eigenvalues $E^n_{\sigma,s}$ are given in Eq. (4.4). The index $\sigma$ in Eq. (4.17) is a sum over electron and positron states while $s$ is a sum over polarizations. The index $s$ refers to the spin along the field axis: parallel ($\uparrow$; $s = +1$) or anti-parallel ($\downarrow$; $s = -1$) for both particle and antiparticle species.

We are explicitly interested in small asymmetries such as baryon excess over antibaryons, or one polarization over another. These are described by Eq. (4.18) as the following two fugacities:

a. Chemical fugacity $\lambda_\sigma$

b. Polarization fugacity $\xi_{\sigma,s}$

For matter ($e^-$; $\sigma = +1$) and antimatter ($e^+$; $\sigma = -1$) particles, a nonzero relativistic chemical potential $\mu_\sigma = \sigma\mu$ is caused by an imbalance of matter and antimatter. While the primordial electron-positron plasma era was overall charge neutral, there was a small asymmetry in the charged leptons (namely electrons) from baryon asymmetry (Fromerth et al., 2012; Canetti et al., 2012) in the universe. Reactions such as $e^+e^- \leftrightarrow \gamma\gamma$ constrains the chemical potential of electrons and positrons (Elze et al., 1980) as

$$\mu \equiv \mu_{e^-} = -\mu_{e^+} \,, \qquad \lambda \equiv \lambda_{e^-} = \lambda^{-1}_{e^+} = \exp \frac{\mu}{T} \,, \tag{4.19}$$

where $\lambda$ is the chemical fugacity of the system.

We can then parameterize the chemical potential of the $e^+e^-$ plasma as a function of temperature $\mu \to \mu(T)$ via the charge neutrality of the universe which implies

$$n_p = n_{e^-} - n_{e^+} = \frac{1}{V}\lambda\frac{\partial}{\partial\lambda}\ln\mathcal{Z}_{e^+e^-}\,. \tag{4.20}$$

In Eq. (4.20), $n_p$ is the observed total number density of protons in all baryon species. The chemical potential defined in Eq. (4.19) is obtained from the requirement that the positive charge of baryons (protons, $\alpha$ particles, light nuclei produced after BBN) is exactly and locally compensated by a tiny net excess of electrons over positrons.

We then introduce a novel polarization fugacity $\xi_{\sigma,s}$ and polarization potential $\eta_{\sigma,s} = \sigma s\eta$. We propose the polarization potential follows analogous expressions as seen in Eq. (4.19) obeying

$$\eta \equiv \eta_{+,+} = \eta_{-,-}\,, \quad \eta = -\eta_{\pm,\mp}\,, \quad \xi_{\sigma,s} \equiv \exp\frac{\eta_{\sigma,s}}{T}\,. \tag{4.21}$$

An imbalance in polarization within a region of volume $V$ results in a nonzero polarization potential $\eta \neq 0$. Conveniently since antiparticles have opposite signs of charge and magnetic moment, the same magnetic moment is associated with opposite spin orientations. A completely particle-antiparticle symmetric magnetized plasma will have therefore zero total angular momentum.

### Euler-Maclaurin integration

Before we proceed with the Boltzmann distribution approximation which makes up the bulk of our analysis, we will comment on the full Fermi-Dirac distribution analysis. The Euler-Maclaurin formula (Abramowitz et al., 1988) is used to convert the

summation over Landau levels $n$ into an integration given by

$$\sum_{n=a}^{b} f(n) - \int_a^b f(x)dx = \frac{1}{2}\left(f(b) + f(a)\right) + \sum_{i=1}^{j} \frac{b_{2i}}{(2i)!}\left(f^{(2i-1)}(b) - f^{(2i-1)}(a)\right) + R(j)\,, \quad (4.22)$$

where $b_{2i}$ are the Bernoulli numbers and $R(j)$ is the error remainder defined by integrals over Bernoulli polynomials. The integer $j$ is chosen for the level of approximation that is desired. Euler-Maclaurin integration is rarely convergent, and in this case serves only as an approximation within the domain where the error remainder is small and bounded; see Greiner et al. (2012b) for the non-relativistic case. In this analysis, we keep the zeroth and first order terms in the Euler-Maclaurin formula. We note that regularization of the excess terms in Eq. (4.22) is done in the context of strong field QED (Greiner and Reinhardt, 2008) though that is outside our scope.

Using Eq. (4.22) allows us to convert the sum over $n$ quantum numbers in Eq. (4.17) into an integral. Defining

$$f^n_{\sigma,s} = \ln\left(1 + \Upsilon_{\sigma,s}\exp\left(-\frac{E^n_{\sigma,s}}{T}\right)\right)\,, \quad (4.23)$$

Eq. (4.17) for $j = 1$ becomes

$$\ln \mathcal{Z}_{e^+e^-} = \frac{eBV}{(2\pi)^2}\sum_{\sigma,s}^{\pm 1}\int_{-\infty}^{+\infty} dp_z \left(\int_0^{+\infty} dn f^n_{\sigma,s} + \frac{1}{2}f^0_{\sigma,s} + \frac{1}{12}\frac{\partial f^n_{\sigma,s}}{\partial n}\bigg|_{n=0} + R(1)\right) \quad (4.24)$$

It will be useful to rearrange Eq. (4.4) by pulling the spin dependency and the ground

state Landau orbital into the mass writing

$$E^n_{\sigma,s} = \tilde{m}_{\sigma,s}\sqrt{1 + \frac{p_z^2}{\tilde{m}^2_{\sigma,s}} + \frac{2eBn}{\tilde{m}^2_{\sigma,s}}}\,, \tag{4.25}$$

$$\varepsilon^n_{\sigma,s}(p_z, B) = \frac{E^n_{\sigma,s}}{\tilde{m}_{\sigma,s}}\,, \qquad \tilde{m}^2_{\sigma,s} = m_e^2 + eB\left(1 + \frac{g}{2}\sigma s\right)\,, \tag{4.26}$$

where we introduced the dimensionless energy $\varepsilon^n_{\sigma,s}$ and effective polarized mass $\tilde{m}_{\sigma,s}$ which is distinct for each spin alignment and is a function of magnetic field strength $B$. The effective polarized mass $\tilde{m}_{\sigma,s}$ allows us to describe the $e^+e^-$ plasma with the spin effects almost wholly separated from the Landau characteristics of the gas when considering the plasma's thermodynamic properties.

With the energies written in this fashion, we recognize the first term in Eq. (4.24) as mathematically equivalent to the free particle fermion partition function with a re-scaled mass $m_{\sigma,s}$. The phase-space relationship between transverse momentum and Landau orbits in Eq. (4.14) and Eq. (4.15) can be succinctly described by

$$p_T^2 \sim 2eBn\,, \qquad 2p_T dp_T \sim 2eBdn\,, \qquad d\boldsymbol{p}^3 = 2\pi p_T dp_T dp_z \tag{4.27}$$

$$\frac{eBV}{(2\pi)^2}\int_{-\infty}^{+\infty} dp_z \int_0^{+\infty} dn \to \frac{V}{(2\pi)^3}\int d\boldsymbol{p}^3 \tag{4.28}$$

which recasts the first term in Eq. (4.24) as

$$\ln \mathcal{Z}_{e^+e^-} = \frac{V}{(2\pi)^3}\sum_{\sigma,s}^{\pm 1}\int d\boldsymbol{p}^3 \ln\left(1 + \Upsilon_{\sigma,s}\exp\left(-\frac{m_{\sigma,s}\sqrt{1 + p^2/m^2_{\sigma,s}}}{T}\right)\right) + \ldots \tag{4.29}$$

As we will see in the proceeding section, this separation of the 'free-like' partition function can be reproduced in the Boltzmann distribution limit as well. This marks the end of the analytic analysis without approximations.

### 4.3.3 Boltzmann approach to electron-positron plasma

Since we address the temperature interval 200 keV $> T >$ 20 keV where the effects of quantum Fermi statistics on the $e^+e^-$ pair plasma are relatively small, but the gas

is still considered relativistic, we will employ the Boltzmann approximation to the partition function in Eq. (4.17). However, we extrapolate our results for presentation completeness up to $T \simeq 4m_e$.

| | aligned: $s=+1$ | anti-aligned: $s=-1$ |
|---|---|---|
| electron: $\sigma=+1$ | $+\mu+\eta$ | $+\mu-\eta$ |
| positron: $\sigma=-1$ | $-\mu-\eta$ | $-\mu+\eta$ |

Table 4.1: Organizational schematic of matter-antimatter ($\sigma$) and polarization ($s$) states with respect to the chemical $\mu$ and polarization $\eta$ potentials as seen in Eq. (4.32). Companion to Table 4.3.

The partition function shown in equation Eq. (4.17) can be rewritten removing the logarithm as

$$\ln \mathcal{Z}_{e^+e^-} = \frac{eBV}{(2\pi)^2} \sum_{\sigma,s}^{\pm 1} \sum_{n=0}^{\infty} \sum_{k=1}^{\infty} \int_{-\infty}^{+\infty} \mathrm{d}p_z \frac{(-1)^{k+1}}{k} \exp\left( k \frac{\sigma\mu + \sigma s\eta - \tilde{m}_{\sigma,s}\varepsilon^n_{\sigma,s}}{T} \right) , \tag{4.30}$$

$$\sigma\mu + \sigma s\eta - \tilde{m}_{\sigma,s}\varepsilon^n_{\sigma,s} < 0 \, , \tag{4.31}$$

which is well behaved as long as the factor in Eq. (4.31) remains negative. We evaluate the sums over $\sigma$ and $s$ as

$$\begin{aligned} \ln \mathcal{Z}_{e^+e^-} = \frac{eBV}{(2\pi)^2} \sum_{n=0}^{\infty} \sum_{k=1}^{\infty} \int_{-\infty}^{+\infty} \mathrm{d}p_z \frac{(-1)^{k+1}}{k} \times \\ \left( \exp\left( k \frac{+\mu+\eta}{T} \right) \exp\left( -k \frac{\tilde{m}_{+,+}\varepsilon^n_{+,+}}{T} \right) + \exp\left( k \frac{+\mu-\eta}{T} \right) \exp\left( -k \frac{\tilde{m}_{+,-}\varepsilon^n_{+,-}}{T} \right) \right. \\ \left. + \exp\left( k \frac{-\mu-\eta}{T} \right) \exp\left( -k \frac{\tilde{m}_{-,+}\varepsilon^n_{-,+}}{T} \right) + \exp\left( k \frac{-\mu+\eta}{T} \right) \exp\left( -k \frac{\tilde{m}_{-,-}\varepsilon^n_{-,-}}{T} \right) \right) \end{aligned} \tag{4.32}$$

We note from Figure 4.3 that the first and forth terms and the second and third terms share the same energies via

$$\varepsilon^n_{+,+} = \varepsilon^n_{-,-} \, , \qquad \varepsilon^n_{+,-} = \varepsilon^n_{-,+} \, . \qquad \varepsilon^n_{+,-} < \varepsilon^n_{+,+} \, , \tag{4.33}$$

Eq. (4.33) allows us to reorganize the partition function with a new magnetization quantum number $s'$ which characterizes paramagnetic flux increasing states ($s' = +1$) and diamagnetic flux decreasing states ($s' = -1$). This recasts Eq. (4.32) as

$$\ln \mathcal{Z}_{e^+e^-} = \frac{eBV}{(2\pi)^2} \sum_{s'}^{\pm 1} \sum_{n=0}^{\infty} \sum_{k=1}^{\infty} \int_{-\infty}^{+\infty} \mathrm{d}p_z \frac{(-1)^{k+1}}{k} \left[ 2\xi_{s'} \cosh \frac{k\mu}{T} \right] \exp\left( -k \frac{\tilde{m}_{s'} \varepsilon^n_{s'}}{T} \right) \quad (4.34)$$

with dimensionless energy $\varepsilon^n_{s'}$, polarization mass $\tilde{m}_{s'}$, and polarization $\eta_{s'}$ redefined in terms of the moment orientation quantum number $s'$

$$\tilde{m}^2_{s'} = m_e^2 + eB \left( 1 - \frac{g}{2} s' \right) , \quad (4.35)$$

$$\eta \equiv \eta_+ = -\eta_- \qquad \xi \equiv \xi_+ = \xi_-^{-1} , \qquad \xi_{s'} = \xi^{\pm 1} = \exp\left( \pm \frac{\eta}{T} \right) . \quad (4.36)$$

We introduce the modified Bessel function $K_\nu$ (see Ch. 10 of Letessier and Rafelski (2023)) of the second kind

$$K_\nu \left( \frac{m}{T} \right) = \frac{\sqrt{\pi}}{\Gamma(\nu - 1/2)} \frac{1}{m} \left( \frac{1}{2mT} \right)^{\nu - 1} \int_0^\infty \mathrm{d}p \, p^{2\nu - 2} \exp\left( -\frac{m\varepsilon}{T} \right) , \quad (4.37)$$

$$\nu > 1/2 , \qquad \varepsilon = \sqrt{1 + p^2/m^2} , \quad (4.38)$$

allowing us to rewrite the integral over momentum in Eq. (4.34) as

$$\frac{1}{T} \int_0^\infty \mathrm{d}p_z \exp\left( -\frac{k\tilde{m}_{s'} \varepsilon^n_{s'}}{T} \right) = W_1 \left( \frac{k\tilde{m}_{s'} \varepsilon^n_{s'}(0, B)}{T} \right) . \quad (4.39)$$

The function $W_\nu$ serves as an auxiliary function of the form $W_\nu(x) = xK_\nu(x)$. The notation $\varepsilon(0, B)$ in Eq. (4.39) refers to the definition of dimensionless energy found in Eq. (4.26) with $p_z = 0$. The standard Boltzmann distribution is obtained by summing only $k = 1$ and neglecting the higher order terms.

We take advantage again of Euler-Maclaurin integration Eq. (4.22) and integrate the partition function. After truncation of the series and error remainder, the parti-

tion function Eq. (4.30) can then be written in terms of modified Bessel $K_\nu$ functions of the second kind and cosmic magnetic scale $b_0$, yielding

$$\boxed{\ln \mathcal{Z}_{e^+e^-} \simeq \frac{T^3 V}{\pi^2} \sum_{s'}^{\pm 1} \left[\xi_{s'} \cosh \frac{\mu}{T}\right] \left(x_{s'}^2 K_2(x_{s'}) + \frac{b_0}{2} x_{s'} K_1(x_{s'}) + \frac{b_0^2}{12} K_0(x_{s'})\right)}, \tag{4.40}$$

$$x_{s'} = \frac{\tilde{m}_{s'}}{T} = \sqrt{\frac{m_e^2}{T^2} + b_0 \left(1 - \frac{g}{2} s'\right)}. \tag{4.41}$$

The latter two terms in Eq. (4.40) proportional to $b_0 K_1$ and $b_0^2 K_0$ are the uniquely magnetic terms present containing both spin and Landau orbital influences in the partition function. The $K_2$ term is analogous to the free Fermi gas (Greiner et al., 2012b) being modified only by spin effects.

This 'separation of concerns' can be rewritten as

$$\ln \mathcal{Z}_{\mathrm{S}} = \frac{T^3 V}{\pi^2} \sum_{s'}^{\pm 1} \left[\xi_{s'} \cosh \frac{\mu}{T}\right] \left(x_{s'}^2 K_2(x_{s'})\right), \tag{4.42}$$

$$\ln \mathcal{Z}_{\mathrm{SO}} = \frac{T^3 V}{\pi^2} \sum_{s'}^{\pm} \left[\xi_{s'} \cosh \frac{\mu}{T}\right] \left(\frac{b_0}{2} x_{s'} K_1(x_{s'}) + \frac{b_0^2}{12} K_0(x_{s'})\right), \tag{4.43}$$

where the spin (S) and spin-orbit (SO) partition functions can be considered independently. When the magnetic scale $b_0$ is small, the spin-orbit term Eq. (4.43) becomes negligible leaving only paramagnetic effects in Eq. (4.42) due to spin. In the non-relativistic limit, Eq. (4.42) reproduces a quantum gas whose Hamiltonian is defined as the free particle (FP) Hamiltonian plus the magnetic dipole (MD) Hamiltonian which span two independent Hilbert spaces $\mathcal{H}_{\mathrm{FP}} \otimes \mathcal{H}_{\mathrm{MD}}$.

Writing the partition function as Eq. (4.40) instead of Eq. (4.30) has the additional benefit that the partition function remains finite in the free gas ($B \to 0$) limit. This is because the free Fermi gas and Eq. (4.42) are mathematically analogous to one another. As the Bessel $K_\nu$ functions are evaluated as functions of $x_\pm$ in Eq. (4.41), the 'free' part of the partition $K_2$ is still subject to spin magnetization effects. In the limit where $B \to 0$, the free Fermi gas is recovered in both the Boltzmann

approximation $k = 1$ and the general case $\sum_{k=1}^{\infty}$.

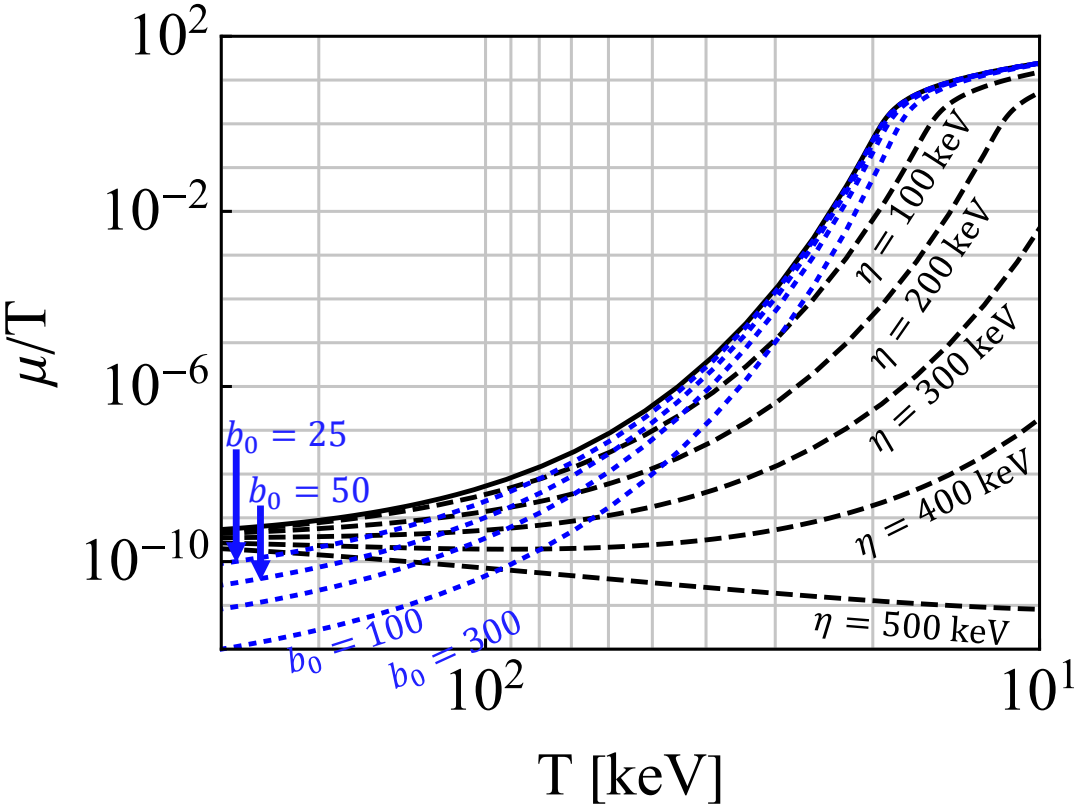


Figure 4.4: The chemical potential over temperature $\mu/T$ is plotted as a function of temperature with differing values of spin potential $\eta$ and magnetic scale $b_0$.

### 4.3.4 Electron-positron chemical potential

In presence of a magnetic field in the Boltzmann approximation, the charge neutrality condition Eq. (4.20) becomes

$$\sinh\frac{\mu}{T} = n_p\frac{\pi^2}{T^3}\left[\sum_{s'}^{\pm 1}\xi_{s'}\left(x_{s'}^2K_2(x_{s'}) + \frac{b_0}{2}x_{s'}K_1(x_{s'}) + \frac{b_0^2}{12}K_0(x_{s'})\right)\right]^{-1}. \tag{4.44}$$

Eq. (4.44) is fully determined by the right-hand-side expression if the spin fugacity is set to unity $\eta = 0$ implying no external bias to the number of polarizations except as a consequence of the difference in energy eigenvalues. In practice, the latter two terms in Eq. (4.44) are negligible to chemical potential in the bounds of the primordial $e^+e^-$

plasma considered and only becomes relevant for extreme (see Figure 4.4) magnetic field strengths well outside our scope.

Eq. (4.44) simplifies if there is no external magnetic field $b_0 = 0$ into

$$\sinh \frac{\mu}{T} = n_p \frac{\pi^2}{T^3} \left[ 2 \cosh \frac{\eta}{T} \left( \frac{m_e}{T} \right)^2 K_2 \left( \frac{m_e}{T} \right) \right]^{-1} . \tag{4.45}$$

In Figure 4.4 we plot the chemical potential $\mu/T$ in Eq. (4.44) and Eq. (4.45) which characterizes the importance of the charged lepton asymmetry as a function of temperature. Since the baryon (and thus charged lepton) asymmetry remains fixed, the suppression of $\mu/T$ at high temperatures indicates a large pair density which is seen explicitly in Figure 4.2. The black line corresponds to the $b_0 = 0$ and $\eta = 0$ case.

The para-diamagnetic contribution from Eq. (4.43) does not appreciably influence $\mu/T$ until the magnetic scales involved become incredibly large well outside the observational bounds defined in Eq. (4.1) and Eq. (4.6) as seen by the dotted blue curves of various large values $b_0 = \{25,\ 50,\ 100,\ 300\}$. The chemical potential is also insensitive to forcing by the spin potential until $\eta$ reaches a significant fraction of the electron mass $m_e$ in size. The chemical potential for large values of spin potential $\eta = \{100,\ 200,\ 300,\ 400,\ 500\}$ keV are also plotted as dashed black lines with $b_0 = 0$.

It is interesting to note that there are crossing points where a given chemical potential can be described as either an imbalance in spin-polarization or presence of external magnetic field. While spin potential suppresses the chemical potential at low temperatures, external magnetic fields only suppress the chemical potential at high temperatures.

The profound insensitivity of the chemical potential to these parameters justifies the use of the free particle chemical potential (black line) in the ranges of magnetic field strength considered for cosmology. Mathematically this can be understood as $\xi$ and $b_0$ act as small corrections in the denominator of Eq. (4.44) if expanded in powers of these two parameters.

## 4.4 Relativistic paramagnetism of electron-positron gas

The total magnetic flux within a region of space can be written as the sum of external fields and the magnetization of the medium via

$$B_{\text{total}} = B + \mathcal{M}\,. \tag{4.46}$$

For the simplest mediums without ferromagnetic or hysteresis considerations, the relationship can be parameterized by the susceptibility $\chi$ of the medium as

$$B_{\text{total}} = (1+\chi)B\,, \qquad \mathcal{M} = \chi B\,, \qquad \chi \equiv \frac{\partial \mathcal{M}}{\partial B}\,, \tag{4.47}$$

with the possibility of both paramagnetic materials ($\chi > 1$) and diamagnetic materials ($\chi < 1$). The $e^+e^-$ plasma however does not so neatly fit in either category as given by Eq. (4.42) and Eq. (4.43). In general, the susceptibility of the gas will itself be a field dependant quantity.

In our analysis, the external magnetic field always appears within the context of the magnetic scale $b_0$, therefore we can introduce the change of variables

$$\frac{\partial b_0}{\partial B} = \frac{e}{T^2}\,. \tag{4.48}$$

The magnetization of the $e^+e^-$ plasma described by the partition function in Eq. (4.40) can then be written as

$$\mathcal{M} \equiv \frac{T}{V}\frac{\partial}{\partial B}\ln \mathcal{Z}_{e^+e^-} = \frac{T}{V}\left(\frac{\partial b_0}{\partial B}\right)\frac{\partial}{\partial b_0}\ln \mathcal{Z}_{e^+e^-}\,, \tag{4.49}$$

Magnetization arising from other components in the cosmic gas (protons, neutrinos, etc.) could in principle also be included. Localized inhomogeneities of matter evolution are often non-trivial and generally be solved numerically using magneto-hydrodynamics (MHD) (Melrose, 2013; Vazza et al., 2017; Vachaspati, 2021). In the context of MHD, primordial magnetogenesis from fluid flows in the electron-positron epoch was considered in Gopal and Sethi (2005); Perrone et al. (2021).

We introduce dimensionless units for magnetization $\mathfrak{M}$ by defining the critical field strength

$$B_C \equiv \frac{m_e^2}{e}\,, \qquad \mathfrak{M} \equiv \frac{\mathcal{M}}{B_C}\,. \tag{4.50}$$

The scale $B_C$ is where electromagnetism is expected to become subject to non-linear effects, though luckily in our regime of interest, electrodynamics should be linear. We note however that the upper bounds of IGMFs in Eq. (4.1) (with $b_0 = 10^{-3}$; see Eq. (4.6)) brings us to within 1% of that limit for the external field strength in the temperature range considered.

The total magnetization $\mathfrak{M}$ can be broken into the sum of magnetic moment parallel $\mathfrak{M}_+$ and magnetic moment anti-parallel $\mathfrak{M}_-$ contributions

$$\mathfrak{M} = \mathfrak{M}_+ + \mathfrak{M}_-\,. \tag{4.51}$$

We note that the expression for the magnetization simplifies significantly for $g = 2$ which is the 'natural' gyro-magnetic factor (Evans and Rafelski, 2022; Rafelski et al., 2023b) for Dirac particles. For illustration, the $g = 2$ magnetization from Eq. (4.49) is then

$$\mathfrak{M}_+ = \frac{e^2}{\pi^2}\frac{T^2}{m_e^2}\xi \cosh\frac{\mu}{T}\left[\frac{1}{2}x_+K_1(x_+) + \frac{b_0}{6}K_0(x_+)\right]\,, \tag{4.52}$$

$$-\mathfrak{M}_- = \frac{e^2}{\pi^2}\frac{T^2}{m_e^2}\xi^{-1} \cosh\frac{\mu}{T}\left[\left(\frac{1}{2} + \frac{b_0^2}{12x_-^2}\right)x_-K_1(x_-) + \frac{b_0}{3}K_0(x_-)\right]\,, \tag{4.53}$$

$$x_+ = \frac{m_e}{T}\,, \qquad x_- = \sqrt{\frac{m_e^2}{T^2} + 2b_0}\,. \tag{4.54}$$

As the $g$-factor of the electron is only slightly above two at $g \simeq 2.00232$ (Tiesinga et al., 2021), the above two expressions for $\mathfrak{M}_+$ and $\mathfrak{M}_-$ are only modified by a small amount because of anomalous magnetic moment (AMM) and would be otherwise invisible on our figures.

### 4.4.1 Evolution of electron-positron magnetization

In Figure 4.5, we plot the magnetization as given by Eq. (4.52) and Eq. (4.53) with the spin potential set to unity $\xi = 1$. The lower (solid red) and upper (solid blue) bounds for cosmic magnetic scale $b_0$ are included. The external magnetic field strength $B/B_C$ is also plotted for lower (dotted red) and upper (dotted blue) bounds. Since the derivative of the partition function governing magnetization may manifest differences between Fermi-Dirac and the here used Boltzmann limit more acutely, out of abundance of caution, we indicate extrapolation outside the domain of validity of the Boltzmann limit with dashes.

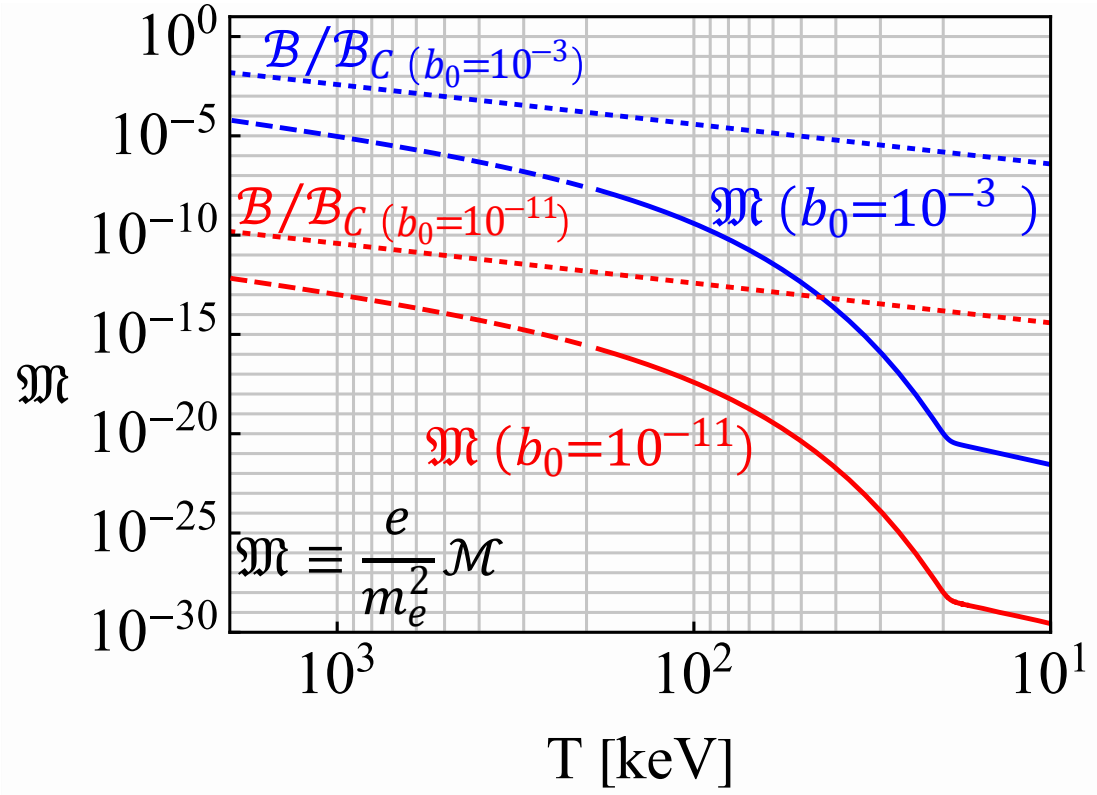


Figure 4.5: The magnetization $\mathfrak{M}$, with $g = 2$, of the primordial $e^+e^-$ plasma is plotted as a function of temperature. Figure made in collaboration with Cheng Tao Yang.

We see in Figure 4.5 that the $e^+e^-$ plasma is overall paramagnetic and yields a positive overall magnetization which is contrary to the traditional assumption that

matter-antimatter plasma lack significant magnetic responses of their own in the bulk. With that said, the magnetization never exceeds the external field under the parameters considered which shows a lack of ferromagnetic behavior.

The large abundance of pairs causes the smallness of the chemical potential seen in Figure 4.4 at high temperatures. As the universe expands and temperature decreases, there is a rapid decrease of the density $n_{e^\pm}$ of $e^+e^-$ pairs. This is the primary the cause of the rapid paramagnetic decrease seen in Figure 4.5 above $T = 21$ keV. At lower temperatures $T < 21$ keV there remains a small electron excess (see Figure 4.2) needed to neutralize proton charge. These excess electrons then govern the residual magnetization and dilutes with cosmic expansion.

An interesting feature of Figure 4.5 is that the magnetization in the full temperature range increases as a function of temperature. This is contrary to Curie's law (Greiner et al., 2012b) which stipulates that paramagnetic susceptibility of a laboratory material is inversely proportional to temperature. However, Curie's law applies to systems with fixed number of particles which is not true in our situation; see Section 4.4.3.

A further consideration is possible hysteresis as the $e^+e^-$ density drops with temperature. It is not immediately obvious the gas's magnetization should simply 'degauss' so rapidly without further consequence. If the very large paramagnetic susceptibility present for $T \simeq m_e$ is the origin of an overall magnetization of the plasma, the conservation of magnetic flux through the comoving surface ensures that the initial residual magnetization is preserved at a lower temperature by Faraday induced kinetic flow processes however our model presented here cannot account for such effects.

Early universe conditions may also apply to some extreme stellar objects with rapid change in $n_{e^\pm}$ with temperatures above $T = 21$ keV. Production and annihilation of $e^+e^-$ plasmas is also predicted around compact stellar objects (Ruffini et al., 2010; Ruffini and Vereshchagin, 2013) potentially as a source of gamma-ray bursts.

### 4.4.2 Dependency on g-factor

As discussed at the end of Section 4.4, the AMM of $e^+e^-$ is not relevant in the present model. However out of academic interest, it is valuable to consider how magnetization is effected by changing the $g$-factor significantly.

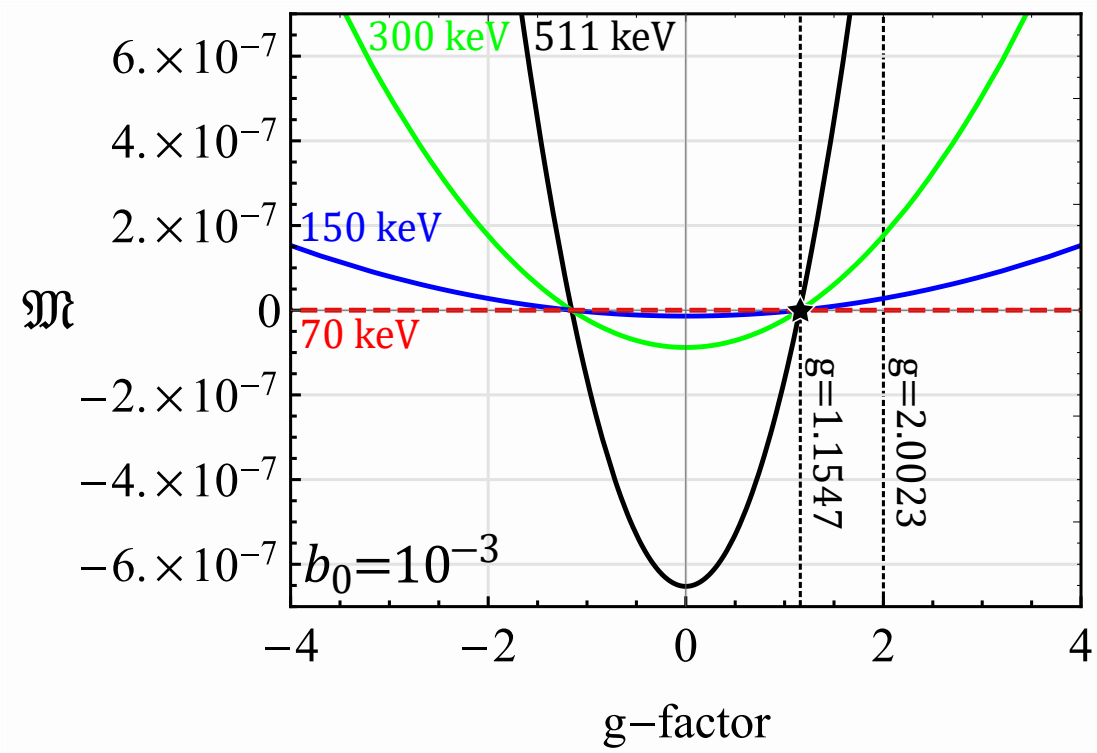


Figure 4.6: The magnetization $\mathfrak{M}$ as a function of $g$-factor plotted for several temperatures with magnetic scale $b_0 = 10^{-3}$ and polarization fugacity $\xi = 1$.

The influence of AMM would be more relevant for the magnetization of baryon gasses since the $g$-factor for protons ($g \approx 5.6$) and neutrons ($g \approx 3.8$) are substantially different from $g=2$. The influence of AMM on the magnetization of thermal systems with large baryon content (neutron stars, magnetars, hypothetical bose stars, etc.) is therefore also of interest (Ferrer and Hackebill, 2019, 2023).

Eq. (4.52) and Eq. (4.53) with arbitrary $g$ reintroduced is given by

$$\mathfrak{M} = \frac{e^2}{\pi^2}\frac{T^2}{m_e^2}\sum_{s'}^{\pm 1}\xi_{s'}\cosh\frac{\mu}{T}\left[C^1_{s'}(x_{s'})K_1(x_{s'}) + C^0_{s'}K_0(x_{s'})\right]\,, \tag{4.55}$$

$$C^1_{s'}(x_\pm) = \left[\frac{1}{2} - \left(\frac{1}{2} - \frac{g}{4}s'\right)\left(1 + \frac{b_0^2}{12x_{s'}^2}\right)\right]x_{s'}\,, \qquad C^0_{s'} = \left[\frac{1}{6} - \left(\frac{1}{4} - \frac{g}{8}s'\right)\right]b_0\,, \tag{4.56}$$

where $x_{s'}$ was previously defined in Eq. (4.41).

In Figure 4.6, we plot the magnetization as a function of $g$-factor between $4 > g > -4$ for temperatures $T = \{511,\ 300,\ 150,\ 70\}$ keV. We find that the magnetization is sensitive to the value of AMM revealing a transition point between paramagnetic ($\mathfrak{M} > 0$) and diamagnetic gasses ($\mathfrak{M} < 0$). Curiously, the transition point was numerically determined to be around $g \simeq 1.1547$ in the limit $b_0 \to 0$. The exact position of this transition point however was found to be both temperature and $b_0$ sensitive, though it moved little in the ranges considered.

It is not surprising for there to be a transition between diamagnetism and paramagnetism given that the partition function (see Eq. (4.42) and Eq. (4.43)) contained elements of both. With that said, the transition point presented at $g \approx 1.15$ should not be taken as exact because of the approximations used to obtain the above results.

It is likely that the exact transition point has been altered by our taking of the Boltzmann approximation and Euler-Maclaurin integration steps. It is known that the Klein-Gordon-Pauli solutions to the Landau problem in Eq. (4.4) have periodic behavior (Steinmetz et al., 2019; Evans and Rafelski, 2022; Rafelski et al., 2023b) for $|g| = k/2$ (where $k \in 1, 2, 3\ldots$).

These integer and half-integer points represent when the two Landau towers of orbital levels match up exactly. Therefore, we propose a more natural transition between the spinless diamagnetic gas of $g = 0$ and a paramagnetic gas is $g = 1$. A more careful analysis is required to confirm this, but that our numerical value is close to unity is suggestive.

### 4.4.3 Magnetization per lepton

Despite the relatively large magnetization seen in Figure 4.5, the average contribution per lepton is only a small fraction of its overall magnetic moment indicating the magnetization is only loosely organized. Specifically, the magnetization regime we are in is described by

$$\mathcal{M} \ll \mu_B \frac{N_{e^+} + N_{e^-}}{V}\,, \qquad \mu_B \equiv \frac{e}{2m_e}\,, \tag{4.57}$$

where $\mu_B$ is the Bohr magneton and $N = nV$ is the total particle number in the proper volume V. To better demonstrate that the plasma is only weakly magnetized, we define the average magnetic moment per lepton given by along the field ($z$-direction) axis as

$$|\vec{m}|_z \equiv \frac{\mathcal{M}}{n_{e^-} + n_{e^+}}\,, \qquad |\vec{m}|_x = |\vec{m}|_y = 0\,. \tag{4.58}$$

Statistically, we expect the transverse expectation values to be zero. We emphasize here that despite $|\vec{m}|_z$ being nonzero, this doesn't indicate a nonzero spin angular momentum as our plasma is nearly matter-antimatter symmetric. The quantity defined in Eq. (4.58) gives us an insight into the microscopic response of the plasma.

The average magnetic moment $|\vec{m}|_z$ defined in Eq. (4.58) is plotted in Figure 4.7 which displays how essential the external field is on the 'per lepton' magnetization. The $b_0 = 10^{-3}$ case (blue curve) is plotted in the Boltzmann approximation. The dashed lines indicate where this approximation is only qualitatively correct. For illustration, a constant magnetic field case (solid green line) with a comoving reference value chosen at temperature $T_0 = 10$ keV is also plotted.

If the field strength is held constant, then the average magnetic moment per lepton is suppressed at higher temperatures as expected for magnetization satisfying Curie's law. The difference in Figure 4.7 between the non-constant (blue solid curve) case and the constant field (solid green curve) case demonstrates the importance of the conservation of primordial magnetic flux in the plasma, required by Eq. (4.5). While

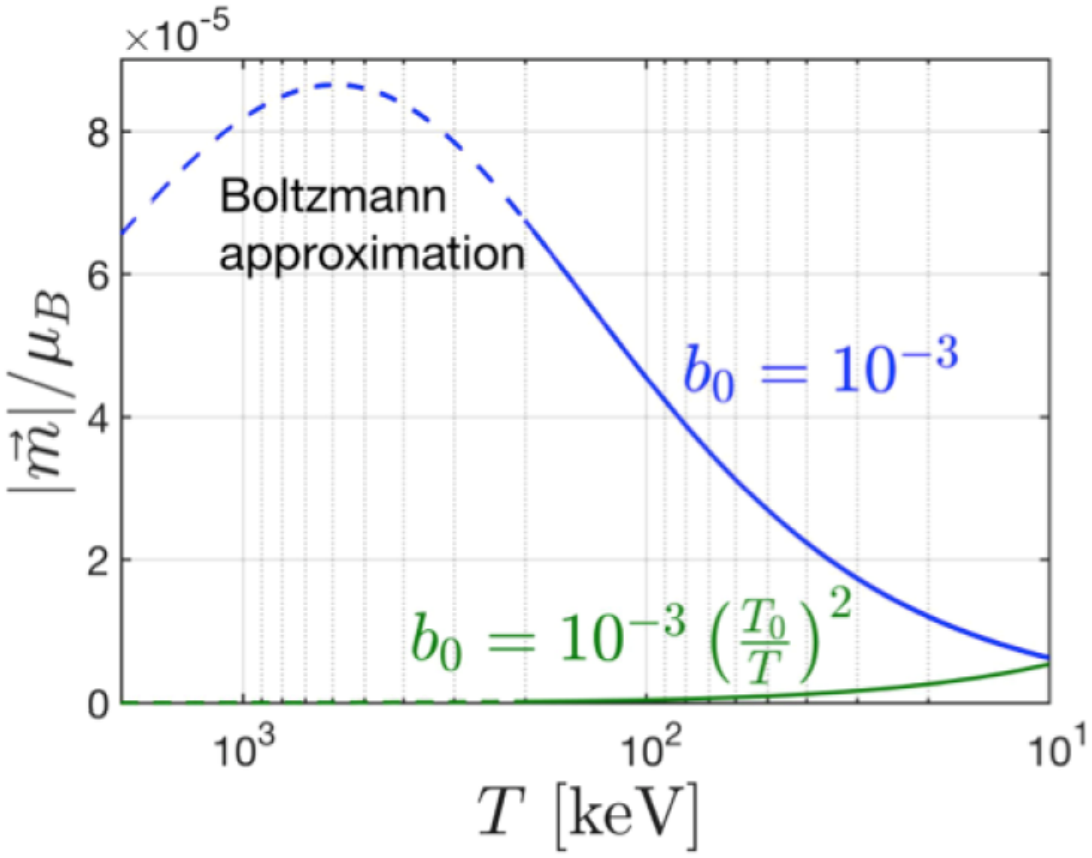


Figure 4.7: The magnetic moment per lepton $|\vec{m}|_z$ along the field axis as a function of temperature. Figure made in collaboration with Cheng Tao Yang.

not shown, if Figure 4.7 was extended to lower temperatures, the magnetization per lepton of the constant field case would be greater than the non-constant case which agrees with our intuition that magnetization is easier to achieve at lower temperatures. This feature again highlights the importance of flux conservation in the system and the uniqueness of the primordial cosmic environment.

## 4.5 Polarization potential and ferromagnetism

Up to this point, we have neglected the impact that a nonzero spin potential $\eta \neq 0$ (and thus $\xi \neq 1$) would have on the primordial $e^+e^-$ plasma magnetization. In the limit that $(m_e/T)^2 \gg b_0$ the magnetization given in Eq. (4.55) and Eq. (4.56) is entirely controlled by the spin fugacity $\xi$ asymmetry generated by the spin potential

$\eta$ yielding up to first order $\mathcal{O}(b_0)$ in magnetic scale

$$\lim_{m_e^2/T^2 \gg b_0} \mathfrak{M} = \frac{g}{2}\frac{e^2}{\pi^2}\frac{T^2}{m_e^2}\sinh\frac{\eta}{T}\cosh\frac{\mu}{T}\left[\frac{m_e}{T}K_1\left(\frac{m_e}{T}\right)\right] + b_0\left(g^2 - \frac{4}{3}\right)\frac{e^2}{8\pi^2}\frac{T^2}{m_e^2}\cosh\frac{\eta}{T}\cosh\frac{\mu}{T}K_0\left(\frac{m_e}{T}\right) + \mathcal{O}\left(b_0^2\right) \quad (4.59)$$

Given Eq. (4.59), we can understand the spin potential as a kind of 'ferromagnetic' influence on the primordial gas which allows for magnetization even in the absence of external magnetic fields. This interpretation is reinforced by the fact the leading coefficient is $g/2$.

We suggest that a variety of physics could produce a small nonzero $\eta$ within a domain of the gas. Such asymmetries could also originate statistically as while the expectation value of free gas polarization is zero, the variance is likely not.

As $\sinh \eta/T$ is an odd function, the sign of $\eta$ also controls the alignment of the magnetization. In the high temperature limit Eq. (4.59) with strictly $b_0 = 0$ assumes a form of to lowest order for brevity

$$\lim_{m_e/T \to 0} \mathfrak{M}|_{b_0=0} = \frac{g}{2}\frac{e^2}{\pi^2}\frac{T^2}{m_e^2}\frac{\eta}{T}\,, \quad (4.60)$$

While the limit in Eq. (4.60) was calculated in only the Boltzmann limit, it is noteworthy that the high temperature (and $m \to 0$) limit of Fermi-Dirac distributions only differs from the Boltzmann result by a proportionality factor.

The natural scale of the $e^+e^-$ magnetization with only a small spin fugacity ($\eta <$ 1 eV) fits easily within the bounds of the predicted magnetization during this era if the IGMF measured today was of primordial origin. The reason for this is that the magnetization seen in Eq. (4.52), Eq. (4.53) and Eq. (4.59) are scaled by $\alpha B_C$ where $\alpha$ is the fine structure constant.

### 4.5.1 Hypothesis of ferromagnetic self-magnetization

One exploratory model we propose is to fix the spin polarization asymmetry, described in Eq. (4.21), to generate a homogeneous magnetic field which dissipates as

the universe cools down. In this model, there is no external primordial magnetic field ($B_{\rm PMF} = 0$) generated by some unrelated physics, but rather the $e^+e^-$ plasma itself is responsible for the field by virtue of spin polarization.

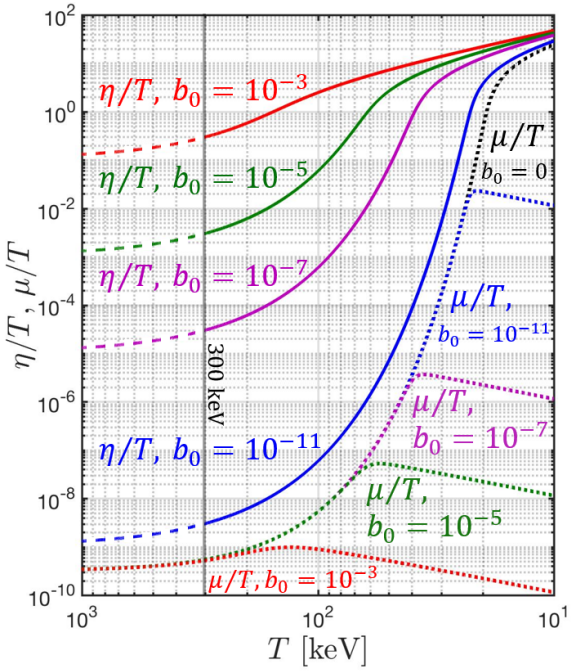


Figure 4.8: The spin potential $\eta$ and chemical potential $\mu$ are plotted under the assumption of self-magnetization through a nonzero spin polarization in bulk of the plasma. Figure made in collaboration with Cheng Tao Yang.

This would obey the following assumption of

$$\mathfrak{M}(b_0) = \frac{\mathcal{M}(b_0)}{B_C} \longleftrightarrow \frac{B}{B_C} = b_0 \frac{T^2}{m_e^2}\,, \tag{4.61}$$

which sets the total magnetization as a function of itself. The spin polarization described by $\eta \to \eta(b_0, T)$ then becomes a fixed function of the temperature and magnetic scale. The underlying assumption would be the preservation of the homogeneous field would be maintained by scattering within the gas (as it is still in thermal equilibrium) modulating the polarization to conserve total magnetic flux.

The result of the self-magnetization assumption in Eq. (4.61) for the potentials is plotted in Figure 4.8. The solid lines indicate the curves for $\eta/T$ for differing values of

$b_0 = \{10^{-11},\ 10^{-7},\ 10^{-5},\ 10^{-3}\}$ which become dashed above $T = 300$ keV to indicate that the Boltzmann approximation is no longer appropriate though the general trend should remain unchanged.

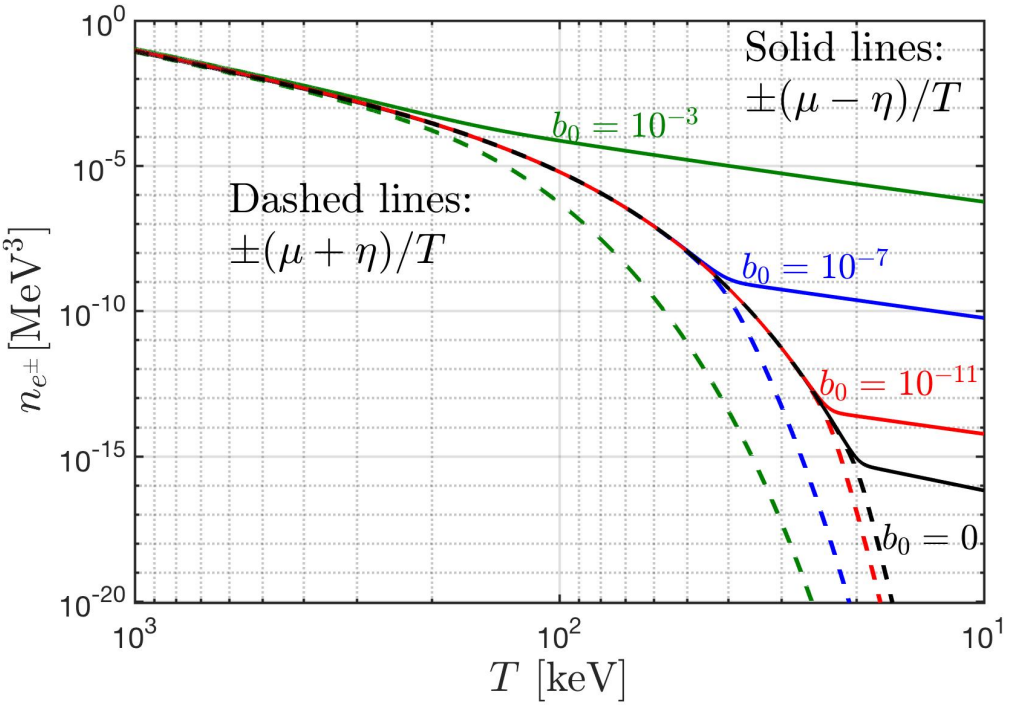


Figure 4.9: The number density $n_{e^\pm}$ of polarized electrons and positrons under the self-magnetization model for differing values of $b_0$. Figure courtesy of Cheng Tao Yang.

The dotted lines are the curves for the chemical potential $\mu/T$. At high temperatures we see that a relatively small $\eta/T$ is needed to produce magnetization owing to the large densities present. Figure 4.8 also shows that the chemical potential does not deviate from the free particle case until the spin polarization becomes sufficiently high which indicates that this form of self-magnetization would require the annihilation of positrons to be incomplete even at lower temperatures.

This is seen explicitly in Figure 4.9 where we plot the numerical density of particles as a function of temperature for spin aligned ($+\eta$) and spin anti-aligned ($-\eta$) species for both positrons ($-\mu$) and electrons ($+\mu$). Various self-magnetization strengths are also plotted to match those seen in Figure 4.8. The nature of $T_{\text{split}}$ changes under

this model since antimatter and polarization states can be extinguished separately. Positrons persist where there is insufficient electron density to maintain the magnetic flux. Polarization asymmetry therefore appears physical only in the domain where there is a large number of matter-antimatter pairs.

### 4.5.2 Matter inhomogeneities in the cosmic plasma

In general, an additional physical constraint is required to fully determine $\mu$ and $\eta$ simultaneously as both potentials have mutual dependency (see Section 4.5). We note that spin polarizations are not required to be in balanced within a single species to preserve angular momentum. For magnetized domains or finite volumes, boundary/surface conditions would also need to be considered.

The CMB (Aghanim et al., 2020) indicates that the early universe was home to domains of slightly higher and lower baryon densities which resulted in the presence of galactic super-clusters, cosmic filaments, and great voids seen today. However, the CMB, as measured today, is blind to the localized inhomogeneities required for gravity to begin galaxy and supermassive black hole formation.

Such acute inhomogeneities distributed like a dust (Grayson et al., 2023) in the plasma would make the proton density sharply and spatially dependant $n_p \to n_p(x)$ which would directly affect the potentials $\mu(x)$ and $\eta(x)$ and thus the density of electrons and positrons locally. This suggests that $e^+e^-$ may play a role in the initial seeding of gravitationally collapsing systems. If the primordial plasma were home to such small localized magnetic domains, the associated nonzero local angular momentum within these domains would provide a natural mechanism for the formation of rotating galaxies today.

Recent measurements by the James Webb Space Telescope (JWST) (Yan et al., 2023; Adams et al., 2023; Haro et al., 2023) indicate that galaxy formation began surprisingly early at large redshift values of $z \gtrsim 10$ within the first 500 million years of the universe requiring gravitational collapse to begin in a hotter environment than expected. The observation of supermassive black holes already present (Larson et al., 2023) in this same high redshift period (with millions of solar masses) indicates the

need for local high density regions in the early universe whose generation is not yet explained and likely need to exist long before the recombination epoch.

# REFERENCES


Abdalla, E., G. F. Abellán, A. Aboubrahim, A. Agnello, Ö. Akarsu, Y. Akrami, G. Alestas, D. Aloni, L. Amendola, L. A. Anchordoqui, et al. (2022). Cosmology intertwined: A review of the particle physics, astrophysics, and cosmology associated with the cosmological tensions and anomalies. *Journal of High Energy Astrophysics*, **34**, pp. 49–211. doi:10.1016/j.jheap.2022.04.002.

Abramowitz, M., I. A. Stegun, and R. H. Romer (1988). *Handbook of mathematical functions with formulas, graphs, and mathematical tables*. American Association of Physics Teachers.

Adams, N. J., C. J. Conselice, L. Ferreira, et al. (2023). Discovery and properties of ultra-high redshift galaxies (9¡ z¡ 12) in the JWST ERO SMACS 0723 Field. *Monthly Notices of the Royal Astronomical Society*, **518**(3), pp. 4755–4766. doi:10.1093/mnras/stac3347.

Adhikary, B., M. Chakraborty, and A. Ghosal (2013). Masses, mixing angles and phases of general Majorana neutrino mass matrix. *JHEP*, **10**, p. 043. doi:10.1007/JHEP10(2013)043. [Erratum: JHEP 09, 180 (2014)].

Aghanim, N. et al. (2020). Planck 2018 results. VI. Cosmological parameters. *Astron. Astrophys.*, **641**, p. A6. doi:10.1051/0004-6361/201833910. [Erratum: Astron.Astrophys. 652, C4 (2021)].

Aguillard, D. P. et al. (2023). Measurement of the Positive Muon Anomalous Magnetic Moment to 0.20 ppm. *arXiv preprint*. doi:10.48550/arXiv.2308.06230.

Aker, M. et al. (2022). Direct neutrino-mass measurement with sub-electronvolt sensitivity. *Nature Phys.*, **18**(2), pp. 160–166. doi:10.1038/s41567-021-01463-1.

Akhmedov, E. (1988). Resonant Amplification of Neutrino Spin Rotation in Matter and the Solar Neutrino Problem. *Phys. Lett. B*, **213**, pp. 64–68. doi:10.1016/0370-2693(88)91048-9.

Akhmedov, E. and P. Martínez-Miravé (2022). Solar $\overline{\nu}_e$ flux: revisiting bounds on neutrino magnetic moments and solar magnetic field. *JHEP*, **10**, p. 144. doi:10.1007/JHEP10(2022)144.

Andreev, V. et al. (2018). Improved limit on the electric dipole moment of the electron. *Nature*, **562**(7727), pp. 355–360. doi:10.1038/s41586-018-0599-8.

Angeles-Martinez, R. and M. Napsuciale (2012). Renormalization of the QED of second order spin 1/2 fermions. *Phys. Rev. D*, **85**, p. 076004. doi:10.1103/PhysRevD.85.076004.

Aoyama, T. et al. (2020). The anomalous magnetic moment of the muon in the Standard Model. *Phys. Rept.*, **887**, pp. 1–166. doi:10.1016/j.physrep.2020.07.006.

Aristizabal Sierra, D., O. G. Miranda, D. K. Papoulias, and G. S. Garcia (2022). Neutrino magnetic and electric dipole moments: From measurements to parameter space. *Phys. Rev. D*, **105**(3), p. 035027. doi:10.1103/PhysRevD.105.035027.

Bahcall, J. N., M. H. Pinsonneault, and S. Basu (2001). Solar Models: Current Epoch and Time Dependences, Neutrinos, and Helioseismological Properties. *The Astrophysical Journal*, **555**(2), p. 990. doi:10.1086/321493.

Bargmann, V., L. Michel, and V. L. Telegdi (1959). Precession of the polarization of particles moving in a homogeneous electromagnetic field. *Phys. Rev. Lett.*, **2**, pp. 435–436. doi:10.1103/PhysRevLett.2.435.

Barut, A. O. and J. Kraus (1975). Resonances in e+ e- System Due to Anomalous Magnetic Moment Interactions. *Phys. Lett. B*, **59**, pp. 175–178. doi:10.1016/0370-2693(75)90696-6.

Barut, A. O. and J. Kraus (1976). Solution of the Dirac Equation with Coulomb and Magnetic Moment Interactions. *J. Math. Phys.*, **17**, pp. 506–508. doi:10.1063/1.522932.

Batista, R. A. and A. Saveliev (2021). The Gamma-ray Window to Intergalactic Magnetism. *Universe*, **7**(7). ISSN 2218-1997. doi:10.3390/universe7070223.

Bethe, H. A. (1986). A Possible Explanation of the Solar Neutrino Puzzle. *Phys. Rev. Lett.*, **56**, p. 1305. doi:10.1103/PhysRevLett.56.1305.

Birrell, J., C. T. Yang, and J. Rafelski (2014). Relic Neutrino Freeze-out: Dependence on Natural Constants. *Nucl. Phys. B*, **890**, pp. 481–517. doi:10.1016/j.nuclphysb.2014.11.020.

Bouchiat, M. A. and C. C. Bouchiat (1974). Weak Neutral Currents in Atomic Physics. *Phys. Lett. B*, **48**, pp. 111–114. doi:10.1016/0370-2693(74)90656-X.

Bouchiat, M. A. and C. C. Bouchiat (1997). Parity violation in atoms. *Rept. Prog. Phys.*, **60**, pp. 1351–1396. doi:10.1088/0034-4885/60/11/004.

Broderick, A., M. Prakash, and J. M. Lattimer (2000). The Equation of state of neutron star matter in strong magnetic fields. *Astrophys. J.*, **537**, p. 351. doi:10.1086/309010.

Buarque Franzosi, D. and C. Zhang (2015). Probing the top-quark chromomagnetic dipole moment at next-to-leading order in QCD. *Phys. Rev. D*, **91**(11), p. 114010. doi:10.1103/PhysRevD.91.114010.

Canas, B. C., O. G. Miranda, A. Parada, M. Tortola, and J. W. F. Valle (2016). Updating neutrino magnetic moment constraints. *Phys. Lett. B*, **753**, pp. 191–198. doi:10.1016/j.physletb.2015.12.011. [Addendum: Phys.Lett.B 757, 568–568 (2016)].

Canetti, L., M. Drewes, and M. Shaposhnikov (2012). Matter and Antimatter in the Universe. *New J. Phys.*, **14**, p. 095012. doi:10.1088/1367-2630/14/9/095012.

Carter, B. (1968). Global structure of the Kerr family of gravitational fields. *Phys. Rev.*, **174**, pp. 1559–1571. doi:10.1103/PhysRev.174.1559.

Chukhnova, A. V. and A. E. Lobanov (2020). Neutrino flavor oscillations and spin rotation in matter and electromagnetic field. *Phys. Rev. D*, **101**(1), p. 013003. doi:10.1103/PhysRevD.101.013003.

Davis, T. M. and C. H. Lineweaver (2004). Expanding confusion: common misconceptions of cosmological horizons and the superluminal expansion of the universe. *Publ. Astron. Soc. Austral.*, **21**, p. 97. doi:10.1071/AS03040.

Delgado-Acosta, E. G., M. Napsuciale, and S. Rodriguez (2011). Second order formalism for spin 1/2 fermions and Compton scattering. *Phys. Rev. D*, **83**, p. 073001. doi:10.1103/PhysRevD.83.073001.

Dunne, G. V. (2014). Extreme quantum field theory and particle physics with IZEST. *Eur. Phys. J. ST*, **223**(6), pp. 1055–1061. doi:10.1140/epjst/e2014-02156-4.

Durrer, R. and A. Neronov (2013). Cosmological magnetic fields: their generation, evolution and observation. *The Astronomy and Astrophysics Review*, **21**, pp. 1–109. doi:10.1007/s00159-013-0062-7.

Ehrenfest, P. (1927). Bemerkung über die angenäherte Gültigkeit der klassischen Mechanik innerhalb der Quantenmechanik. *Z. Phys.*, **45**(7-8), pp. 455–457. doi:10.1007/BF01329203.

Eides, M. I., H. Grotch, and V. A. Shelyuto (2001). Theory of light hydrogen - like atoms. *Phys. Rept.*, **342**, pp. 63–261. doi:10.1016/S0370-1573(00)00077-6.

Elizalde, E., E. J. Ferrer, and V. de la Incera (2004). Neutrino propagation in a strongly magnetized medium. *Phys. Rev. D*, **70**, p. 043012. doi:10.1103/PhysRevD.70.043012.

Elze, H. T., W. Greiner, and J. Rafelski (1980). The relativistic Fermi gas revisited. *J. Phys. G*, **6**, pp. L149–L153. doi:10.1088/0305-4616/6/9/003.

Evans, S. (2022). *Nonperturbative Aspects in the QED Vacuum Related to Anomalous Magnetic Moment*. Ph.D. thesis, Arizona U.

Evans, S. and J. Rafelski (2018). Vacuum stabilized by anomalous magnetic moment. *Phys. Rev. D*, **98**(1), p. 016006. doi:10.1103/PhysRevD.98.016006.

Evans, S. and J. Rafelski (2022). Emergence of periodic in magnetic moment effective QED action. *Phys. Lett. B*, **831**, p. 137190. doi:10.1016/j.physletb.2022.137190.

Ferrara, S., M. Porrati, and V. L. Telegdi (1992). $g = 2$ as the natural value of the tree-level gyromagnetic ratio of elementary particles. *Phys. Rev. D*, **46**, pp. 3529–3537. doi:10.1103/PhysRevD.46.3529.

Ferrer, E. J., V. de la Incera, D. Manreza Paret, A. Pérez Martínez, and A. Sanchez (2015). Insignificance of the anomalous magnetic moment of charged fermions for the equation of state of a magnetized and dense medium. *Phys. Rev. D*, **91**(8), p. 085041. doi:10.1103/PhysRevD.91.085041.

Ferrer, E. J. and A. Hackebill (2019). Thermodynamics of Neutrons in a Magnetic Field and its Implications for Neutron Stars. *Phys. Rev. C*, **99**(6), p. 065803. doi:10.1103/PhysRevC.99.065803.

Ferrer, E. J. and A. Hackebill (2023). The Importance of the Pressure Anisotropy Induced by Strong Magnetic Fields on Neutron Star Physics. *J. Phys. Conf. Ser.*, **2536**(1), p. 012007. doi:10.1088/1742-6596/2536/1/012007.

Feynman, R. P. (1951). An Operator calculus having applications in quantum electrodynamics. *Phys. Rev.*, **84**, pp. 108–128. doi:10.1103/PhysRev.84.108.

Feynman, R. P. and M. Gell-Mann (1958). Theory of Fermi interaction. *Phys. Rev.*, **109**, pp. 193–198. doi:10.1103/PhysRev.109.193.

Fock, V. (1937). Proper time in classical and quantum mechanics. *Phys. Z. Sowjetunion*, **12**, pp. 404–425.

Foldy, L. L. (1952). The Electromagnetic Properties of Dirac Particles. *Phys. Rev.*, **87**, pp. 688–693. doi:10.1103/PhysRev.87.688.

Foldy, L. L. and S. A. Wouthuysen (1950). On the Dirac theory of spin 1/2 particle and its nonrelativistic limit. *Phys. Rev.*, **78**, pp. 29–36. doi:10.1103/PhysRev.78.29.

Formanek, M. (2020). *Revisiting Covariant Particle Dynamics*. Ph.D. thesis, Arizona U.

Formanek, M., S. Evans, J. Rafelski, A. Steinmetz, and C. T. Yang (2018). Strong fields and neutral particle magnetic moment dynamics. *Plasma Phys. Control. Fusion*, **60**, p. 074006. doi:10.1088/1361-6587/aac06a.

Formanek, M., A. Steinmetz, and J. Rafelski (2019). Classical neutral point particle in linearly polarized EM plane wave field. *Plasma Phys. Control. Fusion*, **61**(8), p. 084006. doi:10.1088/1361-6587/ab242e.

Formanek, M., A. Steinmetz, and J. Rafelski (2020). Radiation reaction friction: Resistive material medium. *Phys. Rev. D*, **102**(5), p. 056015. doi:10.1103/PhysRevD.102.056015.

Formanek, M., A. Steinmetz, and J. Rafelski (2021). Motion of classical charged particles with magnetic moment in external plane-wave electromagnetic fields. *Phys. Rev. A*, **103**(5), p. 052218. doi:10.1103/PhysRevA.103.052218.

Frenkel, J. (1926). Die Elektrodynamik des rotierenden Elektrons. *Z. Phys.*, **37**, pp. 243–262. doi:10.1007/BF01397099.

Fritzsch, H. and Z. Z. Xing (1996). Lepton mass hierarchy and neutrino oscillations. *Phys. Lett. B*, **372**, pp. 265–270. doi:10.1016/0370-2693(96)00107-4.

Fritzsch, H. and Z. Z. Xing (1998). Large leptonic flavor mixing and the mass spectrum of leptons. *Phys. Lett. B*, **440**, pp. 313–318. doi:10.1016/S0370-2693(98)01106-X.

Fritzsch, H. and Z. Z. Xing (2000). Mass and flavor mixing schemes of quarks and leptons. *Prog. Part. Nucl. Phys.*, **45**, pp. 1–81. doi:10.1016/S0146-6410(00)00102-2.

Fromerth, M. J., I. Kuznetsova, L. Labun, J. Letessier, and J. Rafelski (2012). From Quark-Gluon Universe to Neutrino Decoupling: $200 < \mathrm{T} < 2$MeV. *Acta Phys. Polon. B*, **43**(12), pp. 2261–2284. doi:10.5506/APhysPolB.43.2261.

Fujikawa, K. and R. E. Shrock (1980). The Magnetic Moment of a Massive Neutrino and Neutrino Spin Rotation. *Phys. Rev. Lett.*, **45**, p. 963. doi:10.1103/PhysRevLett.45.963.

Gaensler, B. M., R. Beck, and L. Feretti (2004). The origin and evolution of cosmic magnetism. *New Astronomy Reviews*, **48**(11-12), pp. 1003–1012. doi:10.1016/j.newar.2004.09.003.

Gerlach, W. and O. Stern (1922). The Magnetic Moment of Silver Atoms. *Z. Phys.*, **9**, pp. 353–355. doi:10.1007/BF01326984.

Gesztesy, F., B. Simon, and B. Thaller (1985). On the selfadjointness of Dirac operators with anomalous magnetic moment. *Proceedings of the American Mathematical Society*, **94**(1), pp. 115–118. doi:10.2307/2044962.

Giovannini, M. (2004). The Magnetized universe. *Int. J. Mod. Phys. D*, **13**, pp. 391–502. doi:10.1142/S0218271804004530.

Giovannini, M. (2018). Probing large-scale magnetism with the Cosmic Microwave Background. *Class. Quant. Grav.*, **35**(8), p. 084003. doi:10.1088/1361-6382/aab17d.

Giovannini, M. (2023). The scaling of primordial gauge fields. *Physics Letters B*, **842**, p. 137967. ISSN 0370-2693. doi:10.1016/j.physletb.2023.137967.

Giunti, C. and C. W. Kim (2007). *Fundamentals of neutrino physics and astrophysics*. Oxford university press. doi:10.1093/acprof:oso/9780198508717.001.0001.

Giunti, C., K. A. Kouzakov, Y. F. Li, A. V. Lokhov, A. Studenikin, and S. Zhou (2016). Electromagnetic neutrinos in laboratory experiments and astrophysics. *Annalen Phys.*, **528**, pp. 198–215. doi:10.1002/andp.201500211.

Giunti, C. and A. Studenikin (2015). Neutrino electromagnetic interactions: a window to new physics. *Rev. Mod. Phys.*, **87**, p. 531. doi:10.1103/RevModPhys.87.531.

Gopal, R. and S. Sethi (2005). Generation of magnetic field in the pre-recombination era. *Mon. Not. Roy. Astron. Soc.*, **363**, pp. 521–528. doi:10.1111/j.1365-2966.2005.09442.x.

Grasso, D. and H. R. Rubinstein (2001). Magnetic fields in the early universe. *Phys. Rept.*, **348**, pp. 163–266. doi:10.1016/S0370-1573(00)00110-1.

Grayson, C., C. T. Yang, M. Formanek, and J. Rafelski (2023). Electron–positron plasma in BBN: Damped-dynamic screening. *Annals Phys.*, **458**, p. 169453. doi:10.1016/j.aop.2023.169453.

Greiner, W. and B. Müller (2009). *Gauge theory of weak interactions*. Springer. doi:10.1007/978-3-540-87843-8.

Greiner, W. and B. Müller (2012). *Quantum mechanics: symmetries*. Springer Science & Business Media. doi:10.1007/978-3-642-57976-9. [orig. pub. 1984].

Greiner, W., B. Muller, and J. Rafelski (2012a). *Quantum electrodynamics of strong fields*. Springer Berlin, Heidelberg. doi:10.1007/978-3-642-82272-8. [orig. pub. 1985].

Greiner, W., L. Neise, and H. Stöcker (2012b). *Thermodynamics and statistical mechanics*. Springer Science & Business Media. doi:10.1007/978-1-4612-0827-3. [orig. pub. 1995].

Greiner, W. and J. Reinhardt (2008). *Quantum electrodynamics*. Springer Science & Business Media. doi:10.1007/978-3-540-87561-1.

Greiner, W., S. Schramm, and E. Stein (2006). *Quantum chromodynamics*. Springer Berlin, Heidelberg. doi:10.1007/978-3-540-48535-3. [orig. pub. 1989].

Hackebill, A. A. (2022). *Magnetic Field Effects on the Physics of Neutron Stars*. Ph.D. thesis, CUNY, Graduate School - U. Ctr.

Haro, P. A., M. Dickinson, S. L. Finkelstein, et al. (2023). Confirmation and refutation of very luminous galaxies in the early universe. *Nature*. doi:10.1038/s41586-023-06521-7.

Hegelich, B. M., G. Mourou, and J. Rafelski (2014). Probing the quantum vacuum with ultra intense laser pulses. *Eur. Phys. J. ST*, **223**(6), pp. 1093–1104. doi:10.1140/epjst/e2014-02160-8.

Hewett, J. L. et al. (2012). Fundamental Physics at the Intensity Frontier. In *Workshop on Fundamental Physics at the Intensity Frontier*. doi:10.2172/1042577.

Itzykson, C. and J. B. Zuber (1980). *Quantum Field Theory*. International Series In Pure and Applied Physics. McGraw-Hill, New York. ISBN 978-0-486-44568-7.

Jancovici, B. (1969). Radiative correction to the ground-state energy of an electron in an intense magnetic field. *Phys. Rev.*, **187**, pp. 2275–2276. doi:10.1103/PhysRev.187.2275.

Jedamzik, K. and T. Abel (2013). Small-scale primordial magnetic fields and anisotropies in the cosmic microwave background radiation. *JCAP*, **10**, p. 050. doi:10.1088/1475-7516/2013/10/050.

Jedamzik, K. and L. Pogosian (2020). Relieving the Hubble tension with primordial magnetic fields. *Physical Review Letters*, **125**(18), p. 181302. doi:10.1103/PhysRevLett.125.181302.

Jedamzik, K. and A. Saveliev (2019). Stringent limit on primordial magnetic fields from the cosmic microwave background radiation. *Physical review letters*, **123**(2), p. 021301. doi:10.1103/PhysRevLett.123.021301.

Jegerlehner, F. (2017). *The Anomalous Magnetic Moment of the Muon*, volume 274. Springer, Cham. doi:10.1007/978-3-319-63577-4.

Jentschura, U. and K. Pachucki (1996). Higher-order binding corrections to the Lamb shift of P-2 states. *Phys. Rev. A*, **54**, pp. 1853–1861. doi:10.1103/PhysRevA.54.1853.

Kaspi, V. M. and A. Beloborodov (2017). Magnetars. *Ann. Rev. Astron. Astrophys.*, **55**, pp. 261–301. doi:10.1146/annurev-astro-081915-023329.

Knecht, M. (2004). The Anomalous magnetic moment of the muon: A Theoretical introduction. *Lect. Notes Phys.*, **629**, pp. 37–84. doi:10.1007/978-3-540-44457-2_2.

Kronberg, P. P. (1994). Extragalactic magnetic fields. *Reports on Progress in Physics*, **57**(4), p. 325. doi:10.1088/0034-4885/57/4/001.

Labun, L. and J. Rafelski (2009). Vacuum Decay Time in Strong External Fields. *Phys. Rev. D*, **79**, p. 057901. doi:10.1103/PhysRevD.79.057901.

Labun, L. and J. Rafelski (2013). Top anomalous magnetic moment and the two photon decay of Higgs boson. *Phys. Rev. D*, **88**, p. 071301. doi:10.1103/PhysRevD.88.071301.

Larson, R. L., S. L. Finkelstein, D. D. Kocevski, T. A. Hutchison, J. R. Trump, P. A. Haro, V. Bromm, N. J. Cleri, M. Dickinson, S. Fujimoto, et al. (2023). A CEERS Discovery of an Accreting Supermassive Black Hole 570 Myr after the Big Bang: Identifying a Progenitor of Massive $z > 6$ Quasars. *arXiv preprint*. doi:10.48550/arXiv.2303.08918. [submitted to ApJ].

Letessier, J. and J. Rafelski (2023). *Hadrons and Quark–Gluon Plasma*. Cambridge Monographs on Particle Physics, Nuclear Physics and Cosmology. Cambridge University Press. doi:10.1017/9781009290753. *Open access.* [orig. pub. 2002].

Lim, C. S. and W. J. Marciano (1988). Resonant Spin - Flavor Precession of Solar and Supernova Neutrinos. *Phys. Rev. D*, **37**, pp. 1368–1373. doi:10.1103/PhysRevD.37.1368.

Martin, P. C. and R. J. Glauber (1958). Relativistic Theory of Radiative Orbital Electron Capture. *Phys. Rev.*, **109**, pp. 1307–1325. doi:10.1103/PhysRev.109.1307.

Martínez-Miravé, P. (2023). *Neutrino properties from the laboratory and the cosmos*. Ph.D. thesis, Valencia U.

Melrose, D. (2013). *Quantum plasmadynamics: Magnetized plasmas*. Springer. doi:10.1007/978-1-4614-4045-1.

Mikheyev, S. P. and A. Y. Smirnov (1985). Resonance Amplification of Oscillations in Matter and Spectroscopy of Solar Neutrinos. *Sov. J. Nucl. Phys.*, **42**, pp. 913–917.

Neronov, A. and I. Vovk (2010). Evidence for strong extragalactic magnetic fields from Fermi observations of TeV blazars. *Science*, **328**(5974), pp. 73–75. doi:10.1126/science.1184192.

Niederle, J. and A. G. Nikitin (2006). Relativistic Coulomb problem for particles with arbitrary half-integer spin. *J. Phys. A*, **39**, pp. 10931–10944. doi:10.1088/0305-4470/39/34/023.

Nieves, J. F. (1982). Electromagnetic Properties of Majorana Neutrinos. *Phys. Rev. D*, **26**, p. 3152. doi:10.1103/PhysRevD.26.3152.

Ohanian, H. C. (1986). What is spin? *American Journal of Physics*, **54**(6), pp. 500–505. doi:10.1119/1.14580.

Ohlsson, T. (2012). *Relativistic quantum physics: From advanced quantum mechanics to introductory quantum field theory*. Cambridge University Press. ISBN 978-1-139-21072-0, 978-0-521-76726-2. doi:10.1017/CBO9781139032681.

Pacetti, S., R. Baldini Ferroli, and E. Tomasi-Gustafsson (2015). Proton electromagnetic form factors: Basic notions, present achievements and future perspectives. *Phys. Rept.*, **550-551**, pp. 1–103. doi:10.1016/j.physrep.2014.09.005.

Pal, P. B. (1992). Particle physics confronts the solar neutrino problem. *Int. J. Mod. Phys. A*, **7**, pp. 5387–5460. doi:10.1142/S0217751X92002465.

Perrone, L. M., G. Gregori, B. Reville, L. O. Silva, and R. Bingham (2021). Neutrino-electron magnetohydrodynamics in an expanding universe. *Phys. Rev. D*, **104**(12), p. 123013. doi:10.1103/PhysRevD.104.123013.

Pomakov, V. P., S. P. O'Sullivan, M. Brüggen, F. Vazza, E. Carretti, G. H. Heald, C. Horellou, T. Shimwell, A. Shulevski, and T. Vernstrom (2022). The redshift evolution of extragalactic magnetic fields. *Monthly Notices of the Royal Astronomical Society*, **515**(1), pp. 256–270. doi:10.1093/mnras/stac1805.

Popov, A. and A. Studenikin (2019). Neutrino eigenstates and flavour, spin and spin-flavour oscillations in a constant magnetic field. *Eur. Phys. J. C*, **79**(2), p. 144. doi:10.1140/epjc/s10052-019-6657-z.

Pshirkov, M. S., P. G. Tinyakov, and F. R. Urban (2016). New limits on extragalactic magnetic fields from rotation measures. *Phys. Rev. Lett.*, **116**(19), p. 191302. doi:10.1103/PhysRevLett.116.191302.

Rafelski, J. and J. Birrell (2014). Traveling Through the Universe: Back in Time to the Quark-Gluon Plasma Era. *J. Phys. Conf. Ser.*, **509**, p. 012014. doi:10.1088/1742-6596/509/1/012014.

Rafelski, J., J. Birrell, A. Steinmetz, and C. T. Yang (2023a). A Short Survey of Matter-Antimatter Evolution in the Primordial Universe. *Universe*, **9**(7), p. 309. doi:10.3390/universe9070309.

Rafelski, J., S. Evans, and L. Labun (2023b). Study of QED singular properties for variable gyromagnetic ratio $g \simeq 2$. *Phys. Rev. D*, **107**. doi:10.1103/PhysRevD.107.076002.

Rafelski, J., M. Formanek, and A. Steinmetz (2018). Relativistic Dynamics of Point Magnetic Moment. *Eur. Phys. J. C*, **78**(1), p. 6. doi:10.1140/epjc/s10052-017-5493-2.

Rafelski, J., L. P. Fulcher, and A. Klein (1978). Fermions and Bosons Interacting with Arbitrarily Strong External Fields. *Phys. Rept.*, **38**, pp. 227–361. doi:10.1016/0370-1573(78)90116-3.

Rafelski, J., J. Kirsch, B. Müller, J. Reinhardt, and W. Greiner (2017). Probing QED Vacuum with Heavy Ions. *FIAS Interdisc. Sci. Ser.*, pp. 211–251. doi:10.1007/978-3-319-44165-8_17.

Rafelski, J., A. Steinmetz, and C. T. Yang (2023c). Dynamic fermion flavor mixing through transition dipole moments. *arXiv preprint*. [submitted to Int. Journal of Mod. Phys. A].

Roussy, T. S. et al. (2023). An improved bound on the electron's electric dipole moment. *Science*, **381**(6653), p. adg4084. doi:10.1126/science.adg4084.

Ruffini, R. and G. Vereshchagin (2013). Electron-positron plasma in GRBs and in cosmology. *Nuovo Cim. C*, **036**(s01), pp. 255–266. doi:10.1393/ncc/i2013-11500-0.

Ruffini, R., G. Vereshchagin, and S. S. Xue (2010). Electron-positron pairs in physics and astrophysics: from heavy nuclei to black holes. *Phys. Rept.*, **487**, pp. 1–140. doi:10.1016/j.physrep.2009.10.004.

Safronova, M. S., D. Budker, D. DeMille, D. F. J. Kimball, A. Derevianko, and C. W. Clark (2018). Search for New Physics with Atoms and Molecules. *Rev. Mod. Phys.*, **90**(2), p. 025008. doi:10.1103/RevModPhys.90.025008.

Sakurai, J. J. (1967). *Advanced quantum mechanics*. Pearson Education India.

Schechter, J. and J. W. F. Valle (1981). Majorana Neutrinos and Magnetic Fields. *Phys. Rev. D*, **24**, pp. 1883–1889. doi:10.1103/PhysRevD.25.283. [Erratum: Phys.Rev.D 25, 283 (1982)].

Schwartz, M. D. (2014). *Quantum Field Theory and the Standard Model*. Cambridge University Press. doi:10.1017/9781139540940.

Schwinger, J. (1974). Spin precession—a dynamical discussion. *American Journal of Physics*, **42**(6), pp. 510–513. doi:10.1119/1.1987764.

Schwinger, J. S. (1951). On gauge invariance and vacuum polarization. *Phys. Rev.*, **82**, pp. 664–679. doi:10.1103/PhysRev.82.664.

Shrock, R. E. (1980). New Tests For, and Bounds On, Neutrino Masses and Lepton Mixing. *Phys. Lett. B*, **96**, pp. 159–164. doi:10.1016/0370-2693(80)90235-X.

Shrock, R. E. (1982). Electromagnetic Properties and Decays of Dirac and Majorana Neutrinos in a General Class of Gauge Theories. *Nucl. Phys. B*, **206**, pp. 359–379. doi:10.1016/0550-3213(82)90273-5.

Smirnov, A. Y. (2003). The MSW effect and solar neutrinos. In *10th International Workshop on Neutrino Telescopes*, pp. 23–43. doi:10.48550/arXiv.hep-ph/0305106.

Steinmetz, A., M. Formanek, and J. Rafelski (2019). Magnetic Dipole Moment in Relativistic Quantum Mechanics. *Eur. Phys. J. A*, **55**(3), p. 40. doi:10.1140/epja/i2019-12715-5.

Steinmetz, A., C. T. Yang, and J. Rafelski (2023). Matter-antimatter origin of cosmic magnetism. doi:10.48550/arXiv.2308.14818. [Submitted to PRD].

Studenikin, A. (2016). Status and perspectives of neutrino magnetic moments. *J. Phys. Conf. Ser.*, **718**(6), p. 062076. doi:10.1088/1742-6596/718/6/062076.

Taylor, A. M., I. Vovk, and A. Neronov (2011). Extragalactic magnetic fields constraints from simultaneous GeV–TeV observations of blazars. *Astronomy & Astrophysics*, **529**, p. A144. doi:10.1051/0004-6361/201116441.

Thaller, B. (2013). *The Dirac equation*. Springer Science & Business Media. ISBN 978-3-662-02753-0. doi:10.1007/978-3-662-02753-0. [orig. pub. 1992].

Tiesinga, E., P. J. Mohr, D. B. Newell, and B. N. Taylor (2021). CODATA recommended values of the fundamental physical constants: 2018. *Rev. Mod. Phys.*, **93**(2), p. 025010. doi:10.1103/RevModPhys.93.025010.

Tsai, W.-Y. and A. Yildiz (1971). Motion of charged particles in a homogeneous magnetic field. *Phys. Rev. D*, **4**, pp. 3643–3648. doi:10.1103/PhysRevD.4.3643.

Vachaspati, T. (2021). Progress on cosmological magnetic fields. *Rept. Prog. Phys.*, **84**(7), p. 074901. doi:10.1088/1361-6633/ac03a9.

Vaquera-Araujo, C. A., M. Napsuciale, and R. Angeles-Martinez (2013). Renormalization of the QED of Self-Interacting Second Order Spin 1/2 Fermions. *JHEP*, **01**, p. 011. doi:10.1007/JHEP01(2013)011.

Vazza, F., M. Brüggen, C. Gheller, S. Hackstein, D. Wittor, and P. M. Hinz (2017). Simulations of extragalactic magnetic fields and of their observables. *Class. Quant. Grav.*, **34**(23), p. 234001. doi:10.1088/1361-6382/aa8e60.

Veltman, M. J. G. (1998). Two component theory and electron magnetic moment. *Acta Phys. Polon. B*, **29**, pp. 783–798.

Vernstrom, T., G. Heald, F. Vazza, T. J. Galvin, J. L. West, N. Locatelli, N. Fornengo, and E. Pinetti (2021). Discovery of magnetic fields along stacked cosmic filaments as revealed by radio and X-ray emission. *Monthly Notices of the Royal Astronomical Society*, **505**(3), pp. 4178–4196. doi:10.1093/mnras/stab1301.

Vryonidou, E. and C. Zhang (2018). Dimension-six electroweak top-loop effects in Higgs production and decay. *JHEP*, **08**, p. 036. doi:10.1007/JHEP08(2018)036.

Weinberg, S. (1972). *Gravitation and cosmology: principles and applications of the general theory of relativity*. John Wiley & Sons.

Weinberg, S. (2005). *The Quantum theory of fields. Vol. 1: Foundations*. Cambridge University Press. ISBN 978-0-521-67053-1, 978-0-511-25204-4. doi:10.1017/CBO9781139644167.

Weisskopf, V. (1936). *The electrodynamics of the vacuum based on the quantum theory of the electron*, p. 206–226. Cambridge University Press. doi:10.1017/CBO9780511608223.018. [translated and reprinted in 1994].

Wolfenstein, L. (1978). Neutrino Oscillations in Matter. *Phys. Rev. D*, **17**, pp. 2369–2374. doi:10.1103/PhysRevD.17.2369.

Workman, R. L. et al. (2022). Review of Particle Physics. *PTEP*, **2022**, p. 083C01. doi:10.1093/ptep/ptac097.

Xing, Z. Z. (2001). Commutators of lepton mass matrices, CP violation, and matter effects in-medium baseline neutrino experiments. *Phys. Rev. D*, **63**, p. 073012. doi:10.1103/PhysRevD.63.073012.

Yan, H., Z. Ma, C. Ling, C. Cheng, and J. Huang (2023). First Batch of z $\approx$ 11–20 Candidate Objects Revealed by the James Webb Space Telescope Early Release Observations on SMACS 0723-73. *Astrophys. J. Lett.*, **942**(1), p. L9. doi:10.3847/2041-8213/aca80c.

Yang, C. T., M. Formanek, A. Steinmetz, and J. Rafelski (2023). Decomposition of Fermi gas into zero and finite temperature distributions with examples. *arXiv preprint*. [submitted to Int. Journal of Theor. Phys.].

Zhang, C. (2012). *Effective field theory for top quark physics*. Ph.D. thesis, Illinois U., Urbana.

Zhang, C. and S. Willenbrock (2011). Effective-Field-Theory Approach to Top-Quark Production and Decay. *Phys. Rev. D*, **83**, p. 034006. doi:10.1103/PhysRevD.83.034006.

# APPENDIX A

## Magnetic dipole moment in relativistic quantum mechanics

Steinmetz, A., Formanek, M. & Rafelski, J. Magnetic dipole moment in relativistic quantum mechanics. European Physical Journal A **55**, 40 (2019). 10.1140/epja/i2019-12715-5

# APPENDIX B

## Strong fields and neutral particle magnetic moment dynamics

Formanek, M., Stefan, E., Rafelski, J., Steinmetz, A., Yang, C. T. Strong fields and neutral particle magnetic moment dynamics. Plasma Physics and Controlled Fusion 60, 7 (2018): 074006. 10.1088/1361-6587/aac06a

# APPENDIX C

## Relativistic dynamics of point magnetic moment

Rafelski, J., Formanek, M., Steinmetz, A. Relativistic dynamics of point magnetic moment. Eur. Phys. J. C **78**, 6 (2018). 10.1140/epjc/s10052-017-5493-2

# APPENDIX D

## Dynamic fermion flavor mixing through transition dipole moments

Rafelski, J., Steinmetz, A., Yang, C.T. Dynamic fermion flavor mixing through transition dipole moments. *arXiv preprint*. 2023.

 Contribution to the book edited by Gerhard Buchalla, Dieter Lüst and Zhi-Zhong Xing dedicated to memory of Harald Fritzsch. Submitted an a separate article to International Journal of Modern Physics A.

# APPENDIX E

## A Short Survey of Matter-Antimatter Evolution in the Primordial Universe

Rafelski, J., Birrell, J., Steinmetz, A., Yang, C.T. A Short Survey of Matter-Antimatter Evolution in the Primordial Universe. Universe 2023, 9, 309. 10.3390/universe9070309

# APPENDIX F

## Matter-antimatter origin of cosmic magnetism

Steinmetz, A., Yang, C.T. & Rafelski, J. Matter-antimatter origin of cosmic magnetism. *arXiv preprint*. 2023. arXiv:2308.14818 [hep-ph]